

1-1-2011

Characterization of poly (rc) binding protein (pcbp2) and frataxin

Sudipa Ghimire-Rijal
Wayne State University

Follow this and additional works at: http://digitalcommons.wayne.edu/oa_theses

 Part of the [Biochemistry Commons](#)

Recommended Citation

Ghimire-Rijal, Sudipa, "Characterization of poly (rc) binding protein (pcbp2) and frataxin" (2011). *Wayne State University Theses*. Paper 71.

**CHARACTERIZATION OF POLY (rC) BINDING PROTEIN (PCBP2) AND
FRATAXIN**

by

SUDIPA GHIMIRE-RIJAL

THESIS

Submitted to the Graduate School

of Wayne State University,

Detroit, Michigan

in partial fulfillment of the requirements

for the degree of

MASTERS IN SCIENCE

2011

MAJOR: BIOCHEMISTRY AND MOLECULAR
BIOLOGY

Approved by:

Advisor

Date

ACKNOWLEDGMENTS

My deepest gratitude goes to my adviser Dr. Timothy L. Stemmler for all his support, encouragement and enthusiasm for the research. He has been very supportive and encouraging through the times which helped me to grow as a budding scientist. I will be forever grateful to you for all the support and guidance that I received while pursuing my MS degree. I am also thankful to my committee members Dr. Brian F. P. Edwards and Dr. Bharati Mitra for their encouragement and constructive comments which helped me to develop a passion for research.

I am thankful to my former and present lab members; Jeremy, Swati, Madhusi, Poorna, Andrea, April, Yogapriya for creating a friendly lab environment. I am also thankful to Asmita Vaishnav for all her suggestions and comments.

My acknowledgement goes to my family members; my parents, my sister Sandipa and in-law Dhiraj whose support and love for education has brought me to this level. I especially want to thank Rajan and Urmila for their motivating talks.

This acknowledgement would not be complete without thanking my husband Keshab, who have been very supportive and encouraging. Thank you very much for your support and care. Lastly and most importantly my acknowledgement goes to my "Lord Krishna" for all the blissful times.

Pursuing my MS at Wayne State University had been a wonderful educational experience to me and I would like to thank everyone who are directly and indirectly involved in this journey of my life.

TABLE OF CONTENTS

Acknowledgements	ii
List of Tables	vii
List of Figures	viii
CHAPTER 1 Iron Chaperones for Mitochondrial Fe-S Cluster Biosynthesis and Ferritin Iron Storage	
1.1 Prelude.....	1
1.2 Introduction.....	2
1.3 Fe-S cluster biosynthesis iron chaperones.....	4
1.4 Ferritin iron chaperones.....	11
1.5 Conclusions	13
CHAPTER 2 Molecular Characteristics of the Drosophila Frataxin-Isu Interaction during Fe-S Cluster Assembly	15
2.1 Prelude.....	15
2.2 Introduction.....	16
2.3 Materials and Methods	19
2.3.1 Cloning, Expression, and Protein Purification.....	19
2.3.2 Isothermal Titration Calorimetry (ITC) Binding Studies.....	21
2.3.3 Fe-S Cluster Assembly Activity Assay	22
2.3.4 X-ray Absorption Spectroscopy (XAS).....	22
2.3.5 Mössbauer Spectroscopy	24
2.3.6 Fluorescence Spectroscopy	25
2.4 Results	26
2.4.1 Isothermal Titration Calorimetry (ITC) Binding Studies.....	26

2.4.2	X-ray Absorption Spectroscopy (XAS).....	28
2.4.3	Mössbauer Spectroscopy	33
2.4.4	Fluorescence Spectroscopy	35
2.5	Discussion.....	37
	CHAPTER 3 Characterization of Poly (rC) binding protein-PCBP2.....	43
3.1	Introduction.....	43
3.2	Materials and Methods	44
3.2.1	Cloning, Optimization of Conditions for Expression of PCBP2	44
3.2.2	Purification of PCBP2	46
3.2.3	Size and Oligomeric State of PCBP2	47
3.2.4	Fold and Stability of PCBP2	48
3.2.5	Substrate and Protein Binding Characteristics	49
3.2.6	XAS Sample Preparation and Analysis	50
3.3	Results.....	52
3.3.1	Optimization of Condition for Expression of Protein	52
3.3.2	Purification of PCBP2	55
3.3.3	Size and Oligomeric State of PCBP2	56
3.3.4	Fold and Stability of PCBP2	58
3.3.5	Metal Binding Properties of PCBP2.....	59
3.3.6	Electronic and Coordination Properties of Bound Iron.....	62
3.4	Conclusion and Discussion.....	64

CHAPTER 4 Activation of the HIF Prolyl Hydroxylase by the Iron Chaperones PCBP1 and PCBP2.....	67
4.1 Prelude.....	67
4.2 Introduction.....	68
4.3 Experimental Procedures.....	72
4.3.1 Cell culture and treatments.....	72
4.3.2 Protein depletion by siRNA.....	72
4.3.3 RNA extraction and Real-time PCR.....	72
4.3.4 Immunoblot analysis.....	73
4.3.5 Luciferase activity assays.....	74
4.3.6 HIF half-life determination.....	74
4.3.7 VHL capture assay.....	75
4.3.8 PHD2 activity assay.....	75
4.3.9 Immunoprecipitation.....	76
4.4 Results.....	77
4.4.1 Accumulation of transcriptionally active HIF1 α in cells lacking PCBPs.....	77
4.4.2 Reduced hydroxylation of HIF1 α in cells lacking PCBPs.....	81
4.4.3 Reduced metallation of PHD2 in cells lacking PCBPs.....	84
4.4.4 Restoration of PHD2 activity with iron or purified PCBP1.....	86
4.4.5 Direct <i>in vivo</i> interactions between PCBP1 and PHD2.....	89
4.4.6 Genetic and physical interactions of PCBP1 with FIH.....	91
4.5 Discussion.....	93
CHAPTER 5 Summary and Future Directions.....	98

5.1 Prelude.....	99
5.2 Summary	100
5.3 Future Directions	101
References.....	102
Abstract.....	123
Autobiographical Statement.....	124

LIST OF TABLES

Table 2.1. Average ITC simulation results. Averaged values for stoichiometry (N_1 and N_2) and dissociation constants (K_{D1} and K_{D2}) are provided with error bars.	27
Table 2.2. Analysis of pre-edge and edge features from Fe-XANES spectra	30
Table 2.3. Summary of best fit EXAFS simulation results for iron at various stages during cofactor formation.....	32
Table 2.4. Analysis of parameters for Mössbauer simulations of iron bound to Dfh.	35
Table 3.1. Different conditions for optimization of expression of PCBP2.	55
Table 3.2. XAS best fit values for Fe(II) bound to PCBP2.....	63

LIST OF FIGURES

Figure 1.1. Major pathways for iron incorporation/utilization within a cell.....	5
Figure 1.2. Molecular details of the 2 Fe ²⁺ binding sites	8
Figure 1.3. Structural details of PCBP's as a ferritin iron chaperone	12
Figure 2.1. Top: ClustalW alignment for Drosophila, Human, Yeast and Bacterial frataxin orthologs.....	18
Figure 2.2. Raw isothermal titration calorimetry data (top) and binding isotherm data (bottom).....	27
Figure 2.3. XANES spectra of Fe bound in the following sample	29
Figure 2.4. EXAFS and Fourier transforms of iron bound to the proteins	31
Figure 2.5. Drosophila Frataxin Homolog (Dfh) Mössbauer spectra	34
Figure 2.6. Fold and structural rearrangement of Dlsu.	36
Figure 3.1. SDS-Page showing the level of expression of apo-PCBP2.	53
Figure 3.2. SDS-PAGES of protein expression of apo-PCBP2 (365aa) before (Panel A), during (Panel B), and after (Panel C) double colony selections	54
Figure 3.3 SDS-Page showing purification of apo-PCBP2.....	56
Figure 3.4. A Determining molecular weight and Oligomeric state of PCBP2.....	57
Figure 3.5. (A) Secondary structure of PCBP2 determined by Circular Dichroism Spectroscopy at 25°C.....	59
Figure 3.6. PCBP2 is a metal binding protein.	60
Figure 3.7. Interaction of Ferritin with apo/holo-PCBP2.	61
Figure 3.8. XANES comparison of iron-PCBP2 with ferrous and ferric models. .	63
Figure 3.9. EXAFS and Fourier transforms of iron loaded human PCBP2.....	64
Figure 4.1. Accumulation of HIF1 α in cells depleted of PCBPs.	78
Figure 4.2. Increase in HIF1 α half-life and activity in cells lacking PCBPs.	80

Figure 4.3. Impaired HIF-1 α hydroxylation and VHL binding after depletion of PCBPs.	83
Figure 4.4. Decrease in PHD2 metallation after depletion of PCBPs.....	85
Figure 4.5. Requirement of PCBPs for iron-dependent PHD activity.	87
Figure 4.6. Direct interaction of PCBP1 with PHD2.	90
Figure 4.7. Genetic and physical interactions of PCBP1 with FIH1.....	92

CHAPTER 1

Iron Chaperones for Mitochondrial Fe-S Cluster Biosynthesis and Ferritin Iron Storage

1.1 Prelude

Even though only a small amount of iron is required on a daily basis, life without iron is impossible. Iron is present as a cofactor in many enzymes that play a vital role in keeping our body healthy. Various proteins help maintain iron-homeostasis by assisting in metal storage, transfer, influx and efflux. Among these proteins, metallo-chaperones bind metal and deliver it to cognate enzymes. While much has been reported about Copper and Nickel chaperones, much less is known about iron-chaperones. The recent identification of cytosolic iron chaperone -Poly (rC) Binding Protein (PCBP1), which transfers iron to the storage protein, ferritin, has sparked interest in the field. The PCBP protein family is hypothesized to serve as iron chaperones in a tissue specific manner. Frataxin, an iron chaperone within the mitochondria, has been shown to participate within the iron sulfur cluster biosynthetic pathway. Therefore, to understand disorders and diseases related to iron transport, investigating iron chaperones at the molecular level is extremely important. My project involved the characterization of the Poly (rC) Binding Protein-2 (PCBP2) and *Drosophila* frataxin at a structural level to determine the molecular details of how these proteins bind and deliver iron.

The first chapter of my thesis describes the current understanding of these Fe-chaperones. This work is being published as a review article and I contributed as a coauthor by writing the first section of the paper and producing the first

figure. This chapter will serve as the background for my thesis. The reference for the article is: Poorna Subramanian, Andria V. Rodrigues, Sudipa Ghimire-Rijal and Timothy L. Stemmler, "Iron Chaperones for Mitochondrial Fe-S Cluster Biosynthesis and Ferritin Iron Storage," *Current Opinion in Chemical Biology*, **2011**, *In press*.

1.2 Introduction

Iron is essential for life and its unique chemical characteristics are often exploited in nature to assist cells in performing inherently complex oxidation chemistry, promote oxygen transport/storage and drive electron transfer pathways (1). Iron is typically absorbed into the body through diet (2) and on average, humans absorb 1 to 2 mg of iron each day (3). Although the amount of iron abstracted from the diet is low, tight regulation of absorbed iron is critical, as humans have no physiologic pathway to excrete iron. Once consumed, over 60% of the iron is incorporated into hemoglobin through developing erythroid precursors and finally into mature red blood cells. Other destinations for Fe include storage inside ferritin or distribution throughout the body for incorporation into cofactor sites of iron metalloproteins. As a cofactor, Fe is often found associated within iron-sulfur (Fe-S) clusters, found as mononuclear Fe-S, 2Fe-2S, 4Fe-4S and higher stoichiometric clusters common to nature (4). Given the body's need to absorb and maintain appropriate iron levels, Fe reuse and recycling from degraded sources is another method the body uses to maintain iron homeostasis. A simple breakdown in any of these pathways can lead to conditions that are detrimental to human health.

When maintained at balanced levels, iron is essential for cellular and organism viability but it leads to a variety of physiological and developmental irregularities when deficient or in excess. (3). Disorders related to a breakdown in iron homeostasis are among the most common human diseases. Diseases of iron overload are highly prevalent, with the hepatological disorder hereditary hemochromatosis being one of the most common (5). Hemochromatosis patients absorb two to three times more iron than normal dietary iron levels. Excess iron is often deposited in the liver and redox chemistry performed by unregulated metal can kill the cell/organism. Neuronal iron accumulation is a phenotype of numerous neurodegenerative disorders (Parkinson's disease, Alzheimer's disease, Friedreich's ataxia, others). In these disorders, unregulated but redox active metal is pooled within specific regions of the brain, generating oxidative stress through iron catalyzed formation of reactive oxygen species (ROS) (6). ROS can damage membrane phospholipids and generate reactive aldehydes that damage proteins, leading to accumulation of misfolded protein aggregates. While examples of the toxic effects of iron overload are numerous, iron deficiency is an even larger human health issue affecting billions (7). Iron deficiency leads to decreased cognitive development in children (8) and continued long-term deficiency leads to numerous other health related issues (3). It is clear that biological pathways controlling iron reactivity are essential; however it is also clear that the pathways ensuring proper iron delivery are equally important for maintaining cell viability.

Many pathways that regulate cellular iron homeostasis are controlled at the genetic and at the protein level (9-10). As outlined in the transferrin cycle, iron is imported through endocytosis of Fe^{3+} loaded transferrin (Tf) interacting with the transferrin receptor (Tf-R), in a tightly regulated feedback loop controlled at the genetic and protein level (Figure 1.1). In eukaryotes, iron can be diverted to the mitochondria where it is utilized during heme production or during Fe-S cluster assembly (pathway #1 in Figure 1.1). During mitochondrial Fe-S cluster assembly, the ISC machinery proteins work together to form clusters that can be loaded onto apo-mitochondrial proteins or pumped out of the mitochondria in some manner (labeled X) to be used by the cytosolic Fe-S cluster assembly machinery (CIA). Cytosolic iron can also be directed for storage into ferritin in an inert form for future use (pathway #2 in Figure 1.1). While there are obviously other fates for cellular iron, recently two iron chaperones have been discovered that control iron delivery in the pathways highlighted above. An overview of the structure and biophysical properties leading to iron binding by these two chaperones is the basis of this review.

1.3 Fe-S cluster biosynthesis iron chaperones

In eukaryotes, the mitochondrial ISC assembly is the major pathway for Fe-S cluster production. Key players in the yeast ISC machinery include the assembly scaffold protein (either Isu1 or 2, for clarity we will refer to only Isu1), the cysteine desulfurase (Nfs1) that provides sulfur to Isu1, the accessory protein

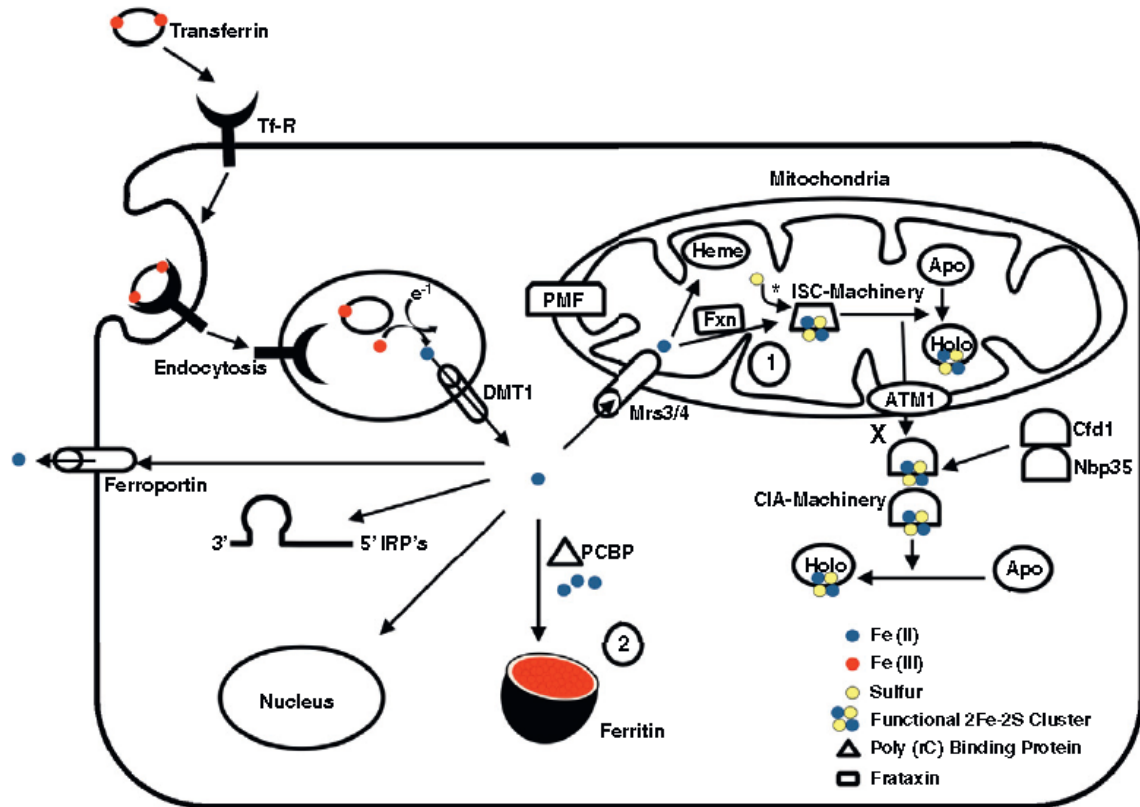


Figure 1.1. Major pathways for iron incorporation/utilization within a cell. Two pathways for Fe^{2+} utilization highlighted within the review include: 1) Frataxin and its role in mitochondrial Fe-S cluster assembly via the ISC-Machinery (* including the cysteine desulfurase/Isd11 complex that provides sulfur); 2) PCBP and its role in ferritin associated iron storage.

(Isd11) that works in complex with Nfs1, a ferredoxin (Yah1) working with a ferredoxin reductase (Arh1) to provide electrons for the reaction, and the putative iron chaperone protein frataxin (Yfh1) (11). Protein orthologs are highly conserved and found in all eukaryotes, while in prokaryotes most are found within the ISC pathway while variants of these proteins exist within the sulfur mobilization (SUF) and the nitrogen fixation (NIF) assembly pathways (12). Isu1

is one of the most conserved proteins (13-14), containing three conserved cysteines critical for *de novo* Fe-S cluster assembly (15-16). Sulfur transfer between Nfs1 and Isu1 occurs as a persulfide (-SSH) through a direct interaction between partners (17); insight into the nature of this interaction has come from a recent structural characterization of bacterial orthologs (18). *In vivo*, Yfh1 is essential for Fe-S cluster maturation (19), and an interaction between Yfh1 and Isu1/Nfs1/Isd11 is critical for cluster biosynthesis (20). *In vitro*, frataxin was shown to deliver iron to the scaffold protein to stimulate Fe-S cluster assembly (21). Based on these and additional reports (see review (11)), frataxin was shown to play a direct role in mitochondrial Fe-S cluster assembly, possibly by serving as the iron chaperone(20, 22), deficiency of which has direct consequences regarding cellular oxidative stress (23).

Insight into frataxin's function has come from investigating the structure and iron binding abilities of numerous orthologs (24). Frataxin is a member of the $\alpha\beta$ sandwich motif family, with N- and C-terminal helices constructing one molecular plane and the second constructed by at least five anti-parallel β -strands (25-30). Key structural features for the frataxin orthologs include highly conserved, surface exposed acidic residues lining the helix-1/strand-1 junction, a short predominately unstructured N-terminal region in eukaryotic orthologs only, and a C-terminal region in the human and bacterial proteins that confers stability (31). The iron binding ability of frataxin was first identified in the yeast ortholog associated with iron-induced aggregation stabilized by low salt/high oxygen solution conditions (32). Monomeric bacterial, yeast, fly and human frataxin have

since been shown to bind iron with micromolar affinity (21, 28, 33-36), and *in vivo* mutations preventing Yfh1 aggregation show no Fe-S cluster phenotypes under normal growth conditions (37), indicating while protein aggregation may be important under oxidative stress, monomeric frataxin is active during Fe-S cluster assembly. Experimental data verify conserved acidic residues on frataxin's helix-1/strand-1 junction are directly involved in iron binding (28, 33, 35). Structural studies confirm that monomeric frataxin binds high spin Fe^{2+} in a symmetric 6-coordinate ligand environment containing only oxygen and nitrogen ligands, in agreement with the conserved acidic residues identified by NMR as iron ligands (35-36, 38). These data suggest as a starting point for iron delivery, frataxin binds iron using carboxylate side chain oxygens from conserved Asp and Glu residues from the helix-1/strand-1 iron binding sites, most likely with assistance from water molecules. Binding in this manner would predispose iron for delivery to Isu1 (Figure 1.2) since the exposed metal would be positioned for delivery to the protein partner and the charged surface surrounding the metal would be amenable for forming an interaction with a complementary charged region of the protein partner.

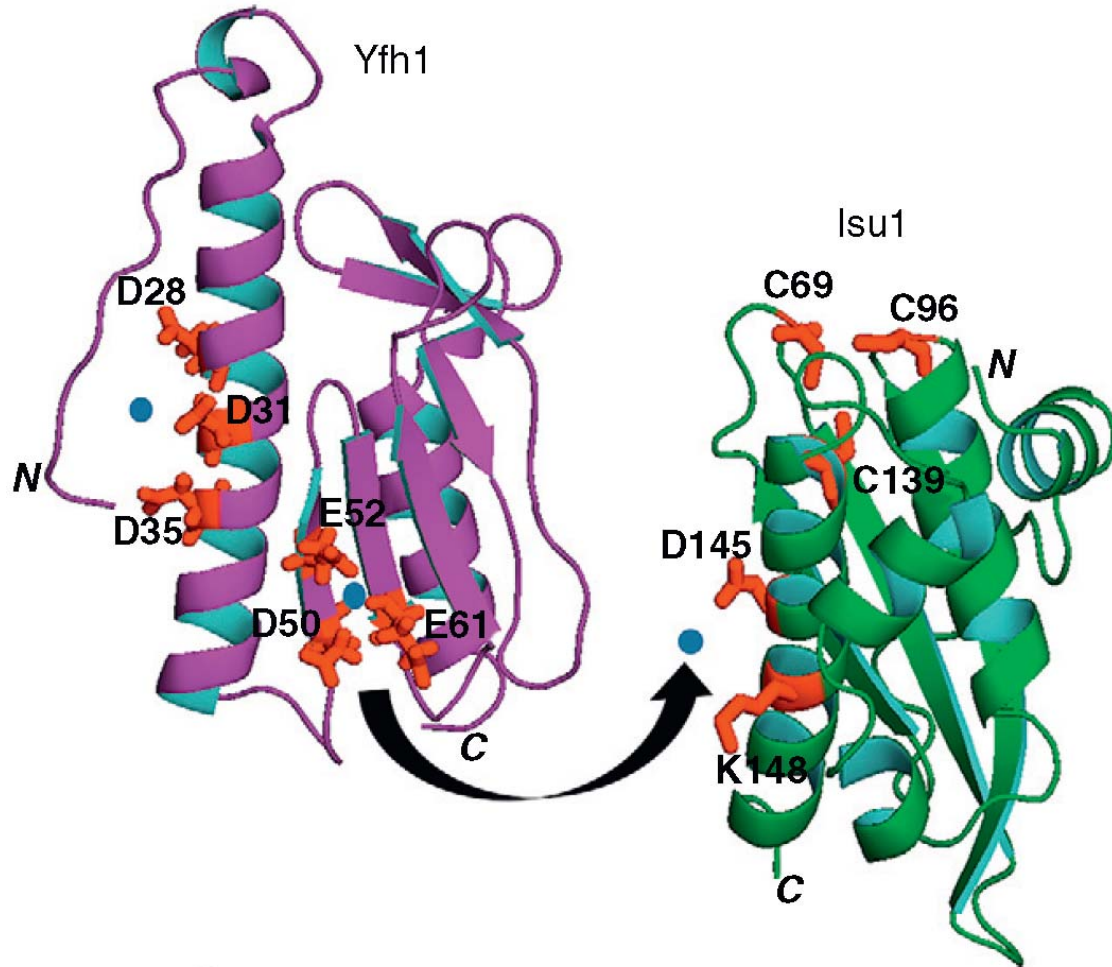


Figure 1.2. Molecular details of the 2 Fe^{2+} binding sites on Yfh1 (PDB #2GA5), and the Cys rich active site on Isu1 (modeled structure) coupled with possible Isu1 Fe^{2+} binding sites on the protein's C-terminus. Ferrous iron (blue dots) shown with arrow denoting Fe transfer events between the two proteins.

Yfh1 undergoes an iron-stimulated interaction with Isu1/Nfs1 (20, 39-40) in agreement with frataxin interacting directly with members of the ISC assembly machinery. *In vivo* mutational studies place frataxin's acidic helix-1/strand-1 ridge, with residues on the Yfh1 β -sheet surface, as interacting with Isu1 (39-43). *In vitro* binding interactions show frataxin/scaffold binding is iron dependent and occurs at nM binding affinity (36, 44-45). Chemical shift mapping studies provide spectroscopic confirmation that Isu1 interacts with Yfh1 on frataxin's acidic helix-1/strand-1 ridge utilizing the protein's β -sheet surface, in close agreement with *in vivo* mutational analysis (45). In eukaryotic systems, activity assays for Fe-S cluster production confirm iron loaded frataxin stimulates *in vitro* Fe-S cluster assembly, possibly by delivering the Fe^{2+} required for cluster production (21, 36, 46). Direct structural details of the frataxin/scaffold interaction are however lacking. Two recent structural papers shed light on the potential binding interaction between these protein partners. Crystallographic data on the *Aquifex aeolicus* IscU ortholog, with cluster bound, confirm the three conserved Cys residues implicated in assembly form the active site of IscU (47). An even more exciting result comes from the structure of the bacterial cysteine desulfurase (IscS) in complex with IscU (18). This structure shows IscU binds to IscS such that the IscU Cys active site is in close contact with the IscS Cys residue implicated in forming the persulfide used for sulfur transfer. Binding of Isu1 to Nfs1 in this manner would prevent frataxin from interacting in this region, assuming sulfur delivery happens before iron delivery. Irrespective of this assumption, mounting evidence suggests all proteins in the ISC machinery form

a complex that promotes the formation of a stable macromolecular complex used to accomplish cluster assembly, so the frataxin piece of this puzzle would need to fit in a unique location on Isu1. A likely candidate for where Yfh1 could bind to Isu1 is on the scaffold protein's C-terminal helix (Figure 1.2) (45). The charge distribution from the electrostatic potential surface of Isu1 in this region matches nicely to the Yfh1 β -sheet surface. Conserved acidic/basic residues on Isu1's C-terminal helix could serve as the initial Fe^{2+} binding residues, metal could then translocate to the scaffold's active site (45). Positional orientation of bacterial frataxin on the IscS/U from small angle X-ray scattering studies (48) suggest that such an orientation may be possible, although this orientation is likely to be altered between the prokaryotic and eukaryotic orthologs since the accessory protein Isd11 found only in eukaryotes is likely also positioned in this region. Following Fe delivery to Isu1 by Yfh1, the binding energetics are reduced, frataxin dissociates from its partner and Isu1 is primed for delivery of the second Fe atom required to make a 2Fe-2S cluster.

Recently it has been suggested frataxin may participate in Fe-S cluster biosynthesis by regulating activity of the cysteine desulfurase. NMR mapping studies of bacterial frataxin (CyaY) onto the bacterial IscS suggest residues lining frataxin's β -sheet ridge tangential to the C-terminus of helix 1, with helix-1 residues, participate in IscS binding (49). Mutagenesis and binding studies implicate a region on one IscS monomer, in proximity to the persulfide site in the second molecule in the dimer, as the CyaY binding surface on IscS (18). Recent studies suggest CyaY acts as an iron-dependent inhibitor of cluster formation by

negatively regulating IscS activity (49). In contrast, another recent report suggests human frataxin acts as an allosteric activator of Nfs1 (50). Regardless, binding of frataxin to the ISC machinery is important during assembly and it will be interesting to see how this binding is finally correlated to iron delivery and assembly.

1.4 Ferritin iron chaperones

Cellular pathways directing iron storage are essential for preventing iron toxicity during overload and ensuring availability during deficiency. Storage is directed by the 4-helix bundle protein ferritin (51). Mammalian cytoplasmic ferritins exist as a 24 subunit multimer of 2 ferritin subunits: H chain (21,000 kDa), which controls the ferroxidase chemistry coupled to iron storage, and the L chain (19,000 kDa). Apo-ferritin H and L chains self-assemble to form a spherical protein shell that stores up to 4500 iron atoms as ferrihydrite within the central cavity. Iron storage involves two key steps: iron oxidation, leading to formation of a μ -oxo(hydroxo)-bridged di-Fe(III) intermediate, and mineralization, depositing the intermediate as inert ferrihydrite mineral. Ferrous iron is first delivered to a hydrophilic channel at three-fold symmetry sites on ferritin. H-chain surface exposed residues H118 (52) and C130 (53), with threefold channel funnel-like forming residues Asp131 and Glu134 (54), are used during iron import. Binding of an iron chaperone must therefore proceed through direct contact with ferritin's three-fold iron entry site (see Figure 1.3).

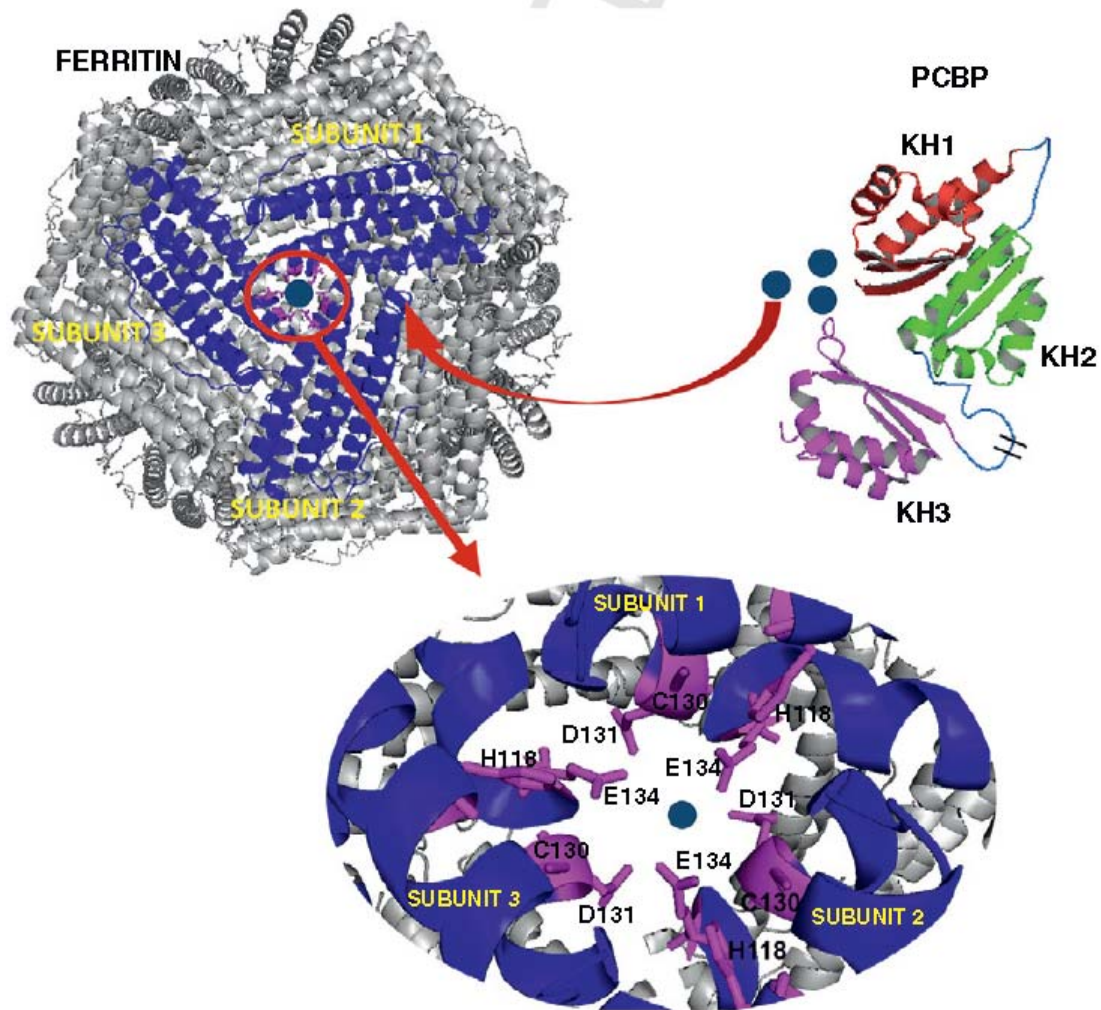


Figure 1.3. Structural details of PCBP's as a ferritin iron chaperone. Top Right: PCBP2 total projected structure based on domains 1,2 (PDB #2JZX) and domain 3 (PDB #2P2R) structure linked together for visual clarity associated with 3 bound iron atoms (blue dots). Top Left: structure of the human ferritin 24-mer (PDB #3AJ0) with iron loaded (blue dot) trimeric symmetry center. Bottom Left: expansion of the ferritin trimeric interface with residues from three subunits involved in Fe^{2+} loading (H118 and C130). In addition, residues (D131, E134) on the inner side of the iron incorporation gate that support metal exchange are also given.

Recently, the human poly (rC)-binding protein (PCBP) was shown to function as a cytosolic iron chaperone that delivers Fe^{2+} to ferritin (55). The RNA-binding PCBP protein family was originally shown to be important in mRNA stabilization and translational activation/silencing (56). PCBPs have 3 KH (hnRNP K homology) domains, with structures of the two N-terminal domains and the third domain of PCBP2 being characterized (57-58). Expression of human PCBP1 recovered an iron loading deficiency for human ferritin expressed in yeast (55). PCBP1 binds to ferritin *in vivo* and *in vitro* facilitates iron loading. PCBP1 binds 3 iron atoms at μM binding affinity comparable to frataxin's iron affinity (24). Metal binding sites on PCBP are unknown; however recent iron structural data indicate PCBP1/2 bind ferrous iron in a 6-coordinate oxygen/nitrogen ligand environment (author's unpublished results). Although molecular details of PCBP as an iron chaperone are still emerging, it is interesting to note that thermodynamic and structural data regarding PCBP iron binding are so similar to that of the Fe-S assembly iron chaperone.

1.5 Conclusions

Evidence that frataxin and PCBP are iron chaperones is compelling, although clarification of their function at the genetic, molecular and atomic levels will be important for understanding how they operate. There are still many questions that remain regarding the identity of other chaperones, how iron is loaded onto a chaperone and what promotes chaperone metal specificity? Possible candidates for the first question are the glutaredoxins Grx3 and 4, which are members of the thioredoxin (Trx) fold family. Grx3/4 are central for cellular

iron trafficking and a strong dependence of iron binding for Grx3/4 on core components in the ISC pathway indicate Grx3/4 bind iron as a Fe-S cluster (59). The ability to form a bridging 2Fe-2S cluster with Fra1/2 for activation of Aft1 (60), coupled with the direct dependence of Grx3/4 on iron loading into heme, Fe-S clusters, and ribonucleotide reductase, suggest iron activated by Grx3/4 may be utilized by other dedicated assembly factors (59). Frataxin and PCBP are most likely the forerunners of more iron chaperones that await discovery.

CHAPTER 2

Molecular Characteristics of the *Drosophila* Frataxin-Isu Interaction during Fe-S Cluster Assembly

2.1 Prelude

Conserved during evolution from prokaryotes to eukaryotes, Frataxin is a nuclear encoded protein targeted to mitochondria that contributes to the maintenance of cellular iron homeostasis. Frataxin is directly involved in the production of Fe-S clusters, which are essential cofactors for proteins in various pathways within the cell. Frataxin is reported to interact directly with other proteins partners in the Iron Sulfur Cluster (ISC) assembly pathway. In order to better understand how these proteins interact, we undertook a study of frataxin with binding partners using proteins in the *Drosophilla* system. My contribution related to this study was to study the interaction between two ISC-scaffold proteins (frataxin and Isu) in the absence of iron with the use of Isothermal Titration Calorimetry (ITC). In addition, I compared the sequence alignment of Frataxin orthologs from different species: bacteria, yeast, *drosophila* and human. The structural correlations I performed were done using ClustalW to show the protein conservation during evolution.

In detail, chapter 2 of this thesis studies molecular characterization of Dfh and DIsu during Fe-S cluster assembly pathway. This work is under preparation for publication. The manuscript in its near final format is listed under the following reference: Swati Rawat, Sudipa Ghimire-Rijal, Yogapriya Murugesan, Gregory Holmes-Hampton, Paul Lindahl and Timothy L. Stemmler, "Molecular

Characteristics of the Drosophila Frataxin-Isu Interaction during Fe-S Cluster Assembly," **2011**, *In preparation*.

2.2 Introduction

Frataxin, a nuclear encoded protein targeted to the mitochondria, is essential for cellular iron homeostasis as part of the mitochondrial iron-sulfur (Fe-S) cluster biosynthesis assembly pathway (19, 61-63). Frataxin deficiency in humans leads to the neurodegenerative disorder Friedreich's Ataxia (FRDA), which affects 1 in 50,000 (61, 64). The disorder is characterized by mitochondrial iron overload, a breakdown in the Fe-S cluster assembly pathway and a general disruption in iron regulation (62, 65). Although numerous roles have been attributed to frataxin, a direct function during mitochondrial Fe-S cluster assembly seems the most likely (21, 36). Recent data suggest frataxin directly participates in Fe-cofactor assembly by possibly serving either as a mitochondrial iron chaperone, supplying the iron required for cluster assembly, or as a regulator for the enzymatic activity of assembly protein partners (49, 66).

In eukaryotes, the major pathway for production of Fe-S clusters is localized within the mitochondria and controlled by the eukaryotic ISC assembly pathway. The ISC machinery in eukaryotes/prokaryotes is constructed of a scaffold assembly protein (Isu/IscU, respectively), a cysteine desulfurase (Nfs/IscS), an accessory protein (Isd11) found in eukaryotes only, and the protein frataxin (20, 67-69). Frataxin has been shown to interact directly with Isu, Nfs and Isd11 individually and within a multiprotein complex in vivo (20, 40, 43, 70). In vitro, frataxin has been shown to both stimulate Isu1 activity and to positively and

negatively regulate Nfs1 activity by interacting directly with the protein partner (49, 66). Frataxin is an iron binding protein and the binding interaction between frataxin and Isu is metal dependent (28, 35, 70-71), suggesting metal sharing is a key component in assembly activity, however the interaction between the bacterial frataxin (CyaY) and cysteine desulfurase (IscS) is metal independent (49, 72), suggesting regulation of the cysteine desulfurase by frataxin is an elastic event. Modelling studies, based on experimental data suggesting frataxin binds to the scaffold/desulfurase complex at the IscS dimer interface cleft with IscU attached (18, 70), was recently confirmed by reconstructions of the X-ray scattering data (72). Combined, these data indicate a direct influence of frataxin on Fe-S cluster assembly by interaction with the multi-protein ISC machinery.

Investigation of frataxin's interaction with each protein in the machinery is essential for understanding the molecular contacts that drive frataxin's participation within the pathway. Genetic and structural studies of frataxin alone show the protein is highly conserved in evolution and has an α - β sandwich architecture (Figure 2.1). Frataxin binds iron at micromolar affinity utilizing key conserved acidic residue side chains on the protein's helix-1/strand-1 ridge (35-36, 71). Iron is bound anaerobically as high spin ferrous metal in a symmetric 6-coordinate ligand environment constructed of only oxygen and nitrogen based ligands (36, 70). Iron loaded frataxin binds to Isu with nanomolar affinity utilizing conserved residues on the protein's β -sheet plane, with support from helix-1 residues (70). When sulfur is supplied chemically to the frataxin/Isu/Fe system, a high percentage of bound iron is converted into a functional 2Fe-2S cluster that

has been confirmed structurally and spectroscopically (36, 70). These data strongly support a direct interaction of frataxin to Isu in a manner highly consistent with frataxin serving as an iron chaperone for the pathway.

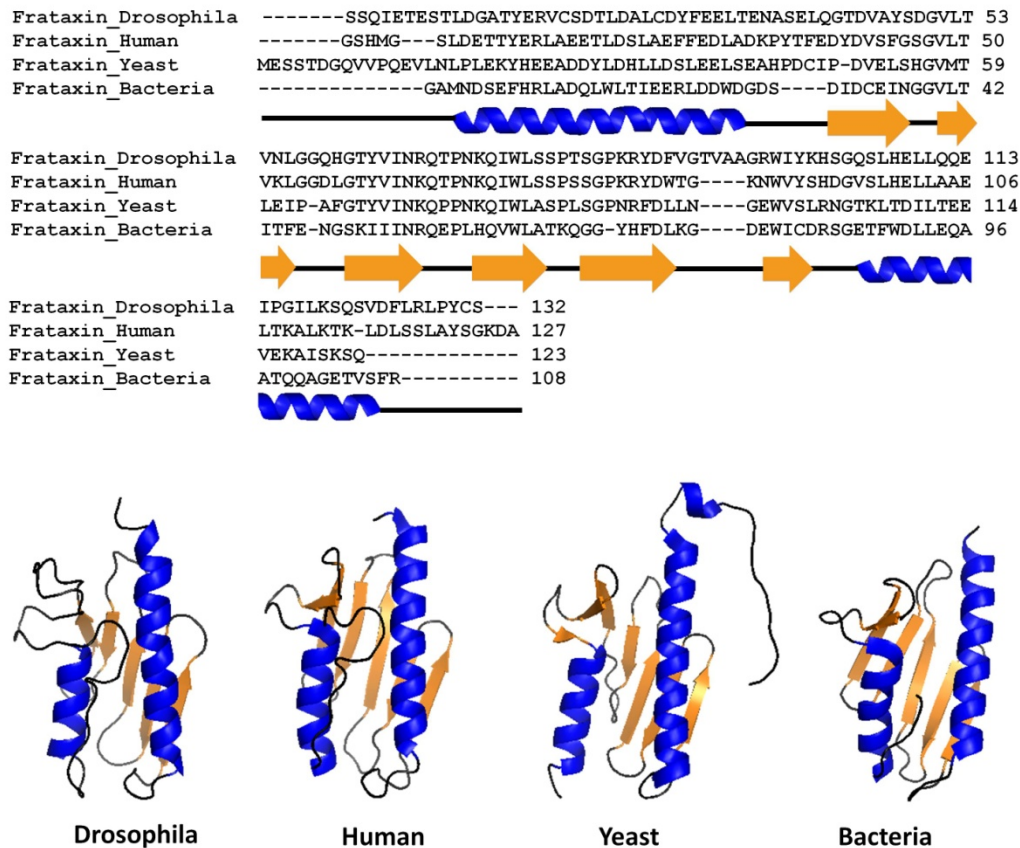


Figure 2.1. Top: ClustalW alignment for Drosophila, Human, Yeast and Bacterial frataxin orthologs. Bottom three sequences represent structurally characterized frataxin orthologs. Secondary structural elements (α -helix in blue and β -sheets in yellow) are given below the sequences. Bottom: Ribbon diagrams for Drosophila, Human, Yeast and Bacterial frataxins. Structural figures were made using crystal structure of Human (PDB ID# 1EKG) while solution structures of Yeast (PDB ID# 2GA5) and Bacterial (PDB ID# 1SOY) frataxins using PYMOL software. The structure of Drosophila frataxin was simulated using Swiss-Prot server with human frataxin as template.

In this report, we utilized proteins in the fly model system to further elucidate the molecular details of how frataxin interacts with the scaffold protein. Our recent characterization studies of *Drosophila* frataxin (Dfh) show the protein is highly stable against degradation/aggregation seen with the human and yeast model systems, and the stability of the fly orthologs is shared with the other proteins in the ISC machinery. Isothermal titration calorimetry (ITC) was used to characterize the binding affinity and stoichiometry between Dlsu and iron, and Dlsu and Dfh in the presence and absence of metal. Frataxin's ability to stimulate 2Fe-2S cluster assembly on the scaffold protein was tested using a previously established activity assay. X-ray absorption spectroscopy was used to characterize the metal spin state and the electronic properties, and the structure of iron bound to Dlsu alone and in the Dlsu ± Fe-Dfh complex in the presence and absence of chemical sulfide. Metal speciation and additional characterization of the iron electronic environments of metal bound to Dfh were characterized by Mössbauer spectroscopy. Finally, the influence of cluster assembly on the Dlsu fold was tested using fluorescence spectroscopy. Combined these data provide structural and mechanistic insight into the frataxin-scaffold interaction that assists in driving the mitochondrial Fe-S cofactor production pathway.

2.3 Materials and Methods

2.3.1 Cloning, Expression, and Protein Purification

The plasmid for expression of mature Dfh (minus 59 amino terminal residues) and protein purification has been described previously (36). Dlsu cDNA was obtained, prepared from the adult head tissue in a pOT2 vector, from the

“Drosophila Genomics Resource Center” (Clone ID: GH01635). DIsu cDNA was PCR amplified and sub-cloned into the directional pET151/D-TOPO expression vector. The sequence represents DIsu residues 25-154 of the complete open reading frame after excluding the predicted mitochondrial targeting sequence but including an N-terminal methionine. Positive clones were verified by DNA sequencing. Recombinant plasmid was transformed into BL21 (DE3) “codon plus” *E. coli* competent cells for protein expression. Expression was optimized by varying induction temperatures and IPTG concentrations. Expression and the stepwise purification of the 130 amino acid DIsu protein closely followed our protocol outlined for the yeast ortholog (36, 70). Briefly, the plasmid was transformed into BL21(DE3) CodonPlus cells and grown by auto induction (73) at 25°C for ca. 24 hrs before harvesting by centrifugation. Protein isolation steps were all performed at 4° C. Cells were resuspended in 50 mM NaPO₄ (pH 7.5), 300 mM NaCl, 20 mM Imidazole and 5 mM β-Me in the presence of Complete EDTA free Protease inhibitor cocktail (Roche). Cells were then lysed by two passes through a French Press cell at high pressure (1100 psi), followed by 2 rounds of sonication (50% power for 20 seconds) and finally centrifuged at high speed (21000 rpm) for 1 hour. Crude soluble fraction was filtered (0.20 μm) and loaded onto a HisPrep FF Ni column (Pharmacia) using an Imidazole gradient in the range of 20 – 500 mM (DIsu protein elutes at ~ 150 mM). DIsu containing fractions were pooled and concentrated to ca. 1mL by centrifugation using 10 kDa cutoff centricons (Millipore) spun at 5000 rpm. The concentrated retentive solution was run over a Sephadex 75 size exclusion column (Pharmacia)

equilibrated with 20 mM HEPES buffer (pH 7.5), 150 mM NaCl and 5 mM β -Me. Following this protocol, we were able to attain high purity DIsu based on gel analysis. Mass spectrometric analysis of DIsu indicated a molecular weight of 18508.4 Da (theoretical molecular weight is 18511.2 Da). Like Dfh, DIsu was very stable against degradation. Protein could be concentrated up to 27 mg/L and stored anaerobically at -20° C and -80° C, retaining complete activity as judged by our Fe-S cluster activity assay, for multiple weeks.

2.3.2 Isothermal Titration Calorimetry (ITC) Binding Studies

The binding affinity and stoichiometry were characterized for the interaction between ferrous iron \pm Dfh and DIsu using ITC. DIsu, Dfh and ferrous ammonium sulfate solutions were prepared anaerobically in 20 mM HEPES (pH 7.5) with 150 mM NaCl. All experiments were conducted anaerobically at 30°C. The Fe into DIsu ITC experiments were conducted using a VP-ITC titration microcalorimeter (MicroCal, Inc.) by titrating a 2.1 mM ferrous iron solution into a 1.4 mL volume of a 90 μ M DIsu solution; Dfh into DIsu experiments were performed by titrating a 0.9 mM solution of either apo- or holo-Dfh into a 70 μ M solution of apo-DIsu. Following an initial 2 μ L titrant solution injection, 29 additional injections of 10 μ L each were titrated into the DIsu solution. The period between injections was 10 min, and the syringe stirring speed was held constant at 500 rpm. All experiments were conducted in duplicate on independent protein and iron samples to ensure data reproducibility. Data analysis was performed utilizing the Origin 5.0 Scientific Graphing and Analysis Software (provided by MicroCal) by applying a nonlinear least-squares curve-fitting algorithm to

determine the stoichiometric ratio and dissociation constant during the reaction.

2.3.3 Fe-S Cluster Assembly Activity Assay

The *in vitro* DIsu Fe-S cluster assembly activity was measured for chemically and DFh assisted delivery of ferrous iron using a previously established activity assay. All protein and substrate samples were made anaerobic on an Schlenk line and stored under positive argon pressure. ApoDfh was incubated with ferrous ammonium sulfate at a metal:protein ratio of 1:1 for 20 min at 30° C. Cluster assembly was initiated by addition of ferrous iron directly, or as part of the HoloDfh complex, to a 500 μ L solution containing 100 μ M DIsu, 4.3 mM DTT, and 2.4 mM sodium sulfide. The final Fe concentration was 100 μ M and all samples were buffered in 20 mM HEPES and 150 mM NaCl (pH 7.5). Controls with DIsu or Dfh alone and with DIsu or Dfh, DTT, and sodium sulfide were prepared under the solution conditions listed above. Fe-S cluster assembly was monitored by UV-visible absorption spectroscopy. Absorption spectra between 200 and 600 nm were recorded. A time course for the reaction progress was prepared by spectral detection every 30 s using the spectral wavelength of 426 nm (a chromophore characteristic for [2Fe-2S] clusters). Assembly data were collected in independent reproducible samples to obtain data statistics.

2.3.4 X-ray Absorption Spectroscopy (XAS)

XAS was used to study the electronic properties and ligand coordination geometry of iron at different stages during Fe-S cluster assembly. All samples

were prepared anaerobically within a glove box (PlasLabs) using protein and iron solutions initially degassed on a Schlenk line and stored under an Ar(g) atmosphere. XAS samples were prepared in 20 mM HEPES buffer (pH 7.5), 150 mM NaCl, 5 mM β -Me and 30% glycerol. Independent duplicate samples were prepared for the following systems: A) Fe-Dlsu was prepared by incubating Dlsu with 0.95 equivalent of ferrous iron, B) Fe-Dfh prepared by incubating 0.95 equivalents of ferrous iron for 10 minutes, C) Fe-Dfh+Dlsu was prepared by first incubating Dfh with 0.95 equivalent of ferrous iron for 10 minutes at room temperature, then adding 1 equivalent of Dlsu and D) Fe-Dfh+Dlsu+S was prepared by first incubating Dfh with 0.95 equivalent of iron for 10 minutes at room temperature, then adding stoichiometric equivalents of Dlsu and Na₂S. All samples were allowed to incubate for an additional 60 minutes in an Ar(g) atmosphere to ensure cluster and complex formation. Samples were loaded into Lucite sample cells wrapped with Kapton tape, flash frozen in liquid nitrogen, removed from the glove box and stored in liquid nitrogen until data collection was performed.

XAS data were collected at the Stanford Synchrotron Radiation Laboratory (SSRL) on beamline 7-3, which is equipped with a single rhodium-coated silicon mirror and a Si [220] double crystal monochromator. Harmonic rejection was achieved by detuning the monochromator 50%. Samples were maintained at 10 K using Oxford Instrument continuous-flow liquid helium cryostat. Protein fluorescence excitation spectra were collected using a 30-element Ge solid-state array detector. XAS spectra were measured using 5 eV steps in the pre-edge

regions (6900 - 7094), 0.25 eV steps in the edge regions (7095-7135 eV) and 0.05 Å⁻¹ increments in the extended X-ray absorption fine structure (EXAFS) region (to k = 13.5 Å⁻¹), integrating from 1 to 20 seconds in a k³ weighted manner for a total scan length of approximately 40 minutes. X-ray energies were calibrated by collecting an iron foil absorption spectrum simultaneously with protein data. Each fluorescence channel of each scan was examined for spectral anomalies prior to averaging and spectra were closely monitored for photoreduction. Protein data represents the average of 5 to 6 scans.

XAS data were processed using the Macintosh OS X version of the EXAMSPAK program suite (74), integrated with Feff version 7.2 for theoretical model generation. Data reduction and processing followed previously established protocols. Analysis of the X-ray absorption near edge structure (XANES) 1s→3d transitions were completed using the EDGE_FIT EXAFSPAK subroutine. EXAFS fitting analysis was performed on raw/unfiltered data following a previously established strategy (35). EXAFS data were fit using both single- and multiple-scattering theoretical model amplitude and phase functions for an Fe-O/N, Fe-S, Fe•••Fe and a Fe-imidazole unit interactions. During spectral simulations, metal-ligand coordination numbers were fixed at half-integer values and only the absorber-scatterer bond length (R) and Debye-Waller factor (σ^2) were allowed to freely vary (75).

2.3.5 Mössbauer Spectroscopy

Mössbauer spectroscopy was used to characterize the speciation and electronic properties of iron bound to Dfh. A sample of Fe⁵⁷ loaded Dfh, 1.8 mM

in concentration, was prepared anaerobically in 20 mM HEPES buffer (pH 7.5) and 150 mM NaCl by first dissolving iron metal in a 1:1 mixture of HCl and HNO₃, diluting the metal with water to a final iron concentration of 80 mM ([HCl] – 120 mM, [HNO₃] – 150 mM). An aliquot of the 80 mM Fe stock solution was removed and reacted with a 1:1 molar ratio of sodium dithionite and added to the protein sample for a final iron concentration of 1.7 mM. The Fe-Dfh sample was then incubated anaerobically for 30 minutes and frozen in Mössbauer sample cups cooled using an aluminium block pre-cooled with liquid nitrogen. All samples were stored under liquid nitrogen until the spectra were collected.

Mössbauer spectra were collected using a MS4 WRC model spectrometer (SEE Co., Edina, MN) equipped with a CCR4K closed cycle helium compressor (Sumitomo Cryogenetics). Spectra were analyzed using the WMOSS software package (SEE Co., Edina, MN). All values for the isomer shift and quadrupole splitting were reported relative to the alpha Fe foil at a temperature of 298 K.

2.3.6 Fluorescence Spectroscopy

Changes in structural characteristics of DIsu in the presence of substrates were monitored using fluorescence spectroscopy. The fluorescent dye 1,8-Anilinonaphthalenesulfonate (ANS), which selectively binds to solvent exposed hydrophobic regions in molten globular proteins (70, 76) was used to probe structure changes on DIsu in the presence and absence of Fe alone, S alone and Fe + S combined. ANS studies were performed using a 3 mL fluorescence cuvette (Starna), equipped with septa, containing a 50 µM DIsu solution in 20 mM HEPES buffer (pH 7.5), 150 mM NaCl. All buffers, samples and the cuvette

were initially degassed using an Ar(g) purged Schlenk line. DIsu samples were prepared in the presence and absence of ferrous iron and sulfide independently and then as a mixture. Single time point fluorescence measurements were made for the protein samples first incubated for 10 minutes, followed by incubation for 10 minutes with 10 μ M ANS ($\lambda_{\text{excite}} = 371 \text{ nm}$, $\lambda_{\text{emission}} = 490 \text{ nm}$). Spectra were collected at room temperature on a QuantaMaster fluorimeter (PTI) at 1 nm intervals with 0.25 second integration times and 5 mm slit widths. Spectra were collected on independent reproducible sample sets.

2.4 Results

2.4.1 Isothermal Titration Calorimetry (ITC) Binding Studies

ITC was used to measure the metal to protein stoichiometry and energetics for association of iron binding to DIsu. Ferrous iron was titrated into apo-DIsu anaerobically under buffer conditions that stabilize the protein (20 mM HEPES, pH=7.5, 150 mM NaCl). Changes in heat associated with iron binding by DIsu are shown in the raw ITC data in Figure 2A (top), with the data following an exothermic iron-binding event. The heat released vs. the molar ratio plot follows biphasic behaviour common to systems with two binding events (Figure 2.2A (bottom)). The best fit simulation to the molar ratio plot was obtained using a two iron binding site model, with ca. 2 iron atoms binding at $475 \pm 166 \text{ nM}$ and $64.5 \pm 17 \text{ nM}$ affinities (Table 2.1).

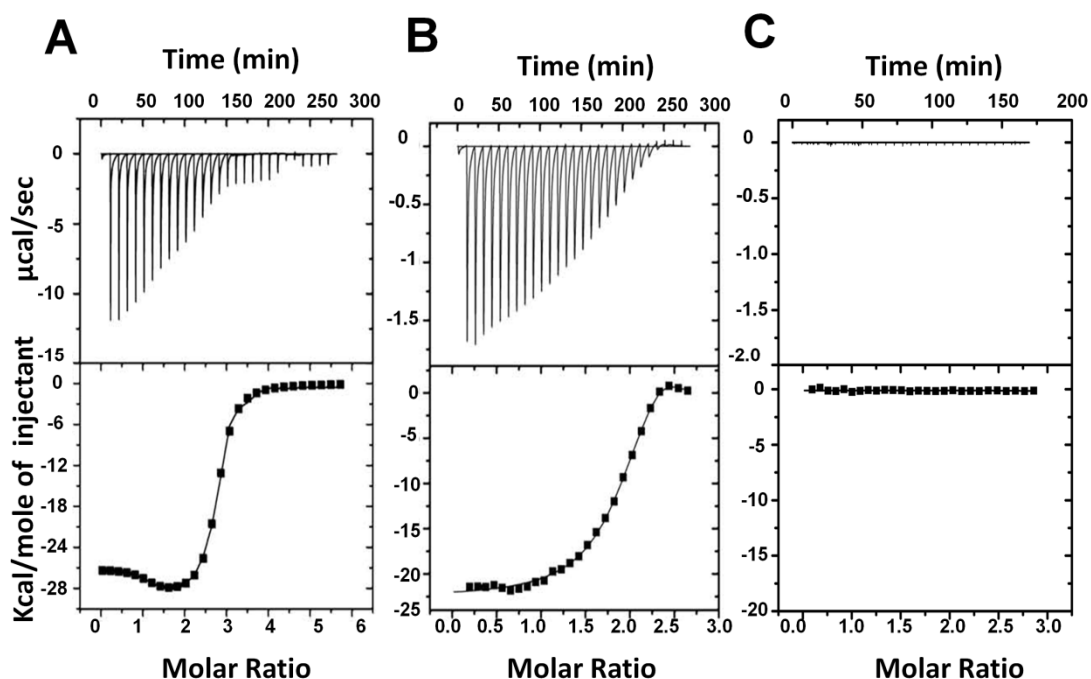


Figure 2.2. Raw isothermal titration calorimetry data (top) and binding isotherm data (bottom) of: A) Fe(II) titration into Dlsu, B) Fe-Dfh titrated into Dlsu and C) Dfh titrated into Dlsu. A grey line in each bottom panel shows the simulated fit to the binding isotherm data. Data were collected anaerobically at 30 C in 20 mM HEPES (pH 7.5) and 150 mM NaCl.

Table 2.1. Average ITC simulation results. Averaged values for stoichiometry (N_1 and N_2) and dissociation constants (K_{D1} and K_{D2}) are provided with error bars.

Sample	N_1	K_{D1}	N_2	K_{D2}
Fe - Dlsu	1.21 ± 0.25	475 ± 166 nM	1.40 ± 0.07	64.5 ± 17 nM
Fe-Dfh + Dlsu	1.72 ± 0.30	530 ± 43.5 nM	0.41 ± 0.22	673 ± 22 nM
Dfh + Dlsu	---	---	---	---

ITC was also used to test the metal dependence as well as binding affinity and stoichiometry of Dfh binding to Dlsu. Experiments were performed under

conditions that stabilize HoloDFh as a protein monomer. In the presence of metal, Dfh binds to DIsu in an exothermic manner (Figure 2.2B (top)). The best-fit simulation of the molar ratio data suggests ca. 2 equivalents of monomeric HoloDFh binds to ApoDIsu with an affinity in the nanomolar range ($K_{D1} = 530 \pm 43.5$ nM and $K_{D2} = 673 \pm 22$ nM) (Table 2.1). However, no appreciable heat is absorbed or released then titrating ApoDfh into ApoDIsu (Figure 2.2C - top).

2.4.2 X-ray Absorption Spectroscopy (XAS)

XAS was used to characterize the electronic and structural properties of iron bound to DIsu at various stages during Fe-S cofactor production. Samples were prepared for: DIsu + iron, Fe-Dfh + DIsu, and Fe-Dfh + DIsu + sulfide. XANES spectra, with an expansion of the pre-edge $1s \rightarrow 3d$ transition features, were offset for clarity and given for each sample in Figure 2.3 and Figure 2.3 (inset), respectively. Pre-edge transition analysis (including pre-edge peak energies and absorption area) were determined for all samples based on simulation analysis, and simulation parameters were most consistent with Fe(II) bound to DIsu, Dfh and Dfh/DIsu alone existing in a high spin, fairly octahedral six coordinate ligand coordination geometry (Table 2.2). In the Fe-Dfh/DIsu/sulfide sample, edge energies and high pre-edge area are most consistent with a portion of the metal existing in a four coordinate tetrahedral ligand coordination geometry consistent with a 2Fe-2S cluster.

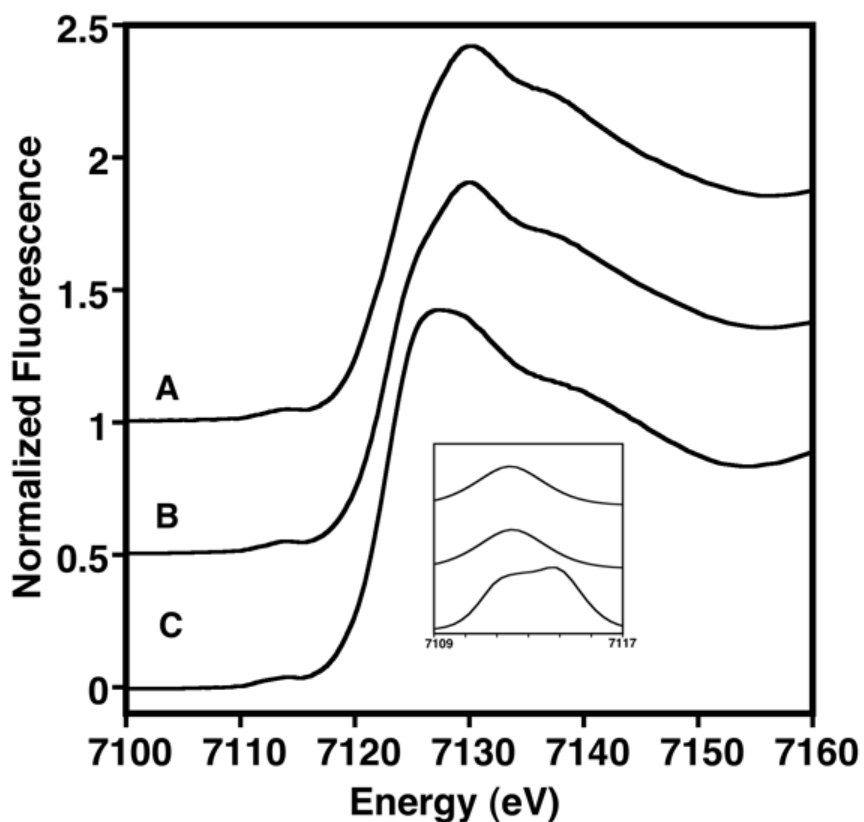


Figure 2.3. XANES spectra of Fe bound in the following sample: A) Fe-Disu, B) Fe-Dfh + Disu and C) Fe-Dfh + S^{2-} + Disu. Individual spectra were equally offset for clarity. Inset: Expansion of the individual $1s \rightarrow 3d$ transition peaks in the same order as listed in the full figure.

Simulations of the EXAFS portion of each XAS spectrum was used to characterize the metal-ligand metrical parameters for iron bound in each sample (Figure 2.4 A,C,E and G). The single pronounced feature in the Fourier transform of the Fe-Disu EXAFS indicates metal is bound in a fairly symmetric ligand environment centered at ca. 2 Å (Figure 2.4B). EXAFS simulations show ferrous iron bound to Disu is stable in a symmetric metal-ligand nearest neighbour coordination environment constructed only by oxygen and nitrogen based ligands (Table 2.3) at average bond lengths of 1.99 Å (coordination number (CN) of 3.0 ± 1.0) and 2.15 Å (CN of 2.0 ± 1.0), respectively. A similar environment is

observed in the Fourier transform of Fe-Dfh (Figure 2.4D). Simulations of the Fe-Dfh EXAFS shows nearest neighbour coordination geometry again constructed of only oxygen and nitrogen based ligands, at average bond lengths of 1.99 and 2.15 respectively.

Table 2.2. Analysis of pre-edge and edge features from Fe-XANES spectra displayed in Figure 2.3. Pre-edge transition energies and areas determined using EDG_FIT software.

Sample	Pre-edge peak energy (eV)	Total pre-edge area	Edge inflection energy (eV)
Fe-Dlsu	7112.41 ± 0.12	3.91 ± 0.5	7122.45 ± 0.1
	7113.78 ± 0.14		
Fe-Dfh + Dlsu	7112.49 ± 0.24	4.01 ± 2.0	7122.48 ± 0.3
	7113.81 ± 0.13		
Fe-Dfh + Dlsu + S	7111.99 ± 0.03	8.01 ± 5.0	7122.66 ± 0.5
	7112.79 ± 0.05		
	7113.95 ± 0.15		

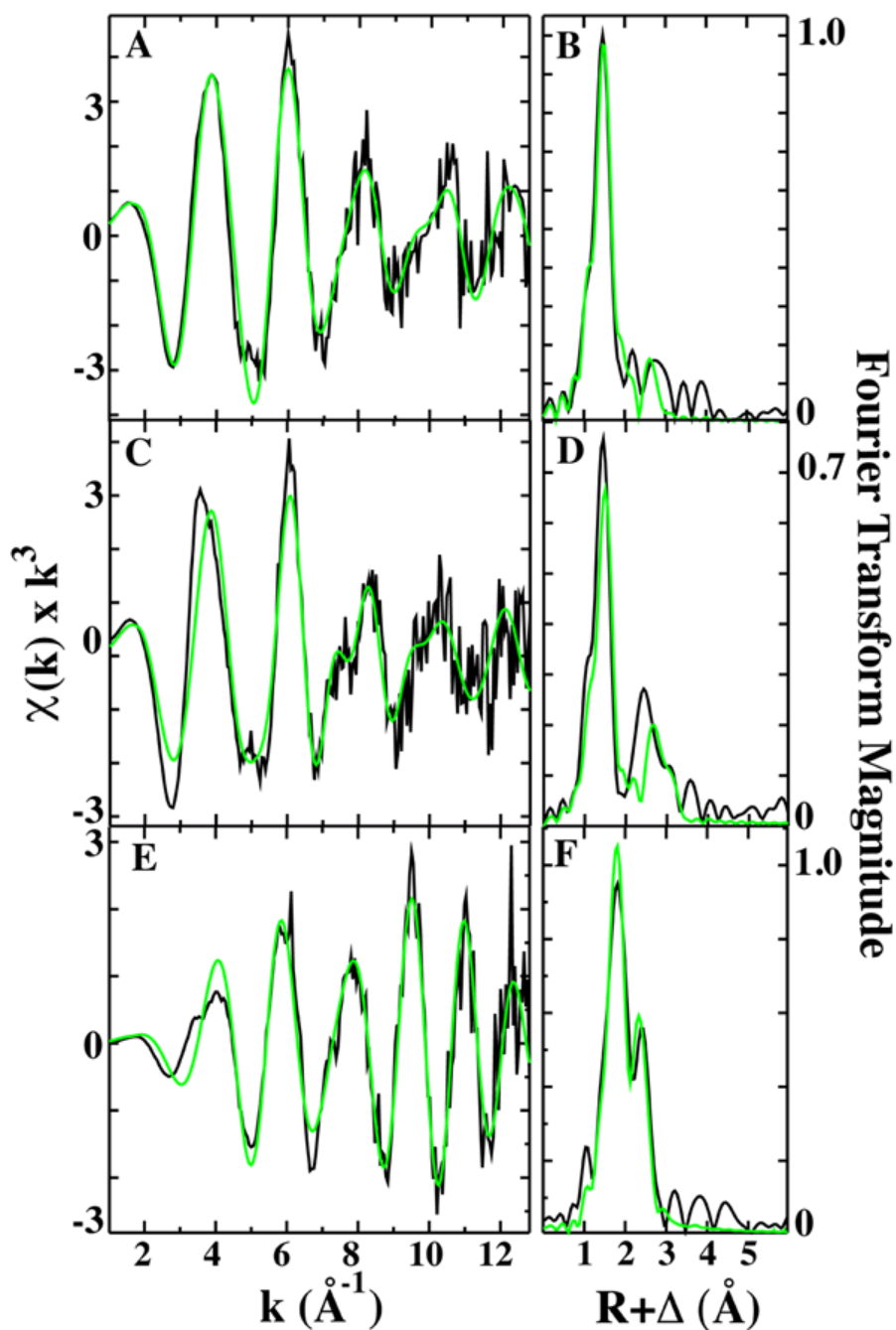


Figure 2.4. EXAFS and Fourier transforms of iron bound to the proteins at various stages during the Fe-S cofactor production. Raw EXAFS data is shown in black with simulated fit in green for: A) Fe-Dlsu, C) Fe-Dfh + Dlsu and E) Fe-Dfh + S^{2-} + Dlsu. Corresponding fourier transform plots of raw EXAFS data in black for: B) Fe-Dlsu, D) Fe-Dfh + Dlsu and F) Fe-Dfh + S^{2-} + Dlsu.

Table 2.3. Summary of best fit EXAFS simulation results for iron at various stages during cofactor formation. Values reported are the average of at least two independent measurements.

Sample	Fe-Nearest Neighbor Ligands ^a				Fe•••Long Range Ligands ^a				F' ^f
	Atom ^b	R(Å) _c	C.N. _d	□ ^{2 e}	Atom ^b	R(Å) _c	C.N. _d	□ ^{2 e}	
Fe - Dlsu	O/N	1.99	3.0	3.78	C	3.13	1.5	3.01	0.32
	O/N	2.15	2.0	2.94					
Fe-Dfh + Dlsu	O/N	1.99	2.0	3.93	C	3.1	2.0	4.32	0.41
	O/N	2.15	1.5	4.27	C	3.51	1.5	3.81	
Fe-Dfh + S + Dlsu	O/N	2.06	1.0	1.07	Fe	2.73	0.5	1.40	0.69
	S	2.28	1.0	1.57					

^a Independent metal-ligand scattering environment

^b Scattering atoms: O (Oxygen), N (Nitrogen), C (Carbon), S (Sulfur) and Fe (Iron)

^c Metal-ligand bond length

^d Metal-ligand coordination number

^e Debye-Waller factor given in Å² x 10³

^f Number of degrees of freedom weighted mean square deviation between data and fit

When Fe-Dfh is added to Dlsu, the average metal ligand nearest neighbour coordination geometry is very similar to that observed in the Fe-Dlsu sample, with only slight variations in the Debye-Waller values (a measure of the metal-ligand bond order), suggesting a dramatic decrease in bond symmetry. Reduction in bond symmetry for Fe-Dfh + Dlsu is further indicated by the unrealistically low CN values obtained for the two independent ligand systems. These ligand systems that have bond lengths (and pre-edge features) consistent

with a 6-coordinate Fe-O/N ligand system, however the low coordination number values suggest a destructive overlap between unique but irresolvable multiple independent metal-ligand systems. In all three cases, long range carbon scattering is observed at ca. 3.1 Å. In the case of the Fe-Dfh/Dlsu sample, an additional ligand environment at 3.51 Å was also observed and the long range scattering for this sample was much more pronounced than the other two. The long range scattering in all samples could not however be fit with any appreciable Fe•••Fe scattering.

Addition of sulfide to the Fe-Dfh/Dlsu system causes a dramatic distortion in the metal-ligand coordination environment compared to the other samples. Fourier transforms of the EXAFS data indicate a nearest-neighbor environment distinct from the other three samples with a well pronounced long range interaction at ca. 2.7 Å (Figure 2.4H). Simulations in the nearest neighbor EXAFS contribution indicate both Fe-ON and Fe-S scattering at averaged values of 2.06 Å and 2.28 Å, respectively. The low coordination numbers for each environment reflect again a highly disordered iron-ligand environment or possibly multiple unique environments with EXAFS that destructively interfere. In this sample only, long range Fe•••Fe scattering is observed at 2.7 Å. This data could not be fitted to long-range carbon scattering in the range of $R > 3.0$ Å.

2.4.3 Mössbauer Spectroscopy

Mössbauer spectroscopy was used to characterize the speciation and electronic environment of the iron bound to Dfh. Mössbauer spectroscopy can give very precise information about chemical, structural and magnetic properties

of bound metal. Figure 2.5 shows Mössbauer spectra of iron bound to Dfh at 5 K (A) and 100 K (B). The spectrum at 100 K looks like typical high-spin Fe (II) metal coordinated by weak field ligands, such as O/N atoms (Figure 2.5).

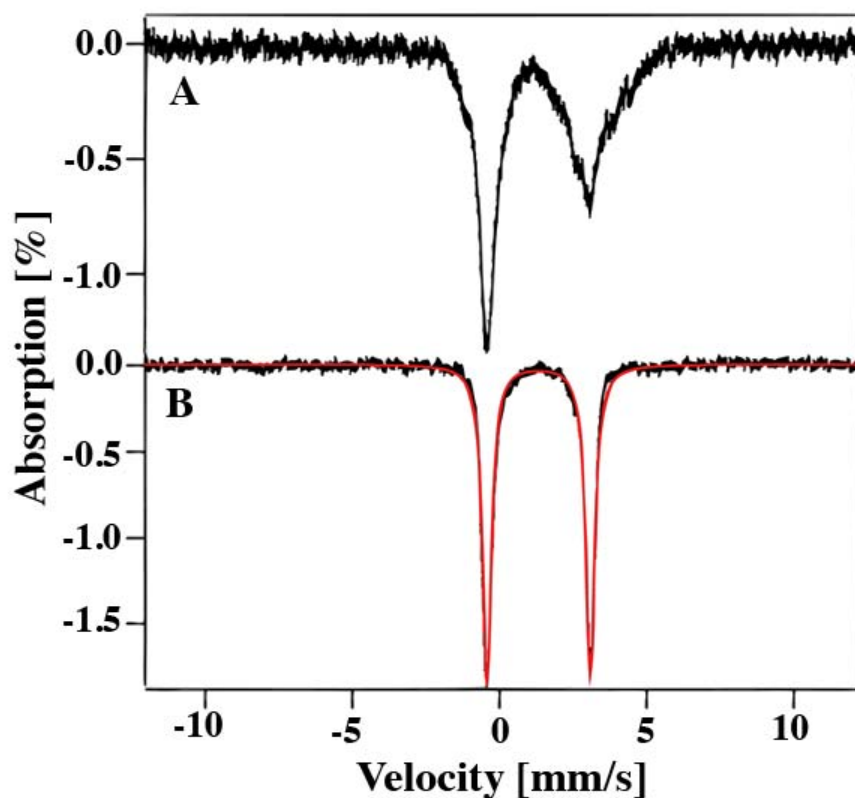


Figure 2.5. Drosophila Frataxin Homolog (Dfh) Mössbauer spectra collected with 0.7G field applied parallel to the sample. A) Spectrum at 5K and B) Spectrum at 100K. Red line is a simulation of the data using $\delta = 1.33$ mm/sec, $\Delta E_q = 3.51$ mm/sec, $\Gamma = 0.367$ mm/sec.

Simulations of these data show quadrupole splitting (ΔE_q) = 3.51 mm/s and an isomer shift (δ) = 1.33 mm/s; results were confirmed by running a ferrous control (Table 2.4). The 5K spectrum shows broadening of the high-energy line (magnetic hyperfine). This data further confirms our previous result that iron

bound to Dfh is high spin using only O/N based ligands. In a previous report, the mössbauer parameters for yeast frataxin (Yfh1) deficient mitochondria showed the presence of typical high-spin ferric iron bound to oxygen/nitrogen in an octahedral arrangement. No ferrous iron was observed in that case (refer Matzanke 2002 paper).

Table 2.4. Analysis of parameters for Mössbauer simulations of iron bound to Dfh.

Sample	δ (mm/sec)	ΔE_Q (mm/sec)	Γ (mm/sec)
Fe (aq)	1.35	3.06	0.591
Dfh	1.33	3.51	0.367

δ – Isomer shift

ΔE_Q – Electric quadrupole

Lw – line width at full width half maximum of signal

2.4.4 Fluorescence Spectroscopy

Fluorescence spectroscopy was used to measure the extent of the molten globular state and fold of DIsu under Fe-S cluster assembly conditions. ANS binding is often used to characterize the globular nature of biomolecules, since this fluorescent probe selectively binds to solvent exposed hydrophobic regions in molten globule proteins. ANS binding induces a fluorescence signal in the vicinity of 500 nm ($\lambda_{\text{excite}} = 371\text{nm}$), whereas well-folded proteins bind little dye and exhibit little fluorescence. A large fluorescence signal centred at 468 nm is observed upon Apo-DIsu exposure to ANS (Figure 2.6, combination of dashed & dotted line), suggesting the presence of exposed hydrophobic residues in a

molten globule form of the Dlsu. At these concentrations, ANS by itself in buffer had negligible fluorescence (control not shown). Addition of Fe (II) or sulfide to Dlsu caused only a minimal change in the ANS fluorescence (Figure 2.6, dashed and dotted lines, respectively), suggesting that binding of each substrate individually does not distort the overall fold of the protein. Incubation of both ferrous iron and sulfide to Dlsu prior to addition of ANS results in a substantial decrease of ANS signal intensity (Figure 2.6, solid line), suggesting a dramatic decrease in solvent accessibility to hydrophobic residues in the protein following or concurrent with the production of the Fe-S cluster.

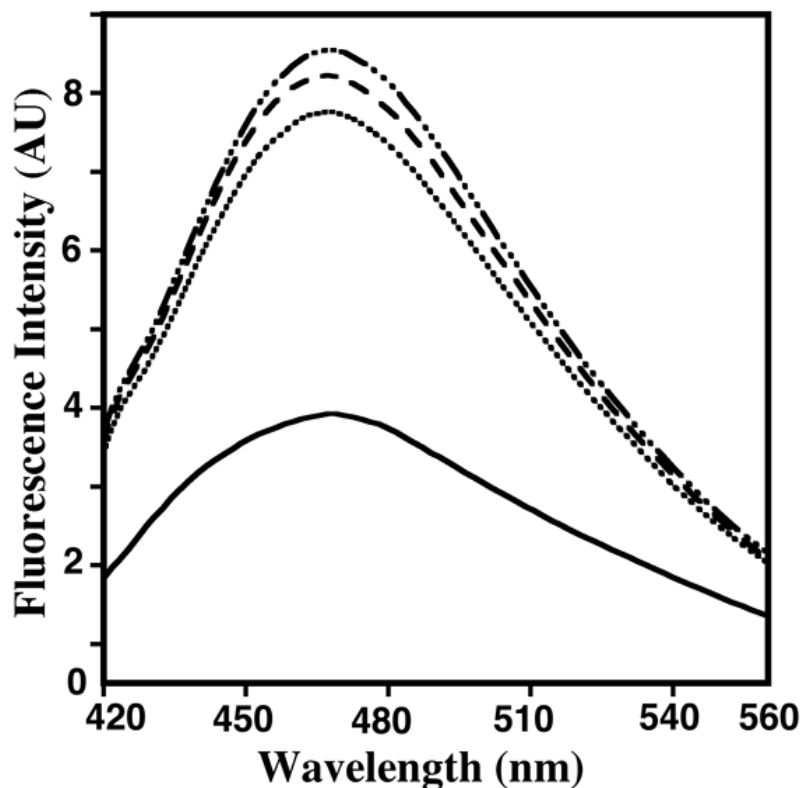


Figure 2.6. Fold and structural rearrangement of Dlsu during cluster formation using ANS fluorescent probe. Fluorescence of ANS bound to Dlsu alone (combination of dashed & dotted line), Dlsu incubated with Fe(II) (dashed line), Dlsu incubated with S²⁻ (dotted line) and Dlsu incubated with Fe(II) and S²⁻ together (solid line).

2.5 Discussion

Biosynthesis of iron sulfur clusters has been an intriguing subject because of the complexity involved in the pathway. Current research on the ISC assembly pathway suggests a multiprotein complex between frataxin, assembly scaffold and cysteine desulfurase/Isc11 exists in eukaryotes. Therefore it involves several protein-protein interactions between these proteins. The interaction between bacterial cysteine desulfurase (IscS) and the scaffold (IscU) has been recently characterized and the Barondeau group has analyzed the entire complex in eukaryotes (human). Their studies suggest the formation of a ~180 kDa hetero octomer ($\alpha_2\beta_2\gamma_2\delta_2$) containing two chains each of frataxin, ISU, NFU, and ISD11. Based on recent studies it occurs that there are significant differences in the assembly process in eukaryotes and prokaryotes. Particularly, the role of frataxin is still controversial, as it has been shown to inhibit the cysteine desulfurase activity in prokaryotes but to activate the cysteine desulfurase activity in eukaryotes. We believe that significant differences between prokaryotic and eukaryotic systems suggest that interaction between protein orthologs may be partially unique for the model system under investigation. In this report we characterize the molecular and structural details of the interaction between the frataxin and the scaffold using *D.melanogaster* proteins. Characterization of these interactions in the fly system may help explain the key differences in the frataxin function among different species (iron chaperone or storage v/s pathway regulator). This study provides details about one of the steps involved in this pathway. Our ultimate goal is to study each of these protein-protein interactions in detail starting with frataxin-scaffold interaction. This will allow us to provide a

detailed multiprotein complex involved in the assembly process. In this report we have characterized the electronic and structural changes in the bound iron at various stages during cluster assembly on *D.melanogaster* Isu (DIsu). We also report here that interaction between *D.melanogaster* frataxin (Dfh) and DIsu is metal dependant. We have also looked into detail on structural changes in DIsu upon cluster binding. In short this report summarizes the biochemical and structural details of frataxin-scaffold interaction enlightening the molecular details of this pathway.

Frataxin has been studied in several orthologs like human, yeast and bacteria. However there have been several issues regarding the stability of the protein in these orthologs. Yeast frataxin is very prone to oxidative damage and subsequent aggregation while human frataxin is susceptible to N-terminal autodegradation. Thus, our finding of Dfh as a stable eukaryotic ortholog was very important as Dfh is highly stable with melting temperature of ~59.2°C. This high stability and resistance to aggregation of Dfh has greatly facilitated our characterization of the DIsu-Dfh interaction in the current paper. Like Dfh, DIsu is also very well behaved protein as compared to other Isu orthologs. Usually wild type Isu is very insoluble and unstable in other eukaryotic orthologs, thus an aspartate mutant (D37A) is usually used for invitro studies in yeast. In case of DIsu, the wild type protein is soluble even under low salt conditions and is stable and active for more than two weeks. It is for these reasons, that we have performed a comprehensive invitro characterization of Dfh-DIsu interaction and the iron delivery to the DIsu protein.

ITC was used to find the iron and partner protein binding ability of Dlsu. The iron binding affinity and optimal metal: protein stoichiometry of Dlsu were characterized to elucidate the biophysical details of iron binding by Dlsu. Under our current solution conditions, Dlsu binds 2 Fe atoms with nanomolar binding affinity ($K_{D1} = 475 \pm 166$ nM and $K_{D2} = 64.5 \pm 17$ nM) (Table 2.1). Similar binding affinities have been observed in other orthologs as well. This iron binding affinity is higher than Dfh's iron binding affinity (average $K_D = 6$ μ M) suggesting that the transfer of iron to Dlsu is thermodynamically favourable. In addition to this, we also observed the interaction between the Dfh and Dlsu using ITC. As shown previously we observed that holo Dfh interacts with apo Dlsu with nanomolar binding affinity ($K_{D1} = 530 \pm 43.5$ nM and $K_{D2} = 673 \pm 22$ nM) (Table 2.1). However, these proteins are not observed to interact in absence of iron. Thus our results suggest that it would be energetically favourable for Dfh to interact with Dlsu in presence of iron. This protein-protein binding will then allow metal transfer to the scaffold and after removal of metal from Dfh would cause Dfh release from Dlsu. Previously, we have characterized the interaction of Dfh with yeast Isu and observed the same result (binding affinity of ca. 0.21 μ M). It is important to note that holo Dfh was able to interact with the yeast Isu. These results closely match the binding affinity of approximately 0.15 μ M obtained between the human proteins, and in both cases, binding is energetically favourable. The fact that the Dfh binding affinity and stoichiometry with respect to Dlsu so closely match those seen for complementary proteins in the human system only further emphasize the idea that the functional role of frataxin toward

Fe-S cluster biosynthesis is conserved between organisms. However, the presence of Nfs1/Isd11 will change the binding affinities between these proteins and future studies in this direction are ongoing in our lab.

We performed structural characterization of bound iron at different stages during assembly of Fe-S cluster on the Dlsu scaffold protein, as this provides insight into how metal is used during cofactor assembly. Our goal was to know the ligand environment and geometry of bound iron at different stages including the intermediates involved in the process. Based on Fe K-edge XANES data for these samples, we observed that Fe is present in high spin ferrous form, which is the biological available form of iron. In absence of sulfide, the iron has all O/N based ligand environment in Dlsu bound Fe and Fe - Dfh - Dlsu bound sample. However, the metrical details of the iron bound in these samples differ suggesting a difference in ligand environment upon delivery to Dlsu. We don't observe any sulfur ligation for iron bound to the Dlsu sample, suggesting a different iron binding site other than the active cysteines involved in cluster binding. While this technique cannot directly distinguish between oxygen- and nitrogen-based ligands, the technique can yield bond length with a very high degree of accuracy (0.02 Å). These accurate values can then be used to provide insight into probable coordination ligand types and geometries. Significant change takes place in the XAS data upon addition of Sulfur to the system. It suggests the formation of multinuclear iron species consisting of 2Fe-2S cluster formations. The EXAFS data of this sample suggests Fe ligation at 2.73 Å and S ligation at 2.28 Å, emphasizing the formation of Fe-S cluster and these values

are consistent with a 2Fe-2S cluster formation. The electronic environment of Fe-bound Dfh was further characterized by using Mössbauer spectroscopy, which again suggests the presence of high spin iron in an all O/N based ligand environment. This further supports our already published XAS results on Fe bound Dfh sample.

Our results indicate that binding of Fe-S cluster on the DIsu scaffold induces a structural change in the protein making it more folded. Isu scaffold proteins in general exist in a dynamic equilibrium between folded and unfolded state in order for them to function as a scaffold. This gives them flexibility to modulate their fold based on interacting protein or substrate to successfully carry a particular reaction. Previously, ANS fluorescence has been used to characterize the molten globule nature of *T. maritime* IscU and yeast Isu in solution. Similar results are observed for DIsu suggesting it also has a molten globule structure. However, no significant change in the fluorescence of the protein is observed upon either Fe or S binding only. We also don't observe any red shift in the data as seen in yeast studies. This can be probably species-specific difference or may be because of wild type nature of the DIsu. Following addition of Fe and S together, Fe-S clusters assemble on the scaffold and significantly decrease the ANS fluorescence due to stabilization of the structure and consequent decrease in the exposure of hydrophobic residues on the protein surface. This is consistent with the well-folded structure of *A. aeolicus* IscU, which was obtained by Fe-S cluster bound to the protein.

Finally, based on the recent research in the field of Fe-S cluster assembly formation and our results, we propose that frataxin and scaffold interact with each other in a metal dependent manner during the assembly process. Dfh binds iron and delivers it to Dlsu during the assembly process via physically interacting with the protein as shown by ITC. This interaction is thermodynamically favourable based on the binding interaction data. Dlsu is structurally stabilized upon cluster binding to the protein. Our structural data suggest that the initial iron-binding site on Dlsu scaffold is separate as compared to the cysteine rich cluster binding site. Iron transfer may take place to the active site during the cluster formation, however this mechanism of transfer to the active cysteine is not yet known.

CHAPTER 3

Characterization of Poly (rC) binding protein-PCBP2

3.1 Introduction

PCBP's were originally identified as RNA binding proteins that share a triple KH domain configuration, characterized by high affinity and sequence-specific interaction with poly (C). PCBP's, also known as α CP proteins (α -complex proteins), are encoded at four dispersed loci and have additional isoforms generated via alternative splicing (56). PCBP protein family members are involved in various biological processes such as mRNA stabilization (77-78), translational silencing (79-80), and translational enhancement (81-82). In addition, these proteins are found to be involved in apoptotic pathways (83-84) and also play a role as determinants of transcriptional controls (85-86).

The PCBP protein family has recently been reported to serve as iron chaperones for the iron storage protein Ferritin (55). Expression of human PCBP1 and PCBP2 in yeast recovered an iron loading deficiency for human Ferritin when it was also expressed in yeast (55). The goal of this portion of my thesis was to identify and characterize the role of PCBP2 in cellular iron homeostasis. My initial goal was to characterize PCBP2 and its iron binding properties. This information will assist in reaching the long term goal of this project, which is to elucidate the functional properties of this protein in terms of cellular iron-homeostasis.

3.2 Materials and Methods

3.2.1 Cloning, Optimization of Conditions for Expression of PCBP2

Human PCBP2 cDNA was supplied in pTYB11 vector by Dr. Caroline C. Philpot at NIH. The target protein is built in frame with the N-terminus of the intein-CBD fusion. The cDNA was amplified by transforming into amplification cell line $\Delta H5\alpha$. Plasmid prep kit was used to extract the amplified plasmid (Qiagen). Thus, amplified plasmid was sequenced to verify the full length protein by GENEWIZ and sequence analysis was done using the program CLUSTALX. The verified plasmid was transformed into BL21 (DE3) *Escherichia Coli* competent cells for protein expression.

Cell growth conditions were optimized by growing cultures in different conditions. First, the induction OD_{600} that gives best level of expression of protein was determined by testing the level of expression of protein in cultures induced at a range of OD_{600} (0.1-1.0). Two different concentration of IPTG (Isopropyl β -D-1-thiogalactopyranoside, Sigma) 0.4, 1mM were used; two different temperature (16, 10) °C and different growth hours (16, 20, 24,) were also explored to determine the best condition for expression of protein (New England Biolabs-impact-kit manual).

It is very important to have a procedure that could give repeatable results on protein expression yield. It was often encountered that the results were not repeatable even with freshly transformed colonies. When started with freshly transformed colony, it sometimes gave an intermediate protein yield but other times the yield was very low even though freshly transformed colonies were used

every time to grow culture following the same procedure. To solve this problem and to get repeatable protein yields, double selection of high level expressing colonies was performed (87). Nine different colonies were picked from a freshly transformed plate and each was used to inoculate 10 ml LB (100ug/ml Amp) taken in a sterilized Falcon tube (50ml). Each culture was grown to OD₆₀₀ of ~0.6 and induced with 0.4 mM IPTG. Immediately after induction, cultures were transferred to a shaker maintained at 16 °C and grown for 20 hours for expression of protein of interest. After 20 hours, 1ml of the cell suspension from each tube was spun down, cell pellet was re-suspended in SDS loading buffer for 10min at 80 °C. The level of expression was checked by running the samples on a SDS gel. The colony showing highest level of expression was chosen and grown to OD₆₀₀ ~ 0.6. A 20 µl of cell suspension was spread onto the plate (LB + Amp), and left in the incubator overnight at 37 °C to allow the colonies to grow. From the plate after the 1st colony selection, eight different colonies were picked, grown and their level of expression was tested by running an SDS page. Again, the best expressing colony from single colony selection was grown till OD₆₀₀ ~ 0.6 and plated onto a (LB+ Amp) plate and allowed to grow on incubator overnight. From the plate of 2nd colony selection, four different colonies were picked and checked for the level of expression by running SDS-Page. Colonies obtained after double selections were used for preparing glycerol stocks that were used for growing cultures in the future.

3.2.2 Purification of PCBP2

Purification of PCBP2 follows an intein-based purification scheme which is a single step purification method. This system utilizes self splicing protein intein in conjunction with the chitin binding domain (CBD) towards the N-terminal of intein, whereas towards the C-terminal region it is fused with target protein. CBD allows fusion protein (Intein + protein of interest) to bind to chitin beads (New England Biolabs) present in the column, allowing the protein of interest to stay bound to the column via the intein domain. Intein can be induced to undergo self cleavage at its C-terminal peptide linkage with 1, 4-dithiothreitol (DTT) which results in the release of target protein (88-89).

After optimization of conditions for the expression of protein, the next step was to purify the protein for conducting the designed experiments. A solution of 10 ml LB with 100ug/ml of Amp was inoculated my glycerol stock and grown overnight as starting culture. This overnight culture was added to 1L LB media (autoclaved prior) with required conc. of Amp. Since the plasmid had amp-resistant marker, 100 µg/ml conc. of Amp was maintained throughout the culture. The culture was grown at 37 °C at 250 rpm, and monitored until it reached OD₆₀₀ ~0.6. It was then induced with 0.4 mM IPTG. After induction, the culture was transferred to a shaker maintained at 16°C and grown for 20 hours at 250 rpm. Cells were harvested by centrifugation for 10 minutes at 8000 rpm. Cells were re-suspended in 20 mM Tris, 500 mM NaCl (pH-8.5) (5mL/g cells) in the presence of complete EDTA free Protease Inhibitor cocktail (Roche), 1% Triton X-100 (Bio-Rad) and final conc of 0.1 mM TCEP [tris-(2 Cyanoethyl)phosphine]. The resuspended solution was lysed by two passes through French press to disrupt

cell and liberate protein. The lysate was then centrifuged at high speed (21000 rpm) for 45 minutes to separate the soluble fraction from the insoluble one. Crude soluble fraction was filtered (0.22 μm) and the lysate was then loaded in the column packed with chitin beads (NEB). The flow was maintained at very low speed (0.2-0.3 ml/min) to allow binding by adsorption onto the chitin column. The immobilized fusion protein remains bound to the column with the chitin beads via CBD. Other proteins remain freely floating in the column and can be washed away. Column loaded with lysate was washed with ~50 column volumes of degassed buffer "A" (20 mM Tris, 500 mM NaCl, pH-8.5), at the flow rate of 1 ml/min. To induce intein to undergo self cleavage and release target protein, 75 mM DTT (Dithiothreitol, Sigma) was added to the column. The column was left to incubate for 30-40 hours at room temperature prior to elution.

After incubation, protein was eluted with buffer A. PCBP2 co-eluted with N-extein, a small protein (~1.6 kDa) which can be dialyzed out by centrifuging for buffer exchange using a 10 kDa cut off Amicons ultra centrifugal filters (Millipore). Concentration of the protein was determined using a Lowry assay.

3.2.3 Size and Oligomeric State of PCBP2

Mass spectrometry was carried out as a next immediate step on the purified protein to verify its mass. A 10 μM concentration of protein was used to confirm the full length polypeptide sequence of the protein sample after purification.

Size-exclusion chromatography was used to determine the oligomeric state of the apo-protein. Samples were prepared in degassed buffer (20 mM Tris,

500 mM NaCl (pH-8.5)). The same buffer was used to equilibrate, wash the column, and also used as a running buffer. Sample was loaded with the help of the syringe onto a 1.2 meter long column attached to AKTA system, and the column was run at 4 °C. Protein controls of vitamin B₁₂ (1.3 kDa), myoglobin (17 kDa), ovalbumin (44 kDa) γ -globulin (158 kDa), and thyroglobulin (670 kDa) were used as a molecular size standards (Bio-Rad).

3.2.4 Fold and Stability of PCBP2

Circular Dichroism spectroscopy was carried out to determine the secondary structure of the protein. Samples were prepared in 1 mM NaPi, pH-7.6 with the protein concentration of 15 μ M. The experiment was performed using a temperature regulated Olis CD spectrometer at 25 °C over the wavelength range of 190-260 nm. A 1.0 nm resolution setup was used to record the spectrum and a baseline was corrected by subtracting the buffer spectrum. Averaging of 10 independent scans followed by data analysis was performed using the OLIS software analysis package.

Protein samples were heated in 5 °C increments over the temperature range of 10 to 95 °C. Thermal unfolding curves were obtained by using 1 nm resolution and monitoring the ellipticity at 208 and 222 nm. The protein melting temperature (T_M) was calculated by analyzing the thermal unfolding curves obtained at 208 nm.

3.2.5 Substrate and Protein Binding Characteristics

Isothermal Titration Calorimetry (ITC) experiments were conducted to determine the metal binding properties of PCBP2. All protein samples and buffer preparation of ferrous ammonium sulfate solutions were degassed on a Schlenk line and samples were stored under Argon. Protein and aqueous ferrous ammonium sulfate solutions were prepared anaerobically in 50 mM Tris, 150 mM NaCl pH-7.6 (ITC buffer). ITC experiments were conducted anaerobically using a VP-ITC titration microcalorimeter (MicroCal, Inc) at 30 °C. A 1 mM ferrous iron solution of was titrated into a 1.4 ml volume of 30 μ M protein solution. The initial 2 μ l injection was followed by 29 additional 10 μ l injections that were titrated into the protein solution. The interval between two injections was 10 min, and the stirring speed of the syringe was held constant at 502 rpm. All data were conducted in triplicate on independent protein and iron samples to ensure data reproducibility. Data analysis was performed using the Origin 7.0 Scientific Graphing and Analysis Software (provided by Micro Cal) to determine the binding affinity and metal-protein stoichiometry.

The binding affinities of other metals such as Zinc were also tested. Samples were prepared in 50 mM Tris, 200 mM NaCl (pH-7.6) and degassed. A 1 mM Zinc solution was titrated as an initial 2 μ l injection, followed by 29 additional 10 μ l injections, into 1.4 ml of a 25 μ M degassed protein sample. The experiment was conducted at 30 °C at a stirring speed held constant at 502 rpm with 10 min interval between injections. The obtained data was analyzed using the software provided by Micro Cal.

Characterization of the interaction between PCBP2 and Ferritin was also conducted using ITC. Samples were prepared in ITC buffer, 150 μ M Ferritin was titrated to 1.4 ml of 15 μ M apo-PCBP2. Both protein samples were degassed in the Schlenk line prior to loading. The experiment was conducted at 30 °C with the stirring speed of 502 rpm. Similarly, the interaction between holo-PCBP2 binding to H-chain Ferritin (Horse spleen-Sigma) was tested. Holo-PCBP2 samples were prepared anaerobically in a glove box, with the metal protein stoichiometry of 3:1 (600 μ M:200 μ M). The 200 μ M holo PCBP2 sample was titrated into 1.4 ml of 20 μ M H-chain Ferritin and the experiment was conducted at 30 °C at 502 rpm.

3.2.6 XAS Sample Preparation and Analysis

X-ray absorption spectroscopy was utilized to investigate the electronic characteristics and ligand co-ordination geometry of iron bound to PCBP2. XAS samples were prepared in 50 mM Tris, 150 mM NaCl (pH-7.6) and 30% glycerol. Multiple independent holo-PCBP2 samples were prepared anaerobically in a glove-box (PlasLabs) purged with argon(at a Fe:PCBP2 ratio of 1:1 and 3:1) using protein samples and iron solutions that were degassed initially in the Schlenk line and stored under an argon atmosphere. Samples were loaded in Lucite XAS cells wrapped with Kapton tape, flash frozen immediately after loading, removed from glovebox and stored immediately in liquid nitrogen until they were used.

XAS data were collected at the Stanford Synchrotron Radiation Laboratory (SSRL) on beamline 9-3. Beamline 9-3 was equipped with a Si (220) double-

crystal monochromator and harmonic rejection mirrors. During data collection, samples were maintained at 10K using an Oxford Instruments continuous-flow liquid helium cryostat. Protein fluorescence excitation spectra were collected using ionization detectors filled with nitrogen gas, placed before and after the cryostat. XAS spectra were measured using 5 eV steps in the pre-edge region (6900-7094), 0.25 eV steps in the edge region (7095-7135) and 0.05 Å⁻¹ increments in the extended X-ray absorption fine structure (EXAFS) region (to $k=13.5 \text{ \AA}^{-1}$), integrating from 1 to 20 s in a k^3 weighted manner for a total scan length of approximately 40 minutes. X-ray energies were calibrated by recording an iron foil absorption spectrum simultaneously with the collection of the protein data. The first inflection point for the iron foil edge was assigned at 7111.3 eV. Each fluorescence channel of each scan was examined for spectral anomalies prior to averaging and spectra were closely monitored for photo-reduction. SSRL data represent average of 100 scans.

XAS data was processed using the Macintosh OS X version of EXAFSPAK manual suite integrated with Feff version 7.2 for theoretical model generation (90-91). Data reduction and processing of the pre-edge transitions utilized a Gaussian function in the pre-edge region and a three-region cubic spline in the EXAFS region. EXAFS data was converted to k-space using an E_0 value of 7130 eV. Data was truncated at 1.0 and 13.5 Å⁻¹ for filtering purposes and Fourier transformed. Fitting analysis was performed on raw/unfiltered data and Fourier transformed. A scale factor (S_c) of 0.95 and threshold shift (ΔE_0) of -11.5 eV were used during the data analysis. The S_c and ΔE_0 were not allowed to

vary as they were calibrated from the Fe(II) model compounds matching the oxidation state of the ferrous iron. When simulating empirical data, metal-ligand coordination numbers were fixed as a half integer values while only the absorber-scatterer bond length (R) and Debye-Waller factor (σ^2) were allowed to vary freely. The criteria for judging the best fit simulation, and for adding ligand environment to the fit, included: A) the lowest mean square deviation between data and fit (F'), a value corrected for number of degrees of freedom in the fit, B) individual shell bond distances must be outside the spectral resolution ($> 0.13 \text{ \AA}$) and finally C) all Debye- Waller factors in the ligand system must have values less than 0.006 \AA^2 (92).

Analysis of X-ray absorption near edge spectroscopy (XANES) $1s \rightarrow 3d$ transition was completed using the EDG_FIT subroutine with EXAFSPAK (90). The data was compared with Fe(II) and Fe(III) models and edge analysis was performed in Kalaiedograph.

3.3 Results

3.3.1 Optimization of Condition for Expression of Protein

The level of expression of the colonies under different growth condition was explored. The different growth conditions explored are listed in Table 3.1. Comparing the level of expression of protein, it was concluded that apo-PCPB2 expresses best when grown at $16 \text{ }^\circ\text{C}$ for 20 hours after induction with 0.4 mM IPTG. The level of expression when induced at different OD_{600} values are shown in Figure 3.1, (Panel A). The lanes from 3-10 show levels of expression when induced at different OD_{600} . Best level of protein expression was obtained when

the culture was induced at OD_{600} 0.6, as shown in lane 8 (Figure 3.1, Panel A). Similarly, higher yields of protein expression were obtained when grown for 20 hours after induction as shown in lane 4 (Figure 3.1, Panel B).

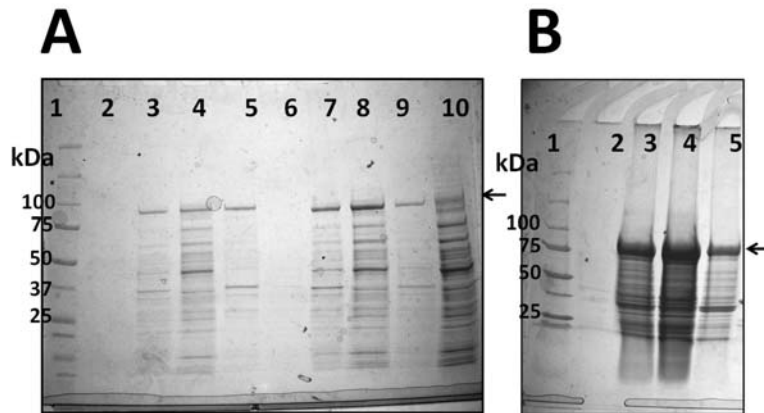


Figure 3.1. SDS-Page showing the level of expression of apo-PCBP2, when induced at different OD_{600} . Panel A: Expected protein band (apo PCBP2+ intein) ~95kDa is shown with an arrow. Induction OD_{600} lanes 3-10 are 0.1, 0.2, 0.3, 0.4, 0.5, 0.6, 0.8, 1.0 respectively. Panel B: shows level of expression of apo-PCBP2 when grown for 16, 20 and 24 hours after induction (lanes 3-5 respectively).

To obtain dependable yields of the protein double colony, selection of the best expressing colony was performed. Figure 3.2 (Panel A) shows a weak level of expression of protein of nine different freshly transformed colonies (Lanes 2-10, Panel A, Figure 3.2). The best expressing colony (Lane 4, Panel A Figure 3.2) was selected and plated on a (LB + Amp) plate. Eight different colonies obtained from single colony selection were tested for level of expression (Panel B, lanes 2-10, Figure 3.2). The level of expression after single colony selection was higher compared to the freshly transformed colonies. Again, the best expressing colony in Panel B (lane 9, Figure 3.2) was selected and plated. The level of expression of four different colonies, after double colony selection, is

shown in Panel C (Lanes 3-6, Figure 3.2). After the colonies were selected for the second time, protein was expressed in higher levels compared to the freshly transformed colonies. These colonies were used for preparing glycerol stocks which were used for growing cultures. Double selection of the high expressing colony produced repeatable results in the yield of protein every time the protein was purified.

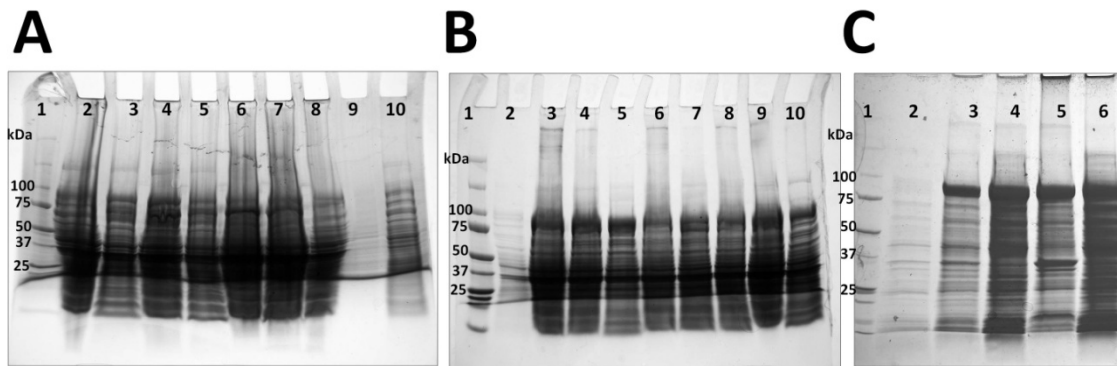
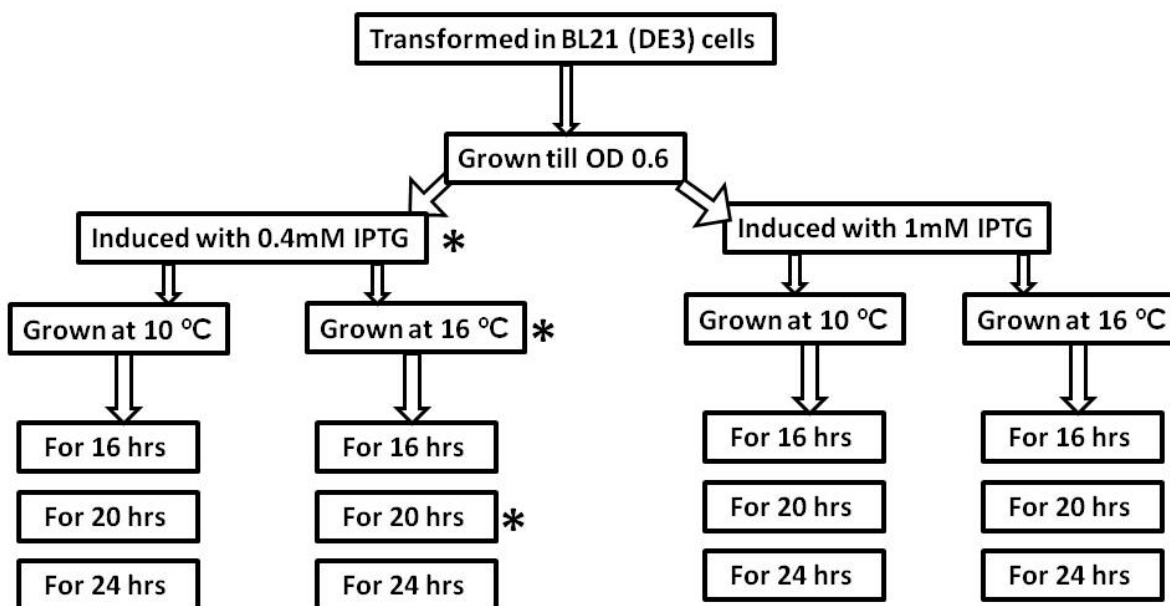


Figure 3.2. SDS-PAGES of protein expression of apo-PCBP2 (365aa) before (Panel A), during (Panel B), and after (Panel C) double colony selections. Expected protein band (~95 kDa, apo PCBP2 (1-365)+ intein) are observed. Panel A shows expression of nine different colonies before colony selection. Panel B shows result of 8 colonies after single colony selection (3rd lane-from Panel A) because this colony gave good level of expression. Panel C shows the results of four colonies selected after double colony selection (lane, 9-from Panel B), indicating high level of protein expression. Molecular weight markers are labeled with kDa. Lane 2 in both panels (B, C) are pre induced samples).

Table 3.1. Different conditions for optimization of expression of PCBP2.



3.3.2 Purification of PCBP2

Purification of PCBP2 follows affinity purification, by which pure protein can be obtained in a single step. PCBP2 is cloned in frame with a self-splicing intein domain that allows it to bind to the chitin beads present in the column. Upon induction with DTT, intein cleaves itself and remains immobilized on the chitin resin with the release of the target protein along with another small protein (~1.6kDa) which cannot be seen on the gel and can be dialyzed away. Figure 3.3 shows the steps on purification of PCBP2. After optimization of conditions, PCBP2 was purified in a single step with ~ 95% purity and 5-8 mg/L yield. Protein concentrations were measured by the Lowry assay before conducting the designed experiments.

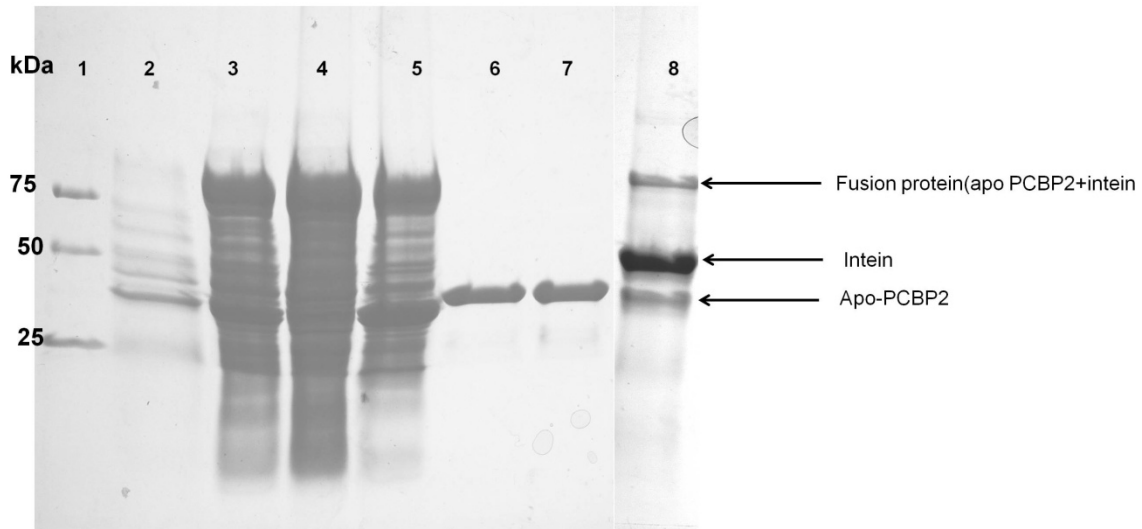


Figure 3.3 SDS-Page showing purification of apo-PCBP2. Protein marker was loaded in first lane and labeled with kDa. Lane 2-pre induction sample, Lane 3- post induction sample, Lane 4, 5 –supernatant and pellet samples respectively. Lanes 2-4 shows fusion protein band (apo-PCBP2+intein), 6-7 are elution's showing apo-PCBP2. Lane 8 shows 3 bands; fusion protein, intein, and apo-PCBP2 respectively.

3.3.3 Size and Oligomeric State of PCBP2

This 365 amino acid protein was expressed in bacteria (5-8 mg/L of medium). Mass spectrometric analysis of apo-PCBP2 indicated the molecular mass of $38,578.4 \pm 5$ Daltons, Figure 3.4, Top panel. Expected mass of full length apo-PCBP2 (Isoform d, 365 amino acids) from the sequence is 38,580 Daltons. Mass spectrometric results showed that full length protein is purified in a single step and PCBP2 elutes out from the column without loss or gain of any additional amino acids.

The oligomeric state of the protein was determined by loading a 200 μ M sample onto a size exclusion column (Sephacryl-200) and collecting 2 ml fractions, which were tested for protein by the quick advanced assay (Biorad).

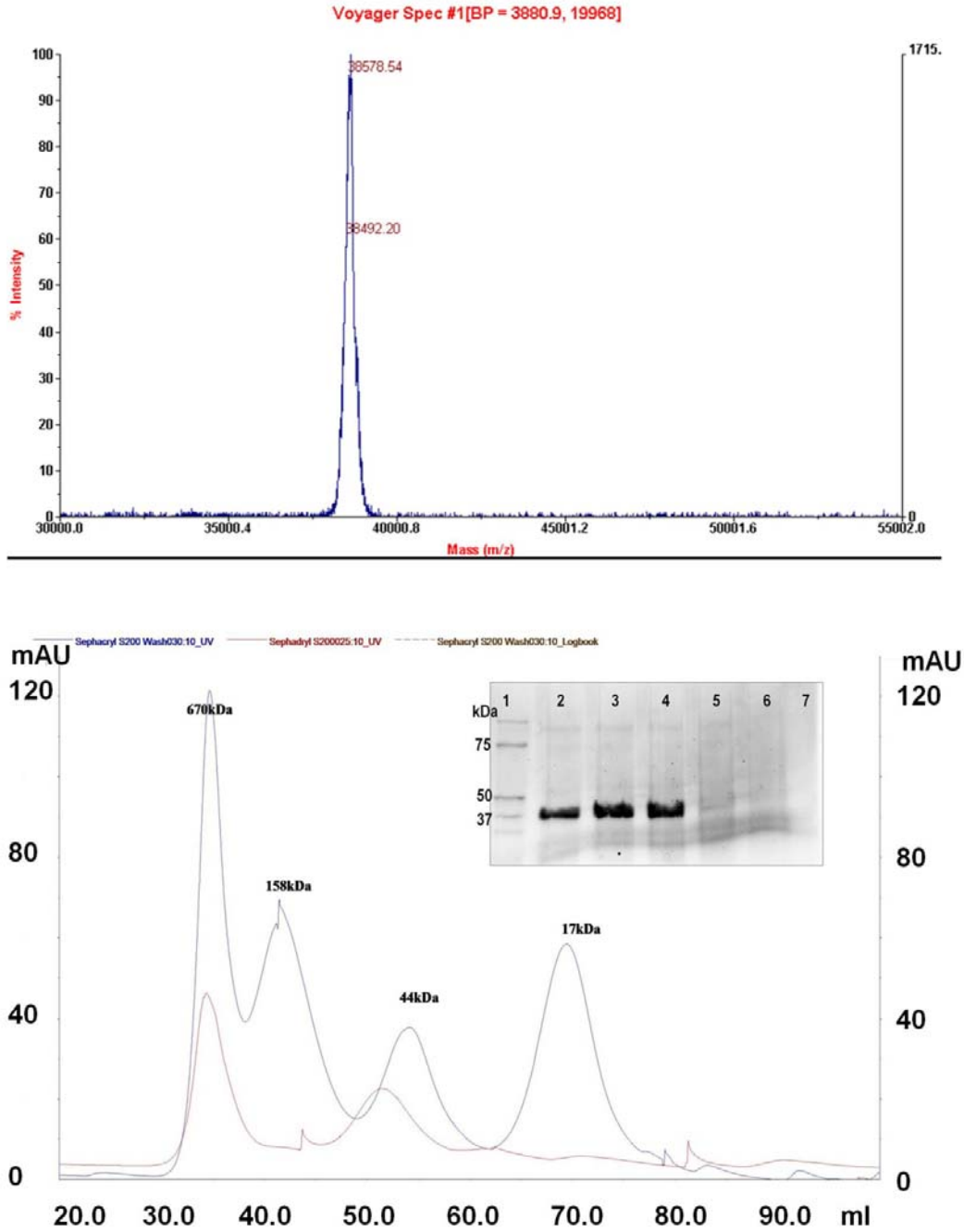


Figure 3.4. A Determining molecular weight and Oligomeric state of PCBP2. The peak was observed with molecular weight $38,580 \pm 2$ Daltons, which is the molecular weight of full length PCBP2. It showed that PCBP2 is successfully purified with full length protein (Top panel). PCBP2 elutes as a dimer in size-exclusion column. Sample was run through S-200 column, and elution peaks were observed. 4 peaks were observed for standards which were compared with the peaks observed for the protein (Bottom panel). First peak, observed in the void volume did not show the any bands showing protein (lanes 5-7). Second peak observed showed protein bands on gel (lanes 2-4), which elutes as a dimer 52-56ml (70 ± 7 kDa).

The fractions that gave positive results in the Biorad assay were run on a SDS gel to confirm the presence of protein in those samples (Bottom Panel, Figure 3.4). Two peaks were observed: a first peak between 30-40ml (void volume of column) and a second peak observed between 52-56 ml. The graph suggests that the protein elutes at 52-56 ml. This was verified by running the samples on SDS-Page (Lanes 2-4, Bottom panel, Figure 3.4). The molecular weight range falls between 70 ± 7 kDa, when compared with the standards, suggesting the protein exists as a dimer. Lanes 5-7 (Bottom panel, Figure 3.4) are the samples taken from the fractions collected between 30-40 ml, which does not appear as a protein band in SDS-page. Elution peaks observed in the range of void volume may be the aggregates of the protein and these eluted out as early fractions.

3.3.4 Fold and Stability of PCBP2

Secondary structure analysis by CD spectra showed that PCBP2 has a high helical content. CD spectral simulations suggested an approximate secondary structure distribution of 59% α -helix, 16% β -sheet and 25% turns/coils, (Standard Deviation: 0.11) (Figure 3.5 A).

A melting temperature for PCBP2 was determined using CD spectroscopy (Figure 3.5 B). Full CD spectra for PCBP2, covering the wavelength range of 190-260 nm, were collected over a broad temperature profile to generate a thermal denaturation plot. The thermal profile was determined by measuring changes in molar ellipticity at both 208 and 222 nm. A representative plot of temperature-dependent fractional fold of the protein utilizing the 10 and 95 °C

spectra as limits is given for the 208 nm signals in the Figure 3.5 B. The melting temperature of the protein was calculated to be 56 ± 2.5 °C.

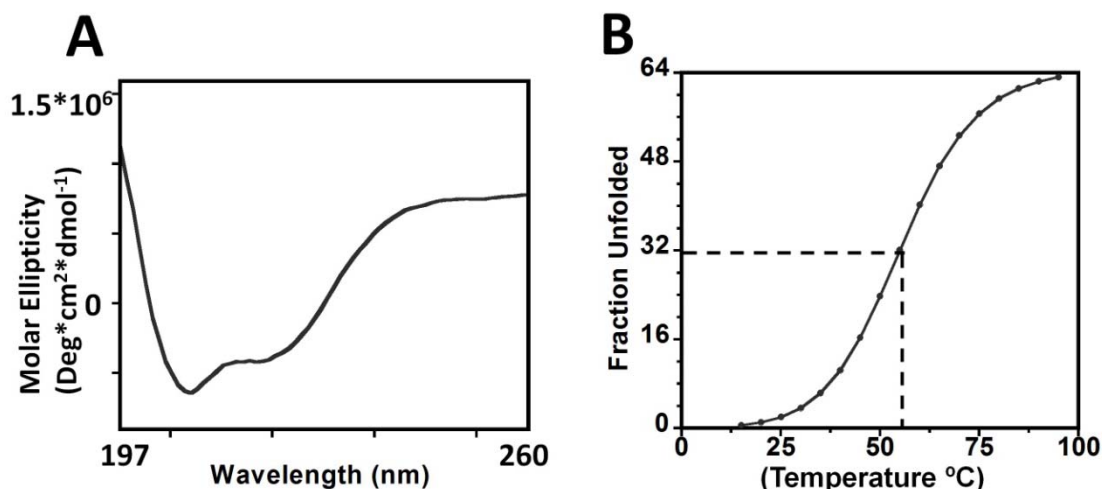


Figure 3.5. (A) Secondary structure of PCBP2 determined by Circular Dichroism Spectroscopy at 25°C in 1mM NaPi (pH-7.6). The displayed spectrum represents an average of 10 consecutive scans. Analysis of the spectrum showed PCBP2 is a folded protein with mainly helical content. Observed secondary structure percents were 59% α -helix, 19% β -sheet, 25% coils/turns (B) The thermal denaturation curve was obtained by measuring changes in molar ellipticity at 208 nm from the CD spectra of protein samples taken at multiple temperatures (10-95 °C) with 5° increment between samples. The dots represent raw data which were simulated using Kalaeidograph. Melting temperature of the protein was determined to be 56 ± 2.5 °C.

3.3.5 Metal Binding Properties of PCBP2

Isothermal Titration Calorimetry (ITC) was used to characterize the ferrous iron binding affinity and maximal metal:protein stoichiometry of iron to PCBP2. A change in the heat associated with titration of anaerobically prepared ferrous iron to apo-PCBP2 is shown as raw ITC data. Raw ITC shows the binding event is an exothermic process since the heat released upon titration being negative. The fit shows that PCBP2 binds iron at two binding sites, one tighter than the other. The first binding site is occupied with 1.46 ± 0.1 Fe atoms with a binding affinity of 0.034 ± 0.023 μ M, while the second binding site is occupied with 2.05 ± 0.09 iron

atoms with the binding affinity of $0.64 \pm 0.1 \mu\text{M}$. The first metal binding event was enthalpically favorable ($\Delta H_1 = -12.2 \text{ kcal/mol}$) and entropically unfavorable ($\Delta S_1 = -5.32 \text{ cal/mol}$) with overall favorable free energy ($\Delta G_1 = -12.205 \text{ kcal/mol}$). Metal binding to the second site was enthalpically favorable ($\Delta H_2 = -6.73 \text{ kcal/mol}$) and entropically favorable ($\Delta S_2 = 6.11 \text{ cal/mol}$) as well with overall favorable free energy ($\Delta G_2 = -6.72 \text{ kcal/mol}$) Figure 3.6, A.

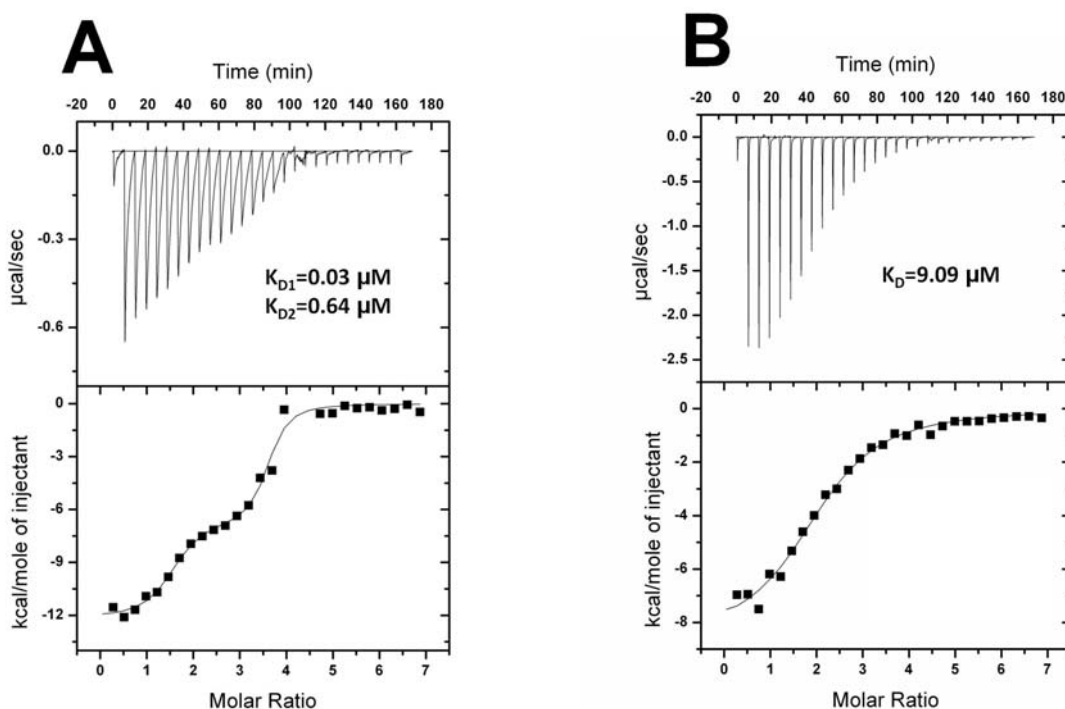


Figure 3.6. PCBP2 is a metal binding protein. (A) Exothermic profile of heat released obtained upon titration of ferrous iron to PCBP2. PCBP2 binds iron at 2 binding sites at micro-molar binding affinity. (B) PCBP2 also binds Zinc, with slightly higher affinity compared to iron.

Further binding of PCBP2 to divalent metal Zinc was also explored. A 1 mM ZnCl_2 solution was prepared in 50 mM Tris, 200 mM NaCl (pH - 7.6) and titrated into 25 μM PCBP2 at 30 °C generated an exothermic profile of heat released. The fitting analysis showed PCBP2 binds 2.08 ± 0.05 Zn atoms with the binding affinity of $9.0 \pm 6.6 \mu\text{M}$. Metal binding event was enthalpically

favorable ($\Delta H = -8.6$ kcal/mol) and entropically unfavorable ($\Delta S = -5.81$ cal/mol) with overall favorable free energy $\Delta G = -8.61$ kcal/mol. (Figure 3.6, B)

Similarly, interaction of PCBP2 to ferritin was also conducted by using ITC. Titration of Ferritin to apo-PCBP2 did not generate a heat release profile suggesting that these two proteins do not interact in the absence of iron (Figure 3.7, A). Titration of holo-PCBP2 to Ferritin generated an exothermic profile in the raw data suggesting a binding event is taking place between Ferritin and PCBP2 in the presence of iron (Figure 3.7, B). Preliminary data suggest the binding process, binding affinity and stoichiometric ratio of Ferritin bound to PCBP2 still needs to be explored with varying buffer conditions to get better data.

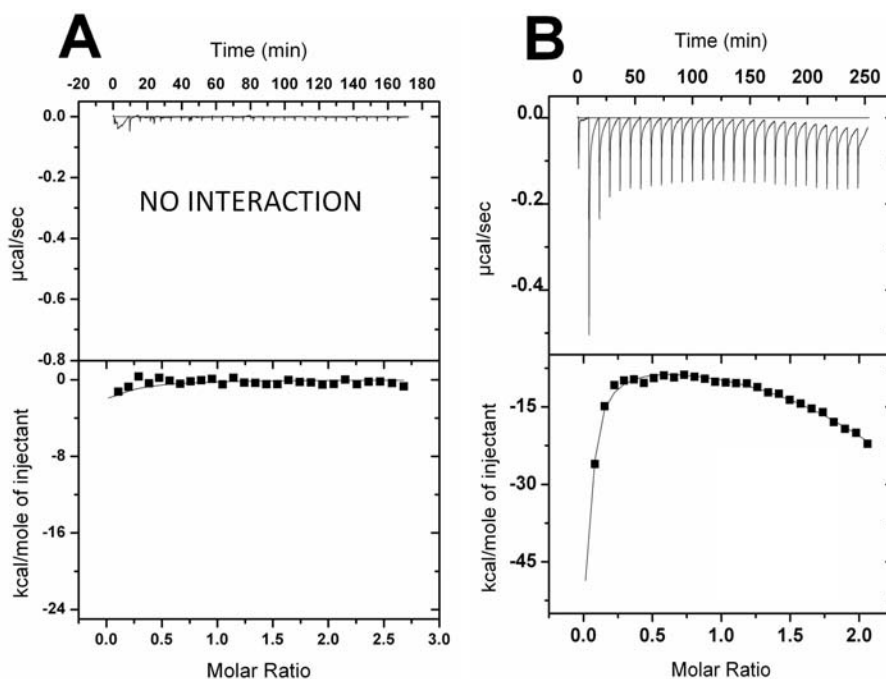


Figure 3.7. Interaction of Ferritin with apo/olo-PCBP2. (A) PCBP2 does not interact with Ferritin in the absence of Iron. (B) Exothermic profile of heat release is obtained upon titration of holo-PCBP2 to Ferritin.

The interaction between PCBP2 and Ferritin in the presence of iron is supported by a previous study conducted with the family member PCBP1, where PCBP1 and Ferritin were co-immunoprecipitated only in the presence of iron (55). However, exact binding parameters are yet to be explored.

3.3.6 Electronic and Coordination Properties of Bound Iron

XAS studies were conducted to characterize the electronic and structural properties of iron bound to PCBP2. K-edge XANES spectra for holo-PCBP2, compared to Fe(II) and Fe(III) controls (35) are given in Figure 3.8. The edge feature of bound iron resembles those observed for our aqueous Fe (II) control. The first inflection edge energy for iron bound to PCBP2 closely matches that obtained for the Fe (II) control (7122.42 ± 0.05 eV and 7123.1 ± 0.06 eV, respectively) as compared to the value obtained for the Fe (III) control (7127 ± 0.02 eV), indicating PCBP2-bound iron is stable as ferrous metal.

EXAFS analysis was used to provide the metal-ligand metric parameters for ferrous iron bound to PCBP2. Raw EXAFS data for Fe:PCBP2 (1:1), has a maximum amplitude of 5.5 \AA^{-1} with the single frequency pattern suggesting the nearest neighbor environment of the Fe-bound to PCBP2 consists of oxygen and/or nitrogen based ligand environment (Figure 3.9, black lines). Spectral simulations showed ligands that directly coordinated with Fe(II) consisted of completely oxygen/nitrogen based environments (Table 3.2). The data is a best fit using 2 O/N shell nearest neighbor environment in the simulations (Fig 3.9, green lines). The sample showed a partially disordered ligand environment with total co-ordination number ~ 6 as expected for the octahedral symmetry generally seen

for ferrous iron. There were no evident iron-sulfur ligation and no long range scattering of atoms were observed.

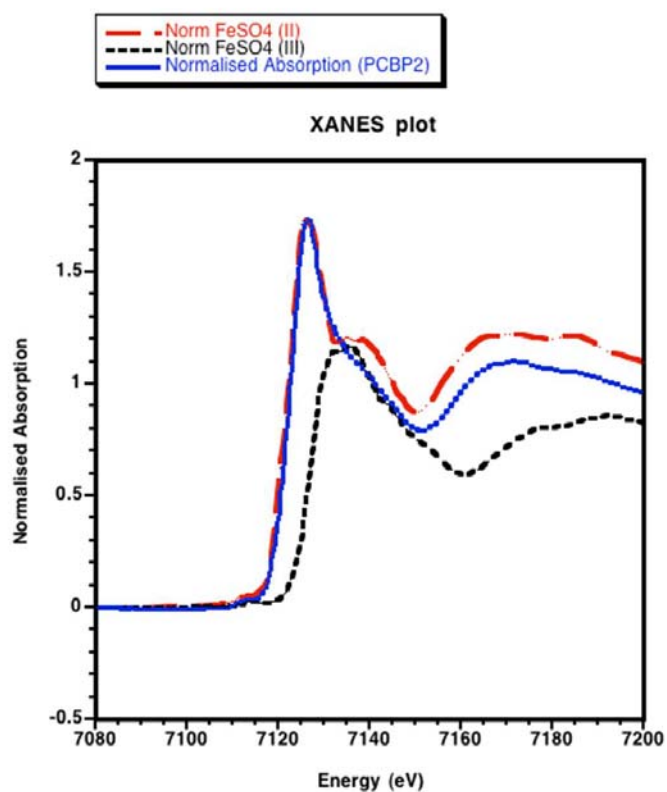


Figure 3.8. XANES comparison of iron loaded PCBP2 with ferrous and ferric models. Full XANES spectra for PCBP2 with 1 iron bound (blue-solid), ferrous ammonium sulfate (red dashed line) and ferric ammonium sulfate (black dotted line) are displayed. XANES analysis of iron bound to PCBP2 showed pre-edge features that resemble the ferrous ammonium sulfate model.

Table 3.2 XAS best fit values for Fe(II) bound to PCBP2.

Shells	Atom	CN	R (Å)	$\chi^2 \sigma^2 \times 10^3$	F' (Red. Error)
2	O/N	4	2.13	3.1	0.92
	O/N	1	2.27	3.2	

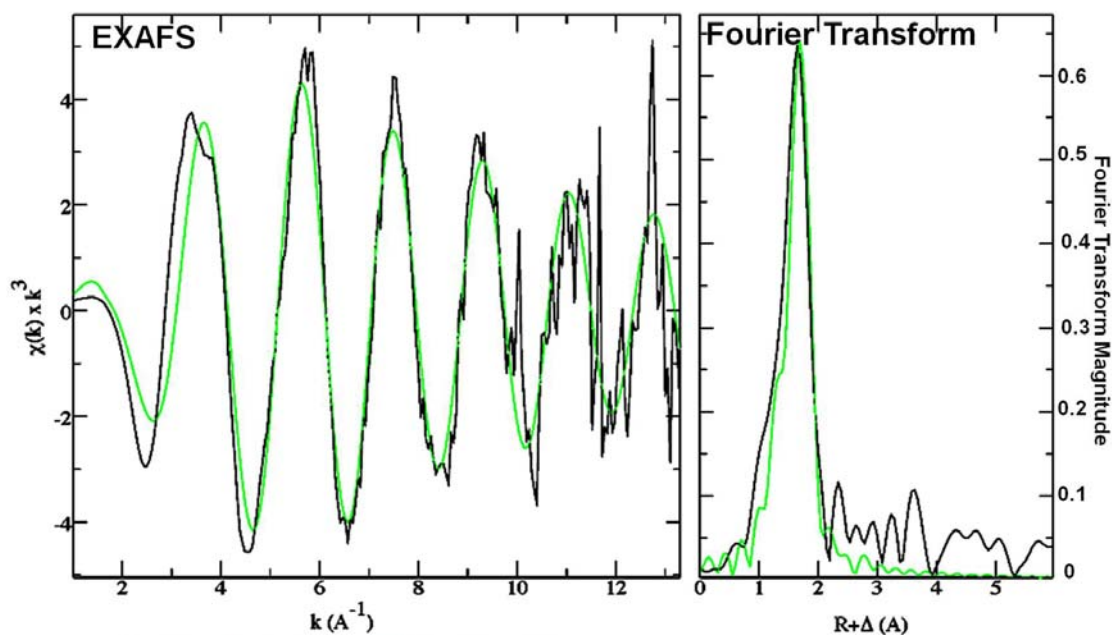


Figure 3.9. EXAFS and Fourier transforms of iron loaded human PCBP2 XAS data. Raw EXAFS spectra (in black) of protein with 1 iron bound, along with corresponding Fourier transform. Simulations of EXAFS and Fourier transform are shown in green.

3.4 Conclusion and Discussion

Uptake of the iron by our body is in milligram range and hence it is considered as a micronutrient (93). Even though this requirement is only in the low milligram range, iron is utilized in almost all biological processes including DNA synthesis, oxygen transport, and cell division (94). Despite the low dietary requirement, iron deficiency is a major global health problem affecting more than 2 billion people worldwide, and it is listed in the group of the top ten leading risk factors for health impairment by World Health Organization (95). As stated in a recent American Heart Association Scientific sessions (2009), “treatment of iron deficiency improves symptoms, functional capacity and quality of life in chronic heart failure patients, independent of presence of ammonia”. Similarly, excess of iron is also detrimental to health, due to of its ability to form metal based reactive

oxygen species (ROS) that destroy cellular DNA and compromises cellular efficacy. Hemochromatosis, along with other iron related disorders such as Friedrich's Ataxia, Parkinson's disease, and Alzheimer's are reported to be associated with dysregulation of iron metabolism (96-99).

Proper level of iron must be balanced in the body to ensure cell can utilize iron when it is needed and to protect themselves against the harmful effects of unregulated metal. Metallochaperones play a vital role in maintaining cellular homeostasis to accommodate these homeostatic requirements. These metallo-chaperones bind metal and deliver it to cognate enzymes that require it (100). Identification of a cytosolic iron chaperone has helped to solve one piece of the puzzle of cellular iron homeostasis and provided new insight for the study of many iron-dependent enzymes in the cytosol. The PCBP family of proteins, which were initially recognized as RNA binding proteins, are identified as players in cellular iron metabolism and serve to deliver iron to cytosolic iron storage protein Ferritin (55). However, the mechanism of iron transport in terms of cellular iron homeostasis and the role played by the PCBP family of proteins is yet to be unfolded.

This thesis studies the biophysical properties of PCBP2 and its metal binding properties. It was found that PCBP2 is a folded protein with high helical content, and Melting Temperature (T_M) of 56 ± 2.5 °C. With respect to its metal binding properties, it was found that PCBP2 binds iron with micromolar binding affinity. This interaction is iron dependent. Also, it has been shown that there is no interaction between the family proteins (PCBP1 and PCBP2) in the absence

of iron. The interaction between PCBP's in the presence of iron is yet to be done. Further, the electronic properties of iron (bound to PCBP2) shows the metal is bound in an O/N based ligand environment in the Fe(II) form.

Given that PCBP binds iron, identification of active sites for metal binding via site directed mutagenesis will further help to decipher the role of PCBP's in iron homeostasis.

CHAPTER 4

Activation of the HIF Prolyl Hydroxylase by the Iron Chaperones PCBP1 and PCBP2

4.1 Prelude

Since free iron is very reactive and can lead to the formation of reactive oxygen species (ROS), iron must be properly regulated so that the body gets iron when and where it is required and at the same time saves itself from the toxic effects of iron. Identification of Poly (rC) Binding Protein 1 (PCBP1) as a cytosolic iron chaperone confirms that the PCBP family of proteins are involved in iron homeostasis in the cytosol. The PCBP family of proteins have been proposed to also serve as iron chaperones for other cytosolic proteins that require iron. There are many iron-dependent enzymes in the cytosol, which may interact with PCBP's. In a final project, we studied the role of PCBP's with respect to iron delivery to the Prolyl-hydroxylase-2 enzyme. My contribution to the corresponding work is related only to the purification of PCBP2 and supplying the protein for studies. I have purified apo-PCBP2 (365 aa) and supplied for conducting the designed experiments.

In detail, this manuscript studies the role of PCBP1 and PCBP2 with relation to Prolyl-hydroxylase-2 activation. A manuscript covering this work is currently under preparation for publication, and the manuscript reference is: Anjali Nandal, Julio C. Ruiz, Poorna Subramanian, Sudipa Ghimire-Rijal, Ruth Ann Sinnamon, Timothy L. Stemmler, Richard K. Bruick, and Caroline C.

Philpott, "Activation of the HIF Prolyl Hydroxylase by the Iron Chaperones PCBP1 and PCBP2" **2011**, *In preparation*.

4.2 Introduction

Mammalian cells express hundreds of metalloproteins. Most of them contain the abundant metals iron and zinc, while others contain various trace metals, such as copper, manganese, molybdenum and cobalt (101). These metals are essential nutrients because metal cofactors activate enzymes and proteins that perform critical functions in virtually every major cellular process (102). Several factors complicate the incorporation of the correct metal ion into a metalloprotein. First, the binding sites for different metals within metalloproteins can be structurally very similar, and incorporation of the non-cognate metal ion is easily achieved *in vitro* for many of these proteins. Second, pools of "free" metal ions in cells may be vanishingly small, as most zinc and copper ions are tightly bound to cytosolic proteins (103). Third, redox-active metals, such as iron and copper ions, can catalyze the production of damaging reactive oxygen species, and cells must maintain tight control over these metals in order to use them while simultaneously avoiding their toxic effects. Fortunately, the majority of metalloproteins receive the correct metal ion *in vivo*, as incorporation of the wrong metal ion typically inactivates the protein.

Although the incorporation of the appropriate metal ion(s) into cellular metalloproteins is a critical, essential process, the mechanism by which most metalloproteins receive their cognate ligand is unknown. Some proteins rely on

metallochaperones: proteins that specifically bind metal ions and deliver them to target enzymes and transporters through direct protein-protein interactions (104). Metallochaperones delivering nickel and copper have been described in prokaryotes and eukaryotes, but much less is known about the delivery of iron and zinc. Frataxin, the protein lacking in the neurodegenerative disease Friedreich's Ataxia, is a mitochondrial protein that functions as an iron chaperone for the assembly of iron-sulfur clusters (105).

More recently, we identified poly (rC) binding protein 1 (PCBP1) as a cytosolic iron chaperone that delivers iron to ferritin (55). In mammals, ferritin is a heteropolymer consisting of 24 subunits of heavy (H) and light (L) peptides that assemble into a hollow sphere into which iron is deposited (106-107). Ferritin serves both to sequester cytosolic iron when it is present in excess and to store iron to meet metabolic needs during periods of iron scarcity. PCBP1 binds Fe(II) with micromolar affinity in a 3 Fe: 1 PCBP1 molar ratio. PCBP1 binds ferritin *in vivo* and can enhance iron incorporation into ferritin *in vitro* and *in vivo*. Mammalian cells lacking PCBP1 exhibit defects in the incorporation of iron into ferritin as well as an increase in the labile pool of cytosolic iron.

PCBP1 (also called α -CP1 or hnRNP E1) has previously been found to function as a RNA and DNA binding protein (56, 108-109). PCBP1 is one member of a family of four homologous proteins containing three heterogeneous nuclear ribonucleoprotein K-homology (KH) domains, an ancient and conserved RNA binding module. PCBP1, an intronless gene, likely arose from the retrotransposition of a splice variant of PCBP2 mRNA, and became fixed in the

genome because it encoded a unique function not shared by the other PCBPs. PCBP1 and 2 bind to cytosolic and viral RNAs, thereby affecting their translation or stability. PCBPs also have a role in transcriptional regulation and participate in several protein-protein interactions.

Numerous cellular proteins require iron for activity. Iron in the form of heme and iron-sulfur clusters are cofactors for proteins involved in a host of metabolic and regulatory functions. Enzymes of the “non-heme” iron families directly coordinate iron ions as cofactors. These families include the diiron monooxygenases, such as the δ -9-fatty acid desaturase and the small subunit of ribonucleotide reductase (110). A second family is the Fe(II)- and 2-oxoglutarate (2-OG)-dependent dioxygenases (111-113). This family is a large, evolutionarily conserved class of enzymes that can oxidatively modify a variety of substrates. In mammals, four members of this class regulate the activity of the transcription factors that control the mammalian response to hypoxia.

Hypoxia-inducible factor (HIF) is a heterodimeric transcription factor that binds DNA at specific sites, termed hypoxia response elements (HREs), and activates the expression of more than 100 genes involved in the adaptation to reduced oxygen levels (111-113). Under hypoxic conditions, the alpha subunit (HIF α) accumulates and binds to the beta subunit (HIF1 β , also called ARNT) to form the active transcription factor. Metazoans express three unstable HIF α subunits. Under conditions of normoxia or hyperoxia, HIF1 α is hydroxylated on proline residues 402 and 564, which allows the protein to be recognized by the von Hippel-Lindau tumor suppressor protein (pVHL), thus targeting HIF1 α for

ubiquitin-mediated degradation in the proteasome (114-115). Three HIF prolyl hydroxylases, PHD1, 2, and 3 (also called HPH-3, -2, and -1 or EGLN2, 1, and 3, respectively) mediate the hydroxylation of proline residues on HIF1 α (116-117), although PHD2 is responsible for nearly all (>95%) of the activity in cells (118). HIF1 α is also hydroxylated on asparagine 803 by an asparaginyl hydroxylase, factor inhibiting HIF (FIH1) (119-120), a modification that inhibits the association of transcriptional coactivators (121). The activities of the HIF hydroxylases are regulated by the availability of the co-substrates, 2-OG and oxygen. Because the hydroxylases exhibit changes in oxygen binding and activity over the range of oxygen concentrations present in tissues, these enzymes are hypothesized to function directly as oxygen sensors.

The activities of the HIF hydroxylases may also be regulated by the availability of iron. HIF hydroxylase activity is stimulated by the addition of Fe(II) *in vitro*, and, in cultured cells, activity is inhibited by iron chelators (111). In mice, HIF2 α accumulates in duodenal enterocytes in response to iron deprivation, which may reflect a localized decrease in HIF hydroxylase activity (122). Cellular factors that control the incorporation of iron into the HIF hydroxylases are unknown.

Here we have addressed the question of whether PCBP1, or its paralog PCBP2, is involved in the delivery of iron to the Fe(II)-dependent prolyl hydroxylases regulating HIF. We found that cells lacking PCBP1 and, to a lesser extent, PCBP2, exhibited increased levels of HIF1 α that was due to a decrease in prolyl hydroxylation and VHL-mediated degradation. The loss of prolyl

hydroxylase activity was traced to a decrease in iron loading of the enzyme, which could be restored with recombinant PCBP1. PCBP1 physically interacted with PHD2, indicating that PCBP1 acts as an iron chaperone for PHD2. Our studies also suggest a role for PCBPs in the activation of the asparaginyl hydroxylase FIH1, as well.

4.3 Experimental Procedures

4.3.1 Cell culture and treatments

Huh7, A549 and HEK293T cells were grown in high glucose Dulbecco's modified Eagle's medium supplemented with 10% fetal bovine serum and antibiotics (penicillin G, 50 U/ml, and streptomycin, 50 µg/ml) (Gibco-BRL). Cells were treated, as indicated, with the following agents: cycloheximide, ferric chloride, desferrioxamine B (DFO) and MG132, all purchased from Sigma.

4.3.2 Protein depletion by siRNA

PCBP1 and 2 were depleted using Stealth Select RNAi (Invitrogen) with the sequences found in Table S1. A non-targeting, scrambled sequence siRNA pool was used as a control. Huh7 or A549 cells were transfected with 50 pMol of siRNA using Lipofectamine RNAiMAX (Invitrogen). Cells were harvested at 3 days after transfection for maximal PCBP1 and 2 depletion. In the HEK293T cell line, two sequential transfections spaced 24 hr apart with the PCBP1 and 2 siRNAs were performed to obtain maximal depletion.

4.3.3 RNA extraction and Real-time PCR

RNA was isolated from cells using the RNeasy RNA Isolation kit according

to the manufacturer's instructions (Qiagen). For reverse transcription, 1 μg of total RNA was used in a reaction mixture containing dNTPs and superscript II as per the manufacturer's instructions (Invitrogen). Reverse transcription was performed for 10 min at 25 °C, 60 min at 42 °C, and 5 min at 70 °C using the PTC200 gradient cycler (MJ Research). Quantitative real-time PCR was performed using the double-stranded DNA dye SYBR Green (Applied Biosystems) on an ABI 7500 system according to the manufacturer's protocols. Experiments were performed in triplicate. The primers used are found in Table S2. The HIF1 α , HIF2 α and PHD2 values were normalized to β -actin according to Pfaffl's mathematical model for relative quantification in real time PCR (123). Actin quantitation did not vary with siRNA or DFO treatment.

4.3.4 Immunoblot analysis

Nuclear and cytoplasmic extracts were prepared using the nuclear extract kit (Active Motif) according to the manufacturer's instructions. Nuclear extracts were used for HIF and CREB Western blots. Membranes were probed using mouse anti-HIF1 α (Transduction, 1:1000), rabbit anti-HIF2 α (GeneTex, 1:1000), or mouse anti-CREB (Cell Signaling, 1:1000) antibodies. For detection of hydroxylated HIF1 α , A549 cells were cultured in DMEM and PCBP α were depleted using siRNAs as described above. After 72 hr, 100 μM MG132 was added for 6 hr followed by 25 μM DFO for 2 hr Nuclear extracts (40 μg) were analyzed by Western blotting with a rabbit antibody that specifically recognizes HIF1 α hydroxylation at proline 564 (gift of O. Aprelikova). Whole cell lysates or cytoplasmic extracts were used for all other Western blotting experiments. Whole

cell extracts were prepared by lysis with buffer A [25 mM Tris (pH 8), 1% Nonidet P40, 0.1% Triton, 1 mM DTT, 1X protease inhibitor cocktail (Roche) and 40 mM KCl]. Membranes were incubated with the indicated primary antibodies, followed by detection with horseradish peroxidase-linked secondary antibodies and enhanced chemiluminescence substrates (Pierce). Antibodies used for Western blotting were rabbit anti-PHD2 (Novus Biologicals), mouse anti-PCBP2 (Novus biologicals), mouse anti-HA (Covance), and horseradish peroxidase-conjugated, mouse anti-FLAG (Sigma). Horseradish peroxidase-conjugated secondary antibodies (Amersham) were used at 1:1000. Antibody against recombinant human PCBP1 (55) was raised in chickens and purified from yolks by the manufacturer (Covance) and used at 1:2000-1:5000.

4.3.5 Luciferase activity assays

HeLa 3XHRE Luc cells (124) were cultured and PCBP1 and/or PCBP2 were depleted as described above. Firefly luciferase activity was assayed using Dual Luciferase reporter assay system (Promega). Samples were read in Lumat LB9507 luminometer (Berthold Tech). For FIH activity, PCBPs were depleted in HEK 293 cells, then plasmids encoding the GalDBD/HIF2 α CADs, G5E1b-Luc reporter, pcDNA3.1-FIH1, and pRL-TK were transfected for 18 hr prior to measurement of luciferase activity. Activity was reported as the ratio to renilla luciferase control.

4.3.6 HIF half-life determination

Huh7 cells were transfected with control or PCBP1 and 2 siRNAs for 3

days then were treated with 25 μ M DFO for 2 hr. Cycloheximide was added at 60 μ g/ml, and the cells collect at intervals. HIF1 α was analyzed in nuclear extracts.

4.3.7 VHL capture assay

HEK293T cells were grown and PCBP1, 2 or both were deleted after sequential transfections of their siRNAs. The cells were lysed by sonication for 5 min. HA-pVHL was synthesized by in vitro transcription/translation reactions using TNT T7 Quick Coupled Rabbit Reticulocyte Lysate kit (Promega). The VHL capture assay was performed as described (125-126).

4.3.8 PHD2 activity assay

Biotinylated peptides derived from the HIF1 α oxygen-dependent degradation domain [Biotin-Acp-DLDLEALAPYIPADDDFQL or a hydroxylated control Biotin-Acp-DLDLEALAP(OH)YIPADDDFQL] were immobilized on Neutravidin-coated 96-well plates. A549 cells were grown and PCBP1 and/or 2 were depleted using siRNA. The cells were harvested and resuspended in 1 ml hypotonic buffer (20 mM Hepes, 5 mM NaF, 10 μ M Na₂MoO₄ or Na₃VO₄, 0.1 mM EDTA, protease inhibitor cocktail and 2 mM DTT) for 15-20 min, then 0.5% NP-40 was added and the samples were vortexed for 10 sec. Clarified lysates (50 μ g/well) were incubated in reaction buffer containing 20 mM Tris-Cl (pH 7.5), 5 mM KCl, 1.5 mM MgCl₂, 2 mM DTT, 0-100 μ M ferrous sulfate, 0.5 mM 2-OG and 1 mM ascorbate for 45 min at room temperature. Purified recombinant PCBP1 or albumin (30 μ M) was loaded with 100 μ M ferrous sulfate for 2 hr at 4°C in an anoxic chamber (Coy Laboratories), then added to lysates at a final

concentration of 3 μM protein/10 μM Fe(II). Peptide hydroxylation was detected using a polyclonal rabbit antibody raised against a hydroxylated HIF peptide epitope, followed by addition of a goat anti-rabbit HRP-conjugated secondary antibody (Santa Cruz). Luminescence was measured in an EnVision plate reader (Perkin Elmer).

4.3.9 Immunoprecipitation

HEK293T cells were depleted of PCBPs, then grown and labeled overnight with addition of 2 μM of $^{55}\text{Fe(II):NTA}$ (1:4 molar ratio). For overexpression of PHD2, cells were transiently transfected with pcDNA3-PHD2-FLAG (1 μg). The cells were lysed in buffer containing 50 mM Tris-HCl, pH 7.5; 150 mM NaCl, 0.5% NP40 and protease (Sigma) and phosphatase inhibitors (Pierce). PHD2 was immunoprecipitated with 5 μg of anti-PHD2 antibody (Novus Biologicals) in 1.5 mg lysate overnight followed by protein A dynabeads (Invitrogen) for 3-4 hours at 4°C. The beads were then washed retained ^{55}Fe measured by scintillation counting (LS6500, Beckman Coulter). For co-immunoprecipitations, anti-PCBP1 antibody or bulk chicken IgY (Gallus Immunotech) was coupled to magnetic M280 tosylactivated dynabeads (Invitrogen) using 100 μg of antibody. Beads were then blocked in 0.5% BSA and washed with PBS (pH 7.4) containing 0.1% BSA prior to use. HEK293T cells were treated overnight with either ferric chloride (20 μM) or DFO (100 μM). The cells were harvested and lysed in buffer A and lysates (1.5 mg for PHD2 overexpression, 3 mg for untransfected cells) were incubated with beads, washed, and the immune complexes analyzed by Western blotting.

4.4 Results

4.4.1 Accumulation of transcriptionally active HIF1 α in cells lacking PCBP_s

The activity of the Fe-dependent prolyl hydroxylases is reflected in the abundance of HIF1 α protein. HIF1 α from nuclear extracts was barely detectable in Huh7 cells grown under normoxia, but was greatly increased in cells treated for 16 hr with the iron chelator desferrioxamine B (DFO) due to the inhibition of the prolyl hydroxylases (Fig. 4.1A). We examined the effects of PCBP depletion on HIF1 α levels by transfecting Huh7 cells with small interfering RNAs (siRNAs) directed against PCBP1 and PCBP2, and with a control siRNA. Depletion of PCBP1 resulted in a three-fold increase in HIF1 α protein when compared to the cells treated with control siRNA, without a significant change in HIF1 α levels in cells treated with siRNAs against PCBP2 and PCBP1 and 2 together (Fig. 4.1A and B). We hypothesized that cells subjected to a mild iron deficiency might show increased sensitivity to PCBP depletion, and briefly treated cells depleted of PCBP_s with DFO then examined the levels of HIF1 α (Fig. 4.1C and 4.1D). When compared to cells treated with control siRNA, cells depleted of PCBP1 exhibited a 7-fold increase in the level of HIF1 α . Cells depleted of both PCBP1 and PCBP2 exhibited similarly high levels of HIF1 α , while cells lacking only PCBP2 exhibited a small and variable increase in HIF1 α levels. We measured the effects of the siRNA treatment on PCBP_s by Western blotting and by quantitative real-time (RT) PCR, and confirmed that our siRNA transfections produced depletion of PCBP1 and PCBP2 in Huh7 cells (Fig. 4.1E).

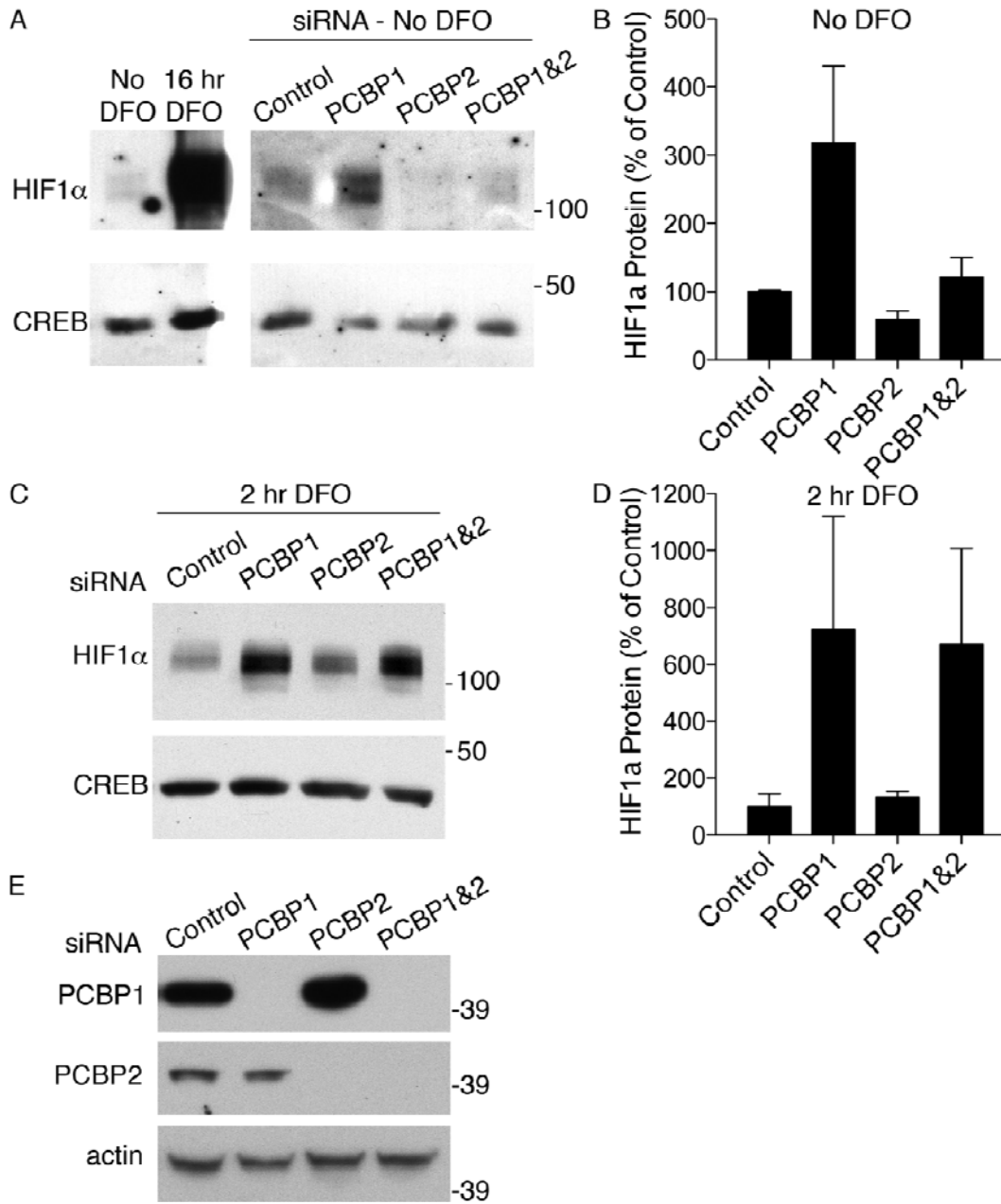


Figure 4.1. Accumulation of HIF1 α in cells depleted of PCBP1 and PCBP2. (A-D) Elevation of HIF1 α protein levels in cells lacking PCBP1 and PCBP2. PCBP1 and PCBP2 were depleted in Huh7 cells using siRNA. After three days cells were treated with no DFO (A and B), 100 μ M DFO for 16h (A) or 2 h (C and D). Nuclear extracts were subjected to SDS-PAGE and Western blotting using anti-HIF1 α and anti-CREB as a loading control (A and C). HIF1 α levels were quantitated from three independent experiments and expressed as a percentage of control-treated cells, \pm SEM (B and D). (E) Confirmation of PCBP1 and PCBP2 depletion by siRNA. Cytoplasmic extracts from Huh7 cells treated with siRNA as in A, above, were subjected to SDS-PAGE and Western blotting using anti-PCBP1 and anti-PCBP2. Membranes were reprobed with mouse anti-actin as a loading control. Molecular weight standards are in kDa.

Although depletion of PCBP1 and 2 appeared complete by Western blot, RT-PCR data suggested that depletion of PCBP2 was less complete than that of PCBP1 (13.3% vs. 5.6% mRNA remaining) and that simultaneous transfection with siRNAs for both PCBP1 and PCBP2 resulted in less efficient depletion of both (9.6% vs. 5.6% remaining for PCBP1 and 16.3% vs. 13.3% for PCBP2). To examine whether the elevated HIF1 α levels in cells lacking PCBPs was due to off-target effects of the siRNAs, we transfected Huh7 cells with alternative siRNAs of different sequences directed against other regions of the PCBP mRNAs and found that these siRNAs also led to increased HIF1 α in cells treated and untreated with DFO. These data indicated that the elevation of HIF1 α in cells depleted of PCBP1 was not due to off target effects of the siRNA.

The elevated levels of HIF1 α detected in cells lacking PCBPs could be due to either an increase in HIF1 α gene expression or a decreased rate of HIF1 α protein degradation. We examined the levels of HIF1 α mRNA in cells depleted of PCBPs using RT-PCR (Fig. 4.2A). Changes in HIF1 α mRNA levels in PCBP-depleted cells were small and not large enough to account for the observed changes in protein levels. We next examined the half-life of HIF1 α protein in Huh7 cells depleted of PCBP1 and 2 versus control cells. Cells were treated with DFO for 2 hr, cycloheximide was added to block new protein synthesis, then cells were collected at intervals and nuclear extracts examined by Western blotting (Fig. 4.2B). HIF1 α protein levels were quantitated and the half-life was calculated

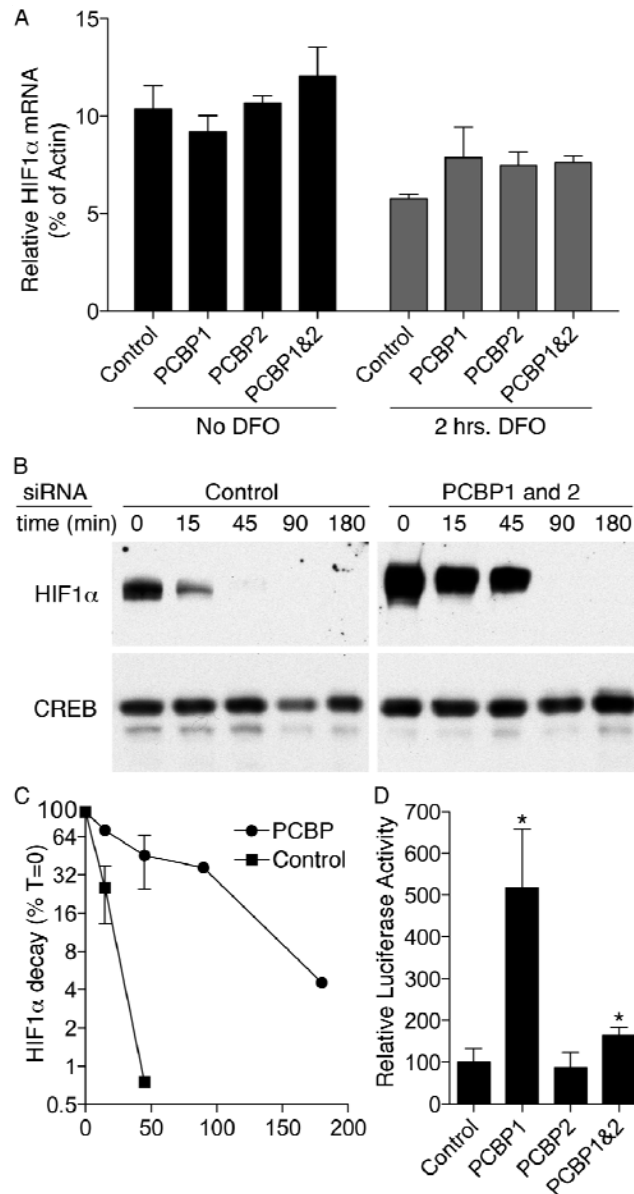


Figure 4.2 Increase in HIF1 α half-life and activity in cells lacking PCBPs. (A) Lack of change in HIF1 α mRNA levels in cells depleted of PCBPs. Huh7 cells were depleted of PCBP1, PCBP2 or both, untreated or treated with DFO for 2 hrs, and HIF-1 α mRNA levels measured by RT-PCR. Data are presented as a percentage of actin mRNA. Samples were analyzed in triplicate and the experiment was repeated three times. Error bars indicated SEM. **(B and C)** Increase in HIF1 α half-life in cells depleted of PCBPs. Huh7 cells were depleted of both PCBP1 and 2, then treated with 25 μ M DFO for 2 h. Cycloheximide was added to the medium and the cells were lysed after 0, 15, 45, 90 and 180 min of treatment. HIF1 α and CREB were detected by Western blotting as in Figure 1 (B). Blots were quantitated, HIF1 α levels were normalized to CREB, and plotted as a percentage of T=0 levels (C). **(D)** Increased HIF1 α transcriptional activity after depletion of PCBP1. A HeLa cell line containing a triple copy of the HRE upstream of a luciferase reporter gene was depleted of PCBP1, PCBP2 or both using siRNA. After 3 days, cells were harvested, lysed, and firefly luciferase activity was measured. The experiment was replicated three times, error bars indicate SEM. * indicates $p < 0.05$.

(Fig. 4.2C). Consistent with previous reports, HIF1 α was rapidly degraded in control cells ($t_{1/2}$ = 8 min.), while HIF1 α exhibited much greater stability in cells depleted of PCBP1 and 2 ($t_{1/2}$ = 50 min.). These data indicated that the accumulation of HIF1 α in cells depleted of PCBP1 was due to impaired degradation of the protein.

We tested whether the increase in HIF1 α protein was associated with an increase in HIF1 α transcriptional activity. A HeLa cell line that contains a stably integrated copy of the firefly luciferase coding sequence under the control of a triple copy of the HRE exhibits luciferase activity in proportion to the activity of the HIF transcription factors (124). This cell line was depleted of PCBP1, PCBP2, or both PCBP1 and 2 and luciferase activity was measured (Fig. 4.2D). Cells treated with PCBP1 siRNA exhibited a 5-fold increase in luciferase activity, while cells treated with siRNAs for both PCBP1 and 2 exhibited a 1.6-fold increase in activity when compared to control cells. These data indicated that cells lacking PCBP1 exhibited both an increase in HIF1 α levels and an increase in HIF-dependent transcription.

4.4.2 Reduced hydroxylation of HIF1 α in cells lacking PCBPs

VHL-mediated degradation of HIF1 α is dependent on the hydroxylation of proline residues 402 and 564 on the oxygen-dependent degradation domain of HIF1 α (114-115). Cells lacking PCBPs may exhibit impaired degradation of HIF1 α because of impaired hydroxylation of these proline residues. We measured the hydroxylation of proline 564 in A549 cells lacking PCBPs by

blocking proteasome-mediated degradation with the inhibitor MG132 and detecting HIF1 α using an antibody that specifically recognizes the hydroxylated form of proline 564 in HIF1 α (HIF1 α -OH) (Fig. 4.3A). A549 cells were selected because they expressed higher levels of PHD2 mRNA than Huh7 cells and HIF1 α -OH was readily detectable. Nuclear extracts were probed for HIF1 α -OH, total HIF1 α , and the nuclear loading control, CREB. HIF1 α -OH was readily detected in cells treated with no or control siRNA, while cells depleted of PCBP1 exhibited dramatically reduced levels of HIF1 α -OH (36% of Control) and cells lacking PCBP2 or PCBP1 and 2 exhibited moderately reduced HIF1 α -OH (66% and 56% of control, respectively). The specificity of the antibody for HIF1 α -OH was demonstrated by the absence of signal in untreated cells (-MG132), which also had no detectable HIF1 α , and the absence of signal in cells treated for 16 hr with DFO alone (+DFO), which had abundant HIF1 α . The decrease in HIF1 α -OH in cells depleted of PCBP1 occurred despite an increase in the level of total HIF1 α , suggesting that depletion of PCBPs was associated with a loss of HIF1 α prolyl hydroxylation.

The activity of the HIF prolyl hydroxylases can be measured using an assay that relies on the specific interaction of pVHL with a HIF1 α -derived peptide containing hydroxyproline 564, but not with a peptide containing an unmodified proline (125-126). We used HEK 293T cell lysates containing PHD to hydroxylate a HIF1 α synthetic peptide corresponding to residues 556-574, which had been bound to magnetic beads. VHL protein was incubated with the peptide, and the amount of pVHL captured by the peptide was measured by Western blotting (Fig.

3B). HEK 293T cells were selected because they expressed more PHD2 than Huh7 cells and depletion of PCBP1 and PCBP2 was very efficient with two sequential

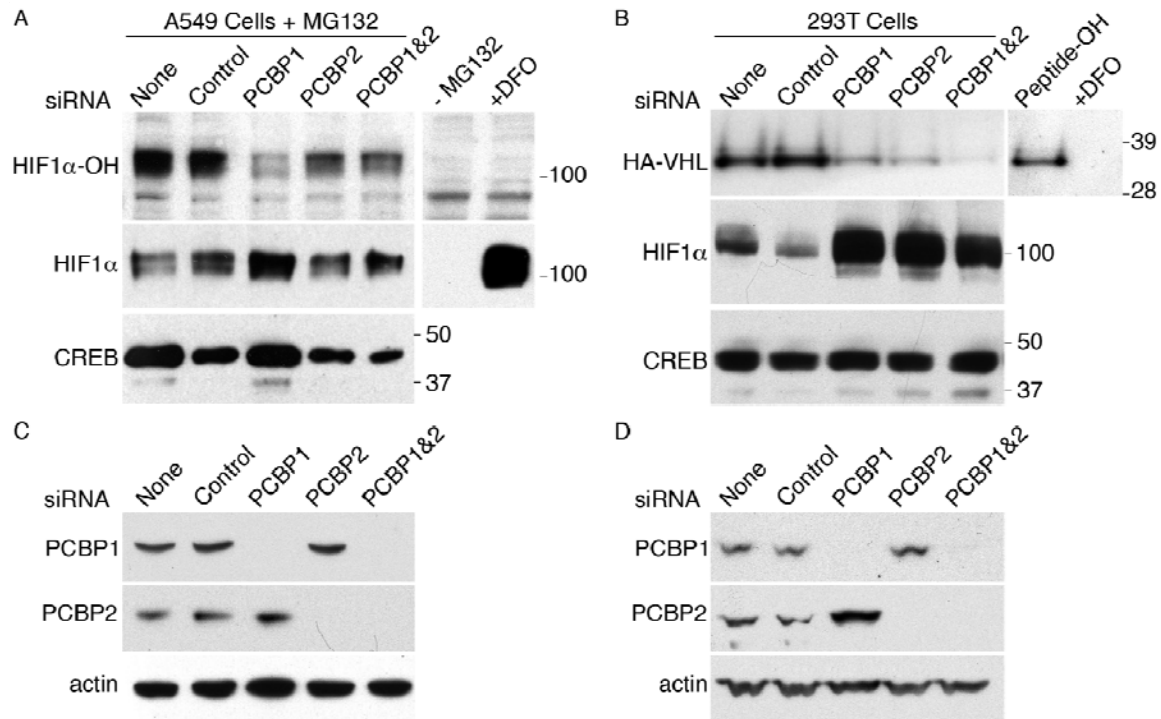


Figure 4.3 Impaired HIF-1 α hydroxylation and VHL binding after depletion of PCBP1 and PCBP2. (A) Decrease in hydroxylated HIF1 α after depletion of PCBP1, PCBP2 or both, then treated with 100 μ M MG132 for 6 h followed by 25 μ M DFO for 2 h. Nuclear extracts were analyzed by Western blotting with anti-HIF1 α -OH, anti-HIF1 α , and anti-CREB. Untreated cells (-MG132) and cells treated with DFO alone were used as controls. (B) Decrease in pVHL binding to hydroxylated HIF1 α after depletion of PCBP1, PCBP2 or both. HEK293T cells depleted of PCBP1, PCBP2 or both were harvested and lysates were added to immobilized synthetic HIF1 α peptide containing proline 564. Peptides were washed and HA-pVHL was allowed to bind to the HIF1 α peptide. Bound HA-pVHL was measured by Western blotting using anti-HA. Hydroxylated synthetic HIF1 α peptide (Peptide-OH) was used as the positive control and DFO treated cells (+DFO) were used as a negative control. Nuclear extracts of HEK293T cells depleted of PCBP1 and PCBP2 were also analyzed for HIF1 α protein and CREB by Western blotting. (C and D) Confirmation of PCBP1 and PCBP2 depletion by siRNA. Cytoplasmic extracts from A549 cells (C) treated with siRNA as in A, above, or HEK293T cells (D) were subjected to SDS-PAGE and Western blotting using anti-PCBP1 and anti-PCBP2 antibodies as in Figure 1. The membranes were reprobed for actin. HEK293T cells were sequentially transfected with siRNAs to deplete PCBP1 and PCBP2.

transfections of siRNAs. Cells were treated with siRNAs for PCBP1 and 2 and control siRNA, then lysed and assayed for PHD activity by the pVHL capture method. Cells transfected with no or control siRNA exhibited readily detectable PHD activity, while cells lacking PCBP1 and PCBP2, individually or in combination, exhibited much lower levels of activity (38-13% of Control). The specificity of the hydroxylated peptide for pVHL capture was confirmed using a hydroxylated synthetic peptide as a positive control (Peptide-OH) and lysate from cells treated with DFO as a negative control (+DFO). Here, HEK 293T cells lacking PCBP2 exhibited a loss of PHD activity that was similar to that of cells lacking PCBP1. Consistent with this observation, the increase in the total amount of HIF1 α in HEK 293T cells lacking PCBP1 and/or PCBP2 was also similar (Fig. 4.3B). Both A549 cells and HEK 293T cells were efficiently depleted of PCBPs using siRNA (Fig. 4.3C and D).

4.4.3 Reduced metallation of PHD2 in cells lacking PCBPs

The reduced hydroxylation of HIF1 α in cells lacking PCBPs could be explained by reduced levels of PHD mRNA or protein, or by reduced specific activity of the enzyme. We measured mRNA levels of PHD2 by RT-PCR and found small differences (less than 2-fold) between control cells and cells lacking PCBPs in Huh7, A549, or HEK 293T cell lines (Fig. 4.4A). PHD2 protein levels did not significantly change in Huh7 (Fig. 4.4B), HEK 293 (Fig. 4.4C), and A549 (Fig. 4.5A) cells after depletion of PCBPs. These data suggested that depletion of PCBPs reduced the specific activity of PHD2 rather than affecting protein

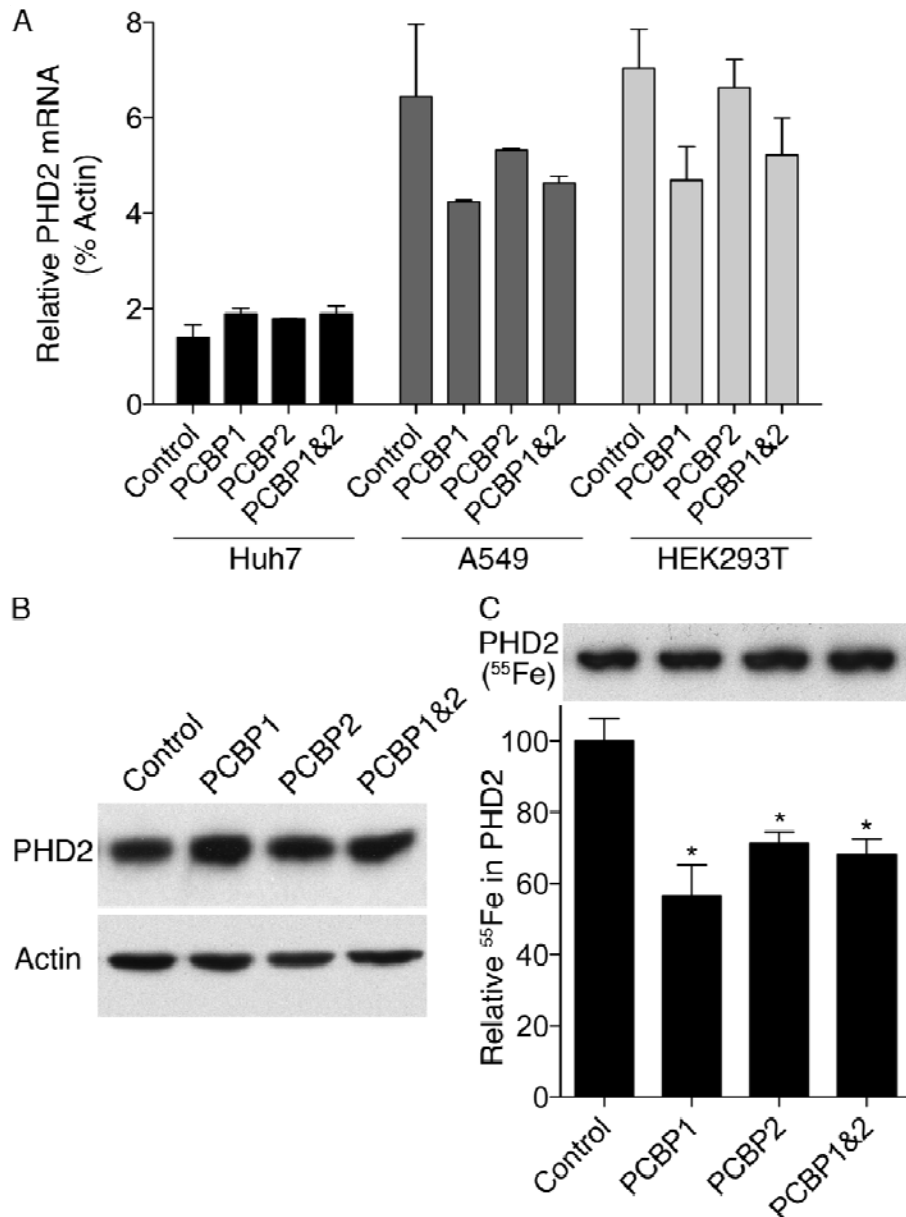


Figure 4.4 Decrease in PHD2 metallation after depletion of PCBP. (A) Lack of change in PHD2 transcript levels after depletion of PCBP. PCBP1, PCBP2 or both were depleted from Huh7, A549 and HEK293T cells by siRNA. PHD2 mRNA levels were measured by RT-PCR and expressed as a percentage of actin. Error bars indicate SEM. (B) Lack of change in PHD2 protein levels after depletion of PCBP. PCBP1, PCBP2 or both were depleted in Huh7 cells. PHD2 was detected in whole cell lysates by Western blotting using anti-PHD2. The blot was reprobed for actin. (C) Less iron in immunoprecipitated PHD2 after depletion of PCBP. PCBP1, PCBP2 or both were depleted from HEK293T cells as in A, then cells were transiently transfected with pcDNA3-PHD2-FLAG to overexpress PHD2. Cells were labeled with ⁵⁵Fe for 16 hrs before harvesting, then PHD2 was detected by Western blotting or PHD2 with its iron ligands was immunoprecipitated using anti-PHD2. Immune complexes were subjected to scintillation counting and the retained ⁵⁵Fe was expressed as a percentage of the ⁵⁵Fe from control lysates. The experiment was replicated four times. Error bars indicate SEM, * indicates $p < 0.05$.

levels. The activity of PHD2 is dependent on the incorporation of iron into the enzyme. Therefore, we measured the amount of iron bound to PHD2 from cells labeled *in vivo* with [^{55}Fe]. HEK 293T cells were depleted of PCBPs, then transiently transfected to overexpress a FLAG-epitope-tagged version of PHD2, and, finally, labeled with [^{55}Fe] for 16 hr. Cells were lysed and PHD2 with its iron ligands was recovered by immunoprecipitation. After washing, immune complexes were subjected to scintillation counting (Fig. 4.4C). The amount of iron bound to PHD2 was significantly reduced in cells lacking PCBP1, PCBP2, or PCBP1 and 2, although the differences measured were not large. There was no difference in the amount of PHD2 protein present in the labeled cell lysates, however (Fig. 4.4C, top panel). These data suggested that the loss of PHD activity in the cells lacking PCBPs was due to a failure to incorporate the Fe(II) cofactor.

4.4.4 Restoration of PHD2 activity with iron or purified PCBP1

We employed a more robust and quantitative assay to further characterize the loss of PHD activity in cells lacking PCBPs. Peptides corresponding to residues 556-574 of HIF1 α were immobilized, then lysates from A549 cells depleted of PCBPs were incubated with the peptides in the presence of 2-oxoglutarate and ascorbate. The amount of hydroxylation of proline 564 was measured using an antibody that specifically recognized hydroxyproline 564 in the HIF1 α -derived peptide. When the hydroxylase assay included a relatively low concentration of Fe(II), robust PHD activity was detected in control lysates, and essentially no activity was detected in lysates from cells treated overnight with DFO (Fig. 4.5A).

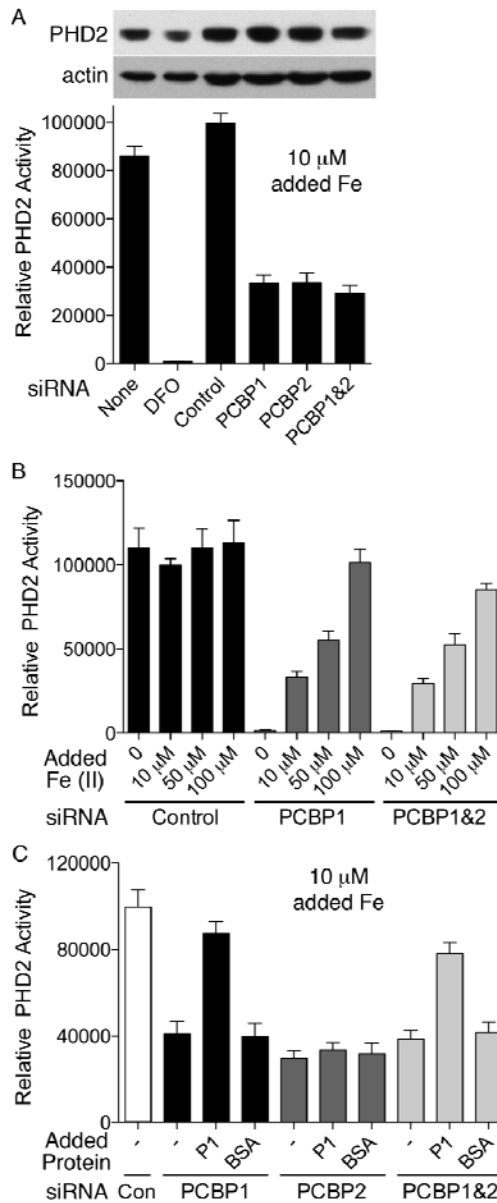


Figure 4.5 Requirement of PCBP1 and PCBP2 for iron-dependent PHD activity. (A) Decrease in PHD activity after depletion of PCBP1 and PCBP2. A549 cells were depleted of PCBP1 and PCBP2 by siRNA. Cells were harvested, lysed, and assayed for PHD protein level (*upper panels*) and activity in the presence of 10 μ M Fe(II). (B) Increased PHD activity after addition of exogenous iron in lysates depleted of PCBP1 and PCBP2. PHD2 activity was measured as in A, above, in assays containing the indicated concentrations of iron. (C) Restoration of PHD activity upon addition of iron-loaded PCBP1 protein to PCBP1-depleted lysates. Purified recombinant PCBP1 and BSA were loaded with Fe(II) and added to lysates prior to measurement of PHD activity. Unliganded Fe(II) was used as an additional control and all assays contained 10 μ M Fe as a final concentration. Activity was expressed as luminescence units. Assays were performed in triplicate, experiments were replicated four or more times. Error bars represent SEM.

Lysates from cells depleted of PCBP1, PCBP2, and PCBP1 and 2 exhibited a 67-71% reduction in PHD2 activity, confirming that PCBPs were required for full PHD activity in cells. Purified recombinant PHD2 that lacks the iron cofactor can be activated *in vitro* with high concentrations of Fe(II). We therefore tested whether PHD activity could be restored in lysates from cells depleted of PCBPs by treating the lysates with Fe(II) *in vitro*. Lysates from control cells exhibited full PHD activity when assayed with or without exogenous iron (Fig. 4.5B), suggesting that the PHD from these cells was fully metallated. In contrast, lysates from cells depleted of PCBP1 and PCBP1 and 2 exhibited virtually no PHD activity in the absence of exogenous iron, but were restored to nearly full activity upon addition of exogenous iron. These data suggested that the loss of PHD activity could be fully explained by the absence of the Fe(II) cofactor from the enzyme in the PCBP-depleted lysates. We next tested whether addition of purified, iron-loaded PCBP1 could restore PHD activity. Purified recombinant PCBP1 (P1) was incubated anaerobically with Fe(II) and added to lysates from cells depleted of PCBPs. The lysates then assayed for PHD activity (Fig. 4.5C). Iron-loaded bovine serum albumin (BSA) and unliganded Fe(II) were used as controls, and the final concentration of iron (10 μ M) was the same for all samples. Purified, iron-loaded PCBP1 was able to restore PHD activity to near control levels in lysates from cells lacking PCBP1 and to partially restore activity in lysates from cells lacking PCBP1 and 2. In contrast, addition of iron-loaded PCBP1 to lysates from cells lacking PCBP2 was no more effective than iron-loaded albumin or iron alone in restoring PHD activity. These data indicated that

iron-loaded PCBP1 could restore PHD activity *in vitro*, and they also suggested that PCBP1 and PCBP2 have non-redundant functions and may cooperate in the delivery of iron to PHD.

4.4.5 Direct *in vivo* interactions between PCBP1 and PHD2

PCBP1 directly binds to ferritin in the process of delivering iron for mineralization, and, in yeast cells, this interaction is dependent on the presence of the iron ligand (55). We examined the *in vivo* binding of PCBP1 to PHD2 in HEK 293T cells by transiently overexpressing PHD2 and testing for the presence of PHD2 in immune complexes precipitated using antibodies against PCBP1 (Fig. 4.6A). To test the effects of iron on interactions between PHD2 and PCBP1, cells overexpressing PHD2 were treated overnight with iron or DFO prior to harvesting. Co-immunoprecipitation of PHD2 with PCBP1 was readily detected in control cells not treated with iron or DFO. No PCBP1 or PHD2 was detected in immunoprecipitates using bulk IgY as a control antibody. Treatment of cells with iron was associated with an increase in the amount of PHD2 bound to precipitated PCBP1 when compared to untreated cells, and treatment of cells with DFO was associated with a large decrease in the co-precipitated PHD2. No significant differences in the amount of PHD2 were apparent in whole cell lysates prior to immunoprecipitation. Because overexpression could favor nonspecific protein-protein interactions, we also tested the binding of endogenous PCBP1 to endogenous PHD2 in the absence of transient overexpression (Fig.4 6B). Again, PHD2 was readily detected in immune complexes obtained after immunoprecipitation of PCBP1, but not in control IgY immunoprecipitations.

Here, the effects of iron manipulation were much less apparent. A measurable increase in PHD2 binding to PCBP1 was occasionally, but not consistently, detected in iron-treated cells when compared to untreated cells. Changes in the amount of bound PHD2 were similarly small in DFO-treated cells. Iron

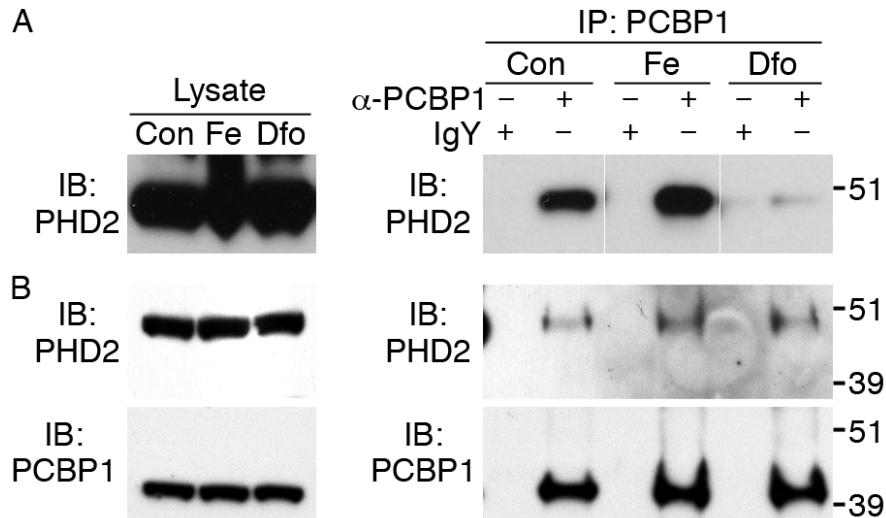


Figure 4.6. Direct interaction of PCBP1 with PHD2. (A) Iron-dependent co-immunoprecipitation of PHD2 with PCBP1 in cells overexpressing PHD2. HEK293T cells were transiently transfected with pcDNA3-PHD2-FLAG followed by overnight addition of 20 μ M ferric chloride or 100 μ M DFO. PCBP1 was immunoprecipitated from 1.5 mg of whole cell lysate using anti-PCBP1 coupled to beads, or bulk IgY coupled to beads as a negative control. In panels on *right*, immune complexes were analyzed by Western blotting for PHD2 and PCBP1. Panels on *left* were Western blots of whole cell lysates before immunoprecipitation. (B) Co-immunoprecipitation of PHD2 with PCBP1 in cells expressing endogenous levels of PHD2. HEK293T cells were treated with either 20 μ M ferric chloride or 100 μ M DFO overnight and immunoprecipitations were carried out as in A, above, using 3 mg of whole cell lysate.

manipulation had no effect on the total levels of PHD2 or PCBP1 in the whole cell lysates. These data showed a direct physical interaction between PCBP1 and PHD2, but whether iron levels affected this interaction appeared to differ depending on the level of expression of PHD2.

4.4.6 Genetic and physical interactions of PCBP1 with FIH

FIH1 is an asparaginyl hydroxylase of the same Fe- and 2-OG-dependent dioxygenase family as the PHDs and we questioned whether FIH1, similar to PHD, also required PCBPs for Fe-dependent activation. FIH1 hydroxylates Asn803 and Asn851 in the carboxyl-terminal transactivation domains (CADs) of HIF1 α and HIF2 α , respectively (120-121). This modification does not lead to degradation of the CADs, but instead prevents the association of transcriptional co-activators with HIF, thereby blocking the activity of the HIF α CADs. Fusion of the CADs to the Gal4 DNA-binding domain (GalDBD) permits the measurement of FIH1 hydroxylase activity through the capacity of FIH1 to inhibit the GalDBD/HIF2 α CAD-dependent transcription of a Gal-responsive luciferase reporter. HEK293 cells were depleted of PCBPs, then co-transfected with plasmids expressing the GalDBD/HIF2 α CAD, wild type FIH1, and a luciferase reporter under the control of a Gal4-responsive promoter (5XGRE). Mutation of Asn851 to Ala in HIF2 α blocks hydroxylation of the Asn residue by FIH1, resulting in constitutive activation of the HIF2 α CAD. Therefore, a second GalDBD/HIF2 α CAD plasmid containing the N851A substitution was also transfected. In cells treated with control siRNA, FIH was fully active, and

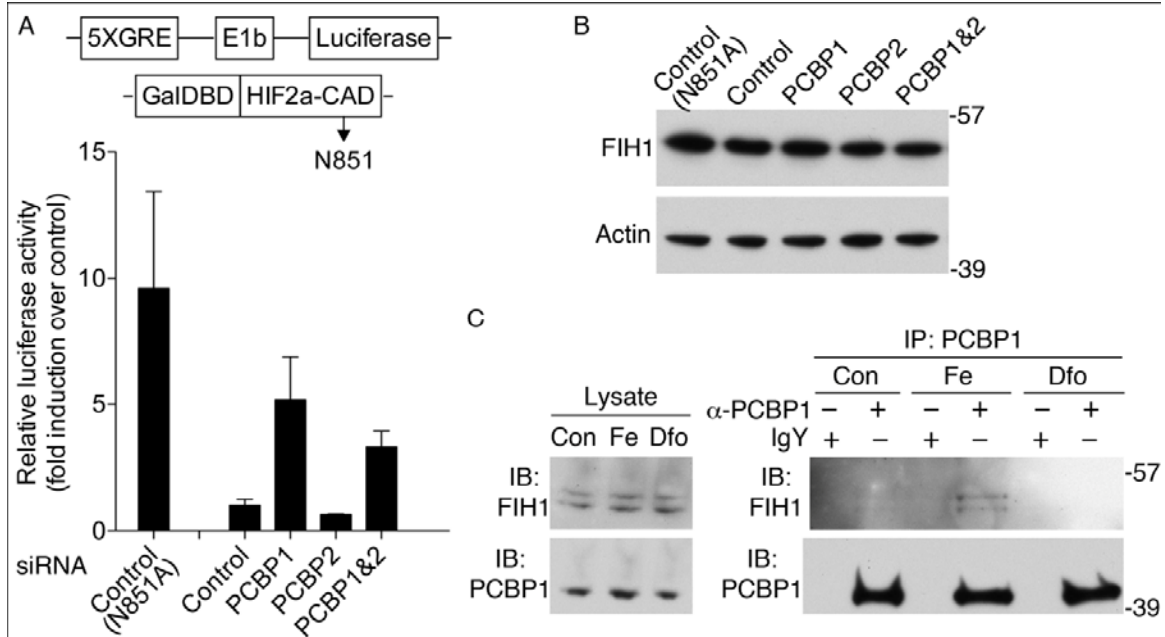


Figure 4.7 Genetic and physical interactions of PCBP1 with FIH1. (A) Loss of FIH1 activity in cells lacking PCBP1. HEK293 cells were depleted of PCBP1 and 2 with siRNA, then co-transfected with plasmids encoding the GalDBD/HIF2 α CAD or the N851A mutant CAD, Gal4-responsive luciferase reporter, control renilla luciferase, and FIH1. Normalized luciferase activity was expressed as a fold-increase over the activity of control siRNA treated cells. Data are the average of three transfections, error bars indicate SEM. **(B)** Lysates from A were subjected to Western blotting for FIH1 and reprobbed for actin. **(C)** Co-immunoprecipitation of FIH1 with PCBP1. HEK293T cells transiently overexpressing FIH1 were treated with iron and DFO, then PCBP1 was immunoprecipitated as in Fig. 6. Whole cell lysates and immune complexes were blotted for FIH1 and PCBP1.

luciferase activity was very low (Fig. 4.7A). In contrast, control cells expressing the N851A CAD exhibited 10-fold higher luciferase activity. Cells depleted of PCBP1 exhibited a 5-fold increase in luciferase activity when compared to control, and cells depleted of PCBP1 and 2 exhibited a 3-fold increase in activity. Similar to PHD2, depletion of PCBPs had no effect on FIH1 protein levels (Fig. 4.7B) and efficient depletion of PCBPs by siRNA was confirmed. These data suggested that cells lacking PCBP1 had reduced FIH1 activity. We tested whether FIH1 was bound to PCBP1 in cells by overexpressing FIH1 in HEK293 cells, immunoprecipitating endogenous PCBP1, and examining immune complexes for co-precipitation of FIH1 (Fig. 4.7C). Similar to PHD2, FIH1 was detectable in immune complexes containing PCBP1, but not in control IgY immunoprecipitations. Unlike PHD2, only immune complexes from cells treated with iron contained significant co-precipitated FIH1. These data suggest that PCBP1 may also act as an iron chaperone for FIH1.

4.5 Discussion

Although most non-heme iron enzymes receive their metal cofactor through an unknown mechanism, our studies indicated that PHDs, the prolyl hydroxylases that modify HIF1 α , require members of the PCBP family of iron chaperones/RNA binding proteins to incorporate Fe(II) into their active sites. Cells lacking PCBP1 exhibited reduced PHD activity, which resulted in less prolyl hydroxylation of HIF1 α , less degradation of HIF1 α through the pVHL-proteasome pathway, accumulation of HIF1 α , and increased HIF1 α transcriptional activity. Because the loss of PHD activity was associated with a loss of the iron cofactor

in vivo and *in vitro*, PCBP1 must be involved in the metallation of PHD. Previously, we have shown that depletion of PCBP1 in Huh7 cells does not result in a change in iron uptake activity; therefore, cellular iron for metallation of PHD must be present. We found that iron-loaded PCBP1 specifically restored activity to inactive PHD *in vitro* and that PCBP1 and PHD2 physically interacted *in vivo* by co-immunoprecipitation. Thus, we propose that PCBP1 is an iron chaperone for PHD as well as for ferritin. The loss of FIH1 activity in cells lacking PCBP1 and the binding of PCBP1 to FIH1 *in vivo* suggest that PCBP1 may act as an iron chaperone for a second member of the Fe- and 2-OG-dependent oxygenases. Treatment of cells with DFO produced a large decrease in the binding of PCBP1 to PHD2 when PHD2 was overexpressed, but not when PHD2 was expressed at endogenous levels. An explanation for this result may be that the affinity of PCBP1 for PHD2 is decreased in the absence of the iron ligand, but iron chelation with DFO only leads to limiting amounts of the Fe-PCBP1 species when PHD2 is present at high levels.

In these studies, depletion of PCBP2 had a variable effect on hydroxylation and degradation of HIF1 α . In Huh7 and A549 cells, the effect of PCBP2 depletion on HIF1 α prolyl hydroxylation and total protein accumulation was small, while in HEK 293T cells, the effect of PCBP1 or PCBP2 depletion was large, and similar for both. In contrast, direct measurement of PHD activity in lysates from A549 cells indicated that depletion of PCBP2 resulted in a dramatic decrease in activity, which was similar to that observed with depletion of PCBP1. One possible explanation for these results is that our depletion of PCBP2 by

siRNA was incomplete, and residual PCBP2 contained sufficient iron chaperone activity to maintain activity in PHDs. This small amount of activity may be sufficient to hydroxylate and destabilize a fraction of the HIF1 α protein, but is too small to measure as significantly greater than the PHD activity of cells lacking PCBP1. Also, PCBP3 and 4 may also have iron chaperone activity and be expressed at different levels in different cell types. We have previously shown that expression of PCBP2 in yeast cells containing human ferritin activates the iron deficiency response of yeast, indicating that PCBP2 can disrupt iron homeostasis in yeast (55). Preliminary data indicate that PCBP2 can bind both iron and ferritin, suggesting that PCBP2 can also function as an iron chaperone (A.N., T.S., and C.C.P., unpublished observations).

Our data do not suggest, however, that PCBP1 and PCBP2 can functionally substitute for each other. Cells lacking PCBP1 or 2 contain wild-type levels of the other paralog. Furthermore, while addition of purified, iron-loaded PCBP1 to lysates lacking PCBP1 fully restored PHD activity, addition of PCBP1 did not restore activity to lysates lacking PCBP2. PCBP1 and PCBP2 may function as a heterooligomeric complex to deliver iron to targets such as ferritin and PHD. PCBP1 and PCBP2 bind to each other when in complex with mRNA (56) and we have confirmed this interaction (data not shown). Our data suggest a model in which PCBP1, in complex with PCBP2 or another PCBP family member, binds iron and interacts with target non-heme iron enzymes to donate metal to the active site. The differences in HIF1 α accumulation that occurred with

depletion of PCBP1 versus PCBP2 may reflect the activity of PCBP1 in complex with PCBP3 or PCBP4, which are generally expressed at lower levels in cells.

Our studies indicate that both ferritin and PHD receive iron from PCBPs. These enzymes are structurally dissimilar, but have certain characteristics in common that may point to mechanisms of iron donation. Both ferritin and PHD2 can fold into their native conformations in the absence of metals. Thus, PCBP1 could interact with these targets posttranslationally to donate iron. The H-chain of ferritin catalyzes the oxidation of Fe(II) to Fe(III) for ferritin core mineralization, and the ferroxidase center structurally and mechanistically resembles the catalytic centers of the oxo-bridged diiron family of monooxygenases (106-107). However, PCBP1 likely does not provide iron directly to the ferroxidase sites of ferritin, as these sites are located on the interior surface of the ferritin sphere. Iron ions are thought to gain access to the ferroxidase sites through pores formed by the subunits arranged along the three-fold axes of symmetry. These pores are lined with hydrophilic residues and PCBP1 could donate Fe(II) to the His, Asp, and Glu residues that line the funnel-shaped channels. The active sites of PHD2 and other enzymes of this class are solvent-exposed and coordinates a single Fe(II) through a His-Xxx-Asp/Glu...His triad located deep in the active site pocket (112-113). Thus, the iron ligands and the coordination environment in these two enzymes are similar.

Given that PCBP1 serves as an iron chaperone for these two diverse target enzymes, we suggest that it is highly likely that other enzymes of the Fe(II)- and 2-OG oxygenase class will require PCBPs for metallation. Sequence

analysis of the human genome indicates the presence of more than 60 enzymes of these classes, many of which have not been functionally characterized, but are predicted to oxidatively modify a broad range of substrates (112-113). Members of the amino acid hydroxylase subclass of these enzymes catalyze the post-translational modification of proteins by hydroxylating the amino acid side chains of proline, lysine, asparagine, aspartate, and tryptophan. In addition to its role in HIF regulation, FIH functions in mice as a regulator of metabolism, likely by hydroxylating asparagine residues on proteins other than HIF (127). This class also includes the collagen prolyl and lysyl hydroxylases, mutations in which cause connective tissue diseases in humans. A subclass of the 2-OG oxygenase family is defined by the presence of the jumonji C domain and members of this sub-class catalyze the oxidative demethylation of mono-, di-, and tri-methylated lysine residues located in histone proteins. The Jhdm2a histone demethylase plays a role in fat and energy metabolism in mice (128). Another subclass of this family resembles the AlkB demethylase of *E. coli*. Eight members of this subclass have been identified in humans with activities that include the dealkylation and oxidative demethylation of modified bases in both DNA and RNA. The activities of these enzymes are predicted to have a major role in DNA repair and the regulation of gene expression. Mutations in the fat-mass and obesity-associated gene, FTO, a 2-OG-dependent enzyme of the AlkB subclass, are associated with obesity in children and adults (129-132). Mice lacking FTO exhibit loss of adipose tissue and increased energy expenditure (133). Perhaps it is a coincidence that, despite having presumably differing activities and specificities, several of the 2-

OG-dependent enzymes seem to function in the regulation of energy metabolism. Alternatively, these enzymes may be poised to respond to changes in cellular energy balance because they require 2-OG, a major product of the TCA cycle, as a co-substrate.

Our studies have not addressed whether PCBP1 is involved in the delivery of iron to the other major class of non-heme iron enzymes, the oxo-bridged diiron family. Ferritin may be a special case, in that PCBP1 cannot interact directly with the active site of the enzyme. Whether PCBPs can deliver iron to the active sites of these enzymes remains to be determined. The mechanism by which PCBPs acquire cytosolic iron is unknown. In yeast, cytosolic monothiol glutaredoxins are required to make iron available to iron-requiring enzymes (59). Whether PCBPs interact with these glutaredoxins awaits further study.

CHAPTER 5

Summary and Future Directions

5.1 Prelude

Iron's unique capacity to accept and donate electrons allows it to play a very important role in almost all possible biological pathways including DNA synthesis, oxygen transport, cell division, etc (2). While low levels of iron accounts for iron deficiency diseases such as anemia, and it impairs cognitive development of the newborns, high levels of iron are associated with disorders like Friedrich's Ataxia, Alzheimer's disease, Parkinson's Disease, etc (99). A reaction between free iron and hydrogen peroxide leads to the formation of reactive oxygen species (ROS) that destroys DNA and compromises cellular efficacy (134). With no known mechanism for excretion, iron levels must be properly regulated when it is in the body.

Various proteins are involved in maintaining cellular iron homeostasis. Transferrin brings iron inside the cell (135), Ferritin stores iron (55), Frataxin possibly serves as iron chaperone for iron-sulfur cluster assembly (136) and there are numerous additional important proteins. These iron binding proteins help to maintain cellular iron homeostasis by allowing the cell to make proper use of iron while at the same time protecting the cell from toxic effects from the metal. Recent breakthroughs regarding the cytosolic iron chaperone for Ferritin have provided new insights in the understanding iron homeostasis at a much deeper level than has previously been attained. Poly (rC) Binding Proteins recovered an iron loading deficiency for Ferritin when both were expressed in yeast, confirming

it plays a role in maintaining cellular iron homeostasis. Using the tools and techniques available in the lab, I have characterized PCBP2 and frataxin, and studied their metal binding properties. The main conclusions of my work are summarized below.

5.2 Summary

PCBP's have been hypothesized to serve as iron chaperones. Following optimization of conditions, PCBP2 was expressed with yield of 5-8mg/L yield and 95% purity in single step purification. Approaches taken to characterize the secondary structure revealed PCBP2 has a high helical content which is consistent with the structure solved of a PCBP2 domain (57-58). With the melting temperature of 56 ± 2.5 °C, PCBP2 appears to be a stable protein.

Using ITC, I was able to show PCBP2 is a metal binding protein, which binds iron at 2 sites with micromolar binding affinity. Furthermore, with the help of ITC, I was able to study the interaction between apo/holo-PCBP2 and Ferritin. Ferritin did not interact with PCBP2 in the absence of iron, but showed an exothermic profile of heat release with holo-PCBP2, confirming PCBP and Ferritin interact with each other only in the presence of iron.

With the use of XAS, the electronic environment of iron bound to PCBP2 was explored. It showed that iron bound to PCBP2 is stable as ferrous metal, and it exists in a nearest ligand environment consisting of 6 coordinate O/N based ligands. These data provide a structural picture of metal bound to PCBP1 that serve as a basis for future studies of iron transfer with ferritin.

5.3 Future Directions:

A long range goal of the lab is to characterize PCBP2 at the atomic, molecular and cellular levels. *The central hypothesis of my project was that the PCBP family of proteins serve as iron chaperones for different tissue specific Ferritins and in additional pathways that require iron.* Understanding the role of the PCBP's at the atomic, molecular, and cellular levels will contribute to the development of a broad understanding of iron storage and utilization events essential for life. With 2 billion of people worldwide suffering from nutritional disorders related to iron deficiency and large number of iron related disorders, the study of iron homeostasis in every detail possible must be explored. The binding affinity of iron to Ferritin, related to the storage and release of metal have been very well documented; whereas, there has been less done to explore how the protein acquires metal from the cytosol. The new finding that PCBP serves as an iron chaperone has given new insights to the understanding of iron homeostasis.

Given that PCBP's bind iron, identification of active sites residues for metal binding via site directed mutagenesis will further help to decipher the role of PCBP's in iron homeostasis. Specifically, by targeting conserved Asp and Glu's in the protein through mutagenesis, we may be able to elucidate how the protein functions during the iron binding and delivery.

REFERENCES

1. Crichton, R. (2001) *Inorganic Biochemistry of Iron Metabolism: From Molecular Mechanisms to Clinical Consequences*, Second ed., John Whiler & Sons, Ltd., West Sussex, England.
2. Andrews, N. C., and Schmidt, P. J. (2007) Iron homeostasis, *Annu Rev Physiol* 69, 69-85.
3. Andrews, N. C. (1999) Disorders of iron metabolism, *N Engl J Med* 341, 1986-1995.
4. Beinert, H., Holm, R.H., Munck, E. (1997) Iron-sulfur clusters: nature's modular, multipurpose structures, *Science* 277, 653-659.
5. Eisenstein, R. S. (1998) Interaction of the hemochromatosis gene product HFE with transferrin receptor modulates cellular iron metabolism, *Nutr Rev* 56, 356-358.
6. Crichton, R. R., Dexter, D. T., and Ward, R. J. (2010) Brain iron metabolism and its perturbation in neurological diseases, *J Neural Transm.*
7. Andrews, N. C. (2008) Forging a field: the golden age of iron biology, *Blood* 112, 219-230.
8. Pollitt, E. (1993) Iron deficiency and cognitive function, *Annu Rev Nutr* 13, 521-537.
9. Hentze, M. W., Muckenthaler, M. U., and Andrews, N. C. (2004) Balancing acts: molecular control of mammalian iron metabolism, *Cell* 117, 285-297.

10. Kaplan, C. D., and Kaplan, J. (2009) Iron acquisition and transcriptional regulation, *Chem Rev.* 109, 4536-4552.
11. Lill, R. (2009) Function and biogenesis of iron-sulphur proteins, *Nature* 460, 831-838.
12. Lill, R., and Muhlenhoff, U. (2008) Maturation of iron-sulfur proteins in eukaryotes: mechanisms, connected processes, and diseases, *Annu Rev Biochem* 77, 669-700.
13. Tokumoto, U., Kitamura, S., Fukuyama, K., and Takahashi, Y. (2004) Interchangeability and distinct properties of bacterial Fe-S cluster assembly systems: functional replacement of the isc and suf operons in *Escherichia coli* with the nifSU-like operon from *Helicobacter pylori*, *J Biochem* 136, 199-209.
14. Schilke, B., Voisine, C., Beinert, H., Craig, E. (1999) Evidence for a conserved system for iron metabolism in the mitochondria of *Saccharomyces cerevisiae*, *Proc. Natl. Acad. Sci. USA* 96, 10206-10211.
15. Yuvaniyama, P., Agar, J. N., Cash, V. L., Johnson, M. K., and Dean, D. R. (2000) NifS-directed assembly of a transient [2Fe-2S] cluster within the NifU protein, *Proc Natl Acad Sci U S A* 97, 599-604.
16. Frazzon, J., and Dean, D. R. (2003) Formation of iron-sulfur clusters in bacteria: an emerging field in bioinorganic chemistry, *Curr Opin Chem Biol* 7, 166-173.

17. Zheng, L., Cash, V. L., Flint, D. H., and Dean, D. R. (1998) Assembly of iron-sulfur clusters. Identification of an iscSUA-hscBA-fdx gene cluster from *Azotobacter vinelandii*, *J Biol Chem* 273, 13264-13272.
18. Shi, R., Proteau, A., Villarroya, M., Moukadiri, I., Zhang, L., Trempe, J. F., Matte, A., Armengod, M. E., and Cygler, M. (2010) Structural basis for Fe-S cluster assembly and tRNA thiolation mediated by IscS protein-protein interactions, *PLoS Biol* 8, 1-18.
19. Muhlenhoff, U., Richhardt, N., Ristow, M., Kispal, G., and Lill, R. (2002) The yeast frataxin homolog Yfh1p plays a specific role in the maturation of cellular Fe/S proteins, *Hum Mol Genet* 11, 2025-2036.
20. Gerber, J., Muhlenhoff, U., and Lill, R. (2003) An interaction between frataxin and Isu1/Nfs1 that is crucial for Fe/S cluster synthesis on Isu1, *EMBO Rep* 4, 906-911.
21. Yoon, T., and Cowan, J. A. (2003) Iron-sulfur cluster biosynthesis. Characterization of frataxin as an iron donor for assembly of [2Fe-2S] clusters in ISU-type proteins., *J. Am. Chem. Soc.* 125, 6078-6084.
22. Layer, G., Ollagnier-de Choudens, S., Sanakis, Y., and Fontecave, M. (2006) Iron-sulfur cluster biosynthesis: characterization of *Escherichia coli* CYaY as an iron donor for the assembly of [2Fe-2S] clusters in the scaffold IscU, *J Biol Chem* 281, 16256-16263.
23. Moreno-Cermeno, A., Obis, E., Belli, G., Cabisco, E., Ros, J., and Tamarit, J. Frataxin depletion in yeast triggers upregulation of iron

- transport systems before affecting iron-sulfur enzyme activities, *J Biol Chem*.
24. Bencze, K. Z., Kondapalli, K. C., Cook, J. D., McMahon, S., Millan-Pacheco, C., Pastor, N., and Stemmler, T. L. (2006) The structure and function of frataxin, *Crit Rev Biochem Mol Biol* 41, 269-291.
 25. Dhe-Paganon, S., Shigeta, R., Chi, Y. I., Ristow, M., and Shoelson, S. E. (2000) Crystal structure of human frataxin, *J Biol Chem* 275, 30753-30756.
 26. Musco, G., Stier, G., Kolmerer, B., Adinolfi, S., Martin, S., Frenkiel, T., Gibson, T., and Pastore, A. (2000) Towards a Structural Understanding of Friedreich's Ataxia: The Solution Structure of Frataxin, *Structure* 8, 695-707.
 27. Cho, S. J., Lee, M. G., Yang, J. K., Lee, J. Y., Song, H. K., and Suh, S. W. (2000) Crystal structure of Escherichia coli CyaY protein reveals a previously unidentified fold for the evolutionarily conserved frataxin family, *Proc Natl Acad Sci U S A* 97, 8932-8937.
 28. He, Y., Alam, S. L., Proteasa, S. V., Zhang, Y., Lesuisse, E., Dancis, A., and Stemmler, T. L. (2004) Yeast frataxin solution structure, iron binding, and ferrochelatase interaction, *Biochemistry* 43, 16254-16262.
 29. Nair, M., Adinolfi, S., Pastore, C., Kelly, G., Temussi, P., and Pastore, A. (2004) Solution structure of the bacterial frataxin ortholog, CyaY: mapping the iron binding sites, *Structure (Camb)* 12, 2037-2048.

30. Karlberg, T., Schagerlof, U., Gakh, O., Park, S., Ryde, U., Lindahl, M., Leath, K., Garman, E., Isaya, G., and Al-Karadaghi, S. (2006) The structures of frataxin oligomers reveal the mechanism for the delivery and detoxification of iron, *Structure* *14*, 1535-1546.
31. Adinolfi, S., Nair, M., Politou, A., Bayer, E., Martin, S., Temussi, P., and Pastore, A. (2004) The Factors Governing the Thermal Stability of Frataxin Orthologues: How To Increase a Protein's Stability, *Biochemistry* *43*, 6511-6518.
32. Adamec, J., Rusnak, F., Owen, W. G., Naylor, S., Benson, L. M., Gacy, A. M., and Isaya, G. (2000) Iron-dependent self-assembly of recombinant yeast frataxin: implications for Friedreich ataxia, *Am J Hum Genet* *67*, 549-562.
33. Bou-Abdallah, F., Adinolfi, S., Pastore, A., Laue, T. M., and Dennis Chasteen, N. (2004) Iron binding and oxidation kinetics in frataxin CyaY of *Escherichia coli*, *J Mol Biol* *341*, 605-615.
34. O'Neill, H. A., Gakh, O., Park, S., Cui, J., Mooney, S. M., Sampson, M., Ferreira, G. C., and Isaya, G. (2005) Assembly of human frataxin is a mechanism for detoxifying redox-active iron, *Biochemistry* *44*, 537-545.
35. Cook, J. D., Bencze, K. Z., Jankovic, A. D., Crater, A. K., Busch, C. N., Bradley, P. B., Stemmler, A. J., Spaller, M. R., and Stemmler, T. L. (2006) Monomeric yeast frataxin is an iron-binding protein, *Biochemistry* *45*, 7767-7777.

36. Kondapalli, K. C., Kok, N. M., Dancis, A., and Stemmler, T. L. (2008) *Drosophila* frataxin: an iron chaperone during cellular Fe-S cluster bioassembly, *Biochemistry* 47, 6917-6927.
37. Aloria, K., Schilke, B., Andrew, A., and Craig, E. A. (2004) Iron-induced oligomerization of yeast frataxin homologue Yfh1 is dispensable in vivo, *EMBO Rep* 5, 1096-1101.
38. Bencze, K. Z., Yoon, T., Millan-Pacheco, C., Bradley, P. B., Pastor, N., Cowan, J. A., and Stemmler, T. L. (2007) Human frataxin: iron and ferroxidase binding surface, *Chem Commun (Camb)*, 1798-1800.
39. Ramazzotti, A., Vanmansart, V., and Foury, F. (2004) Mitochondrial functional interactions between frataxin and Isu1p, the iron-sulfur cluster scaffold protein, in *Saccharomyces cerevisiae*, *FEBS Lett* 557, 215-220.
40. Wang, T., and Craig, E. A. (2008) Binding of yeast frataxin to the scaffold for Fe-S cluster biogenesis, Isu, *J Biol Chem* 283, 12674-12679.
41. Correia, A. R., Wang, T., Craig, E. A., and Gomes, C. M. Iron-binding activity in yeast frataxin entails a trade off with stability in the alpha1/beta1 acidic ridge region, *Biochem J* 426, 197-203.
42. Foury, F., Pastore, A., and Trincal, M. (2007) Acidic residues of yeast frataxin have an essential role in Fe-S cluster assembly, *EMBO Rep* 8, 194-199.
43. Leidgens, S., De Smet, S., and Foury, F. (2010) Frataxin interacts with Isu1 through a conserved tryptophan in its beta-sheet, *Hum Mol Genet* 19, 276-286.

44. Wu, S. P., Wu, G., Surerus, K. K., and Cowan, J. A. (2002) Iron-sulfur cluster biosynthesis. Kinetic analysis of [2Fe-2S] cluster transfer from holo ISU to apo Fd: role of redox chemistry and a conserved aspartate., *Biochemistry* 41, 8876-8885.
45. Cook, J. D., Kondapalli, K. C., Rawat, S., Childs, W. C., Murugesan, Y., Dancis, A., and Stemmler, T. L. (2010) Molecular Details of the Yeast Frataxin-Isu1 Interaction during Mitochondrial Fe-S Cluster Assembly, *Biochemistry* 49, 8756-8765.
46. Li, H., Gakh, O., Smith, D. Y. t., and Isaya, G. (2009) Oligomeric yeast frataxin drives assembly of core machinery for mitochondrial iron-sulfur cluster synthesis, *J Biol Chem* 284, 21971-21980.
47. Shimomura, Y., Wada, K., Fukuyama, K., and Takahashi, Y. (2008) The asymmetric trimeric architecture of [2Fe-2S] IscU: implications for its scaffolding during iron-sulfur cluster biosynthesis, *J Mol Biol* 383, 133-143.
48. Prischi, F., Konarev, P. V., Iannuzzi, C., Pastore, C., Adinolfi, S., Martin, S. R., Svergun, D. I., and Pastore, A. (2010) Structural bases for the interaction of frataxin with the central components of iron-sulphur cluster assembly, *Nat Commun* 1, 95.
49. Adinolfi, S., Iannuzzi, C., Prischi, F., Pastore, C., Iametti, S., Martin, S. R., Bonomi, F., and Pastore, A. (2009) Bacterial frataxin CyaY is the gatekeeper of iron-sulfur cluster formation catalyzed by IscS, *Nat Struct Mol Biol* 16, 390-396.

50. Tsai, C. L., and Barondeau, D. P. (2010) Human frataxin is an allosteric switch that activates the Fe-S cluster biosynthetic complex, *Biochemistry* 49, 9132-9139.
51. Liu, X., and Theil, E. C. (2005) Ferritin: dynamic management of biological iron and oxygen chemistry, *Acc. Chem. Res.* 38, 167-175.
52. Granier, T., Langlois d'Estaintot, B., Gallois, B., Chevalier, J. M., Precigoux, G., Santambrogio, P., and Arosio, P. (2003) Structural description of the active sites of mouse L-chain ferritin at 1.2 Å resolution, *J Biol Inorg Chem* 8, 105-111.
53. Takeda, S., Yamaki, M., Ebina, S., and Nagayama, K. (1995) Site-specific reactivities of cysteine residues in horse L-apoferritin, *J Biochem* 117, 267-270.
54. Levi, S., Santambrogio, P., Corsi, B., Cozzi, A., and Arosio, P. (1996) Evidence that residues exposed on the three-fold channels have active roles in the mechanism of ferritin iron incorporation., *Biochem. J.* 317, 467-473.
55. Shi, H., Bencze, K. Z., Stemmler, T. L., and Philpott, C. C. (2008) A cytosolic iron chaperone that delivers iron to ferritin, *Science* 320, 1207-1210.
56. Makeyev, A. V., and Liebhaber, S. A. (2002) The poly(C)-binding proteins: a multiplicity of functions and a search for mechanisms, *RNA* 8, 265-278.
57. Du, Z., Fenn, S., Tjhen, R., and James, T. L. (2008) Structure of a construct of a human poly(C)-binding protein containing the first and

- second KH domains reveals insights into its regulatory mechanisms, *J Biol Chem* 283, 28757-28766.
58. Fenn, S., Du, Z., Lee, J. K., Tjhen, R., Stroud, R. M., and James, T. L. (2007) Crystal structure of the third KH domain of human poly(C)-binding protein-2 in complex with a C-rich strand of human telomeric DNA at 1.6 Å resolution, *Nucleic Acids Res* 35, 2651-2660.
59. Muhlenhoff, U., Molik, S., Godoy, J. R., Uzarska, M. A., Richter, N., Seubert, A., Zhang, Y., Stubbe, J., Pierrel, F., Herrero, E., Lillig, C. H., and Lill, R. (2010) Cytosolic monothiol glutaredoxins function in intracellular iron sensing and trafficking via their bound iron-sulfur cluster, *Cell Metab* 12, 373-385.
60. Li, H., Mapolelo, D. T., Dingra, N. N., Naik, S. G., Lees, N. S., Hoffman, B. M., Riggs-Gelasco, P. J., Huynh, B. H., Johnson, M. K., and Outten, C. E. (2009) The yeast iron regulatory proteins Grx3/4 and Fra2 form heterodimeric complexes containing a [2Fe-2S] cluster with cysteinyl and histidyl ligation, *Biochemistry* 48, 9569-9581.
61. Campuzano, V., Montermini, L., Molto, M. D., Pianese, L., Cossee, M., Cavalcanti, F., Monros, E., Rodius, F., Duclos, F., Monticelli, A., Zara, F., Canizares, J., Koutnikova, H., Bidichandani, S. I., Gellera, C., Brice, A., Trouillas, P., De Michele, G., Filla, A., De Frutos, R., Palau, F., Patel, P. I., Di Donato, S., Mandel, J. L., Coccozza, S., Koenig, M., and Pandolfo, M. (1996) Friedreich's ataxia: autosomal recessive disease caused by an intronic GAA triplet repeat expansion, *Science* 271, 1423-1427.

62. Babcock, M., de Silva, D., Oaks, R., Davis-Kaplan, S., Jiralerspong, S., Montermini, L., Pandolfo, M., and Kaplan, J. (1997) Regulation of mitochondrial iron accumulation by Yfh1p, a putative homolog of frataxin, *Science* 276, 1709-1712.
63. Rotig, A., de Lonlay, P., Chretien, D., Foury, F., Koenig, M., Sidi, D., Munnich, A., and Rustin, P. (1997) Aconitase and mitochondrial iron-sulphur protein deficiency in Friedreich ataxia, *Nat Genet* 17, 215-217.
64. Cossee, M., Puccio, H., Gansmuller, A., Koutnikova, H., Dierich, A., LeMeur, M., Fischbeck, K., Dolle, P., and Koenig, M. (2000) Inactivation of the Friedreich ataxia mouse gene leads to early embryonic lethality without iron accumulation, *Hum Mol Genet* 9, 1219-1226.
65. Huang, M. L., Becker, E. M., Whitnall, M., Rahmanto, Y. S., Ponka, P., and Richardson, D. R. (2009) Elucidation of the mechanism of mitochondrial iron loading in Friedreich's ataxia by analysis of a mouse mutant, *Proc Natl Acad Sci U S A* 106, 16381-16386.
66. Tsai, C. L., and Barondeau, D. P. (2010) Human Frataxin Is an Allosteric Switch That Activates the Fe-S Cluster Biosynthetic Complex, *Biochemistry* E-published ahead of print.
67. Garland, S. A., Hoff, K., Vickery, L. E., and Culotta, V. C. (1999) *Saccharomyces cerevisiae* ISU1 and ISU2: members of a well-conserved gene family for iron-sulfur cluster assembly, *J Mol Biol* 294, 897-907.

68. Adam, A. C., Bornhovd, C., Prokisch, H., Neupert, W., and Hell, K. (2006) The Nfs1 interacting protein Isd11 has an essential role in Fe/S cluster biogenesis in mitochondria, *Embo J* 25, 174-183.
69. Wiedemann, N., Urzica, E., Guiard, B., Muller, H., Lohaus, C., Meyer, H. E., Ryan, M. T., Meisinger, C., Muhlenhoff, U., Lill, R., and Pfanner, N. (2006) Essential role of Isd11 in mitochondrial iron-sulfur cluster synthesis on Isu scaffold proteins, *Embo J* 25, 184-195.
70. Cook, J. D., Kondapalli, K. C., Rawat, S., Childs, W. C., Murugesan, Y., Dancis, A., and Stemmler, T. L. (2010) Molecular Details of the Yeast Frataxin-Isu1 Interaction during Mitochondrial Fe-S Cluster Assembly, *Biochemistry E-published ahead of print*.
71. Huang, J., Dizin, E., and Cowan, J. A. (2008) Mapping iron binding sites on human frataxin: implications for cluster assembly on the ISU Fe-S cluster scaffold protein, *J Biol Inorg Chem* 13, 825-836.
72. Prischi, F., Konarev, P. V., Iannuzzi, C., Pastore, C., Adinolfi, S., Martin, S. R., Svergun, D. I., and Pastore, A. Structural bases for the interaction of frataxin with the central components of iron-sulphur cluster assembly, *Nat Commun* 1, 95.
73. Studier, F. W. (2005) Protein production by auto-induction in high density shaking cultures, *Protein Expr Purif* 41, 207-234.
74. George, G. N., George, S. J., and Pickering, I. J. (2001) EXAFSPAK, <http://www-ssrl.slac.stanford.edu/~george/exafspak/exafs.htm>, Menlo Park, CA.

75. Bencze, K. Z., Kondapalli, K. C., and Stemmler, T. L. (2007) X-Ray Absorption Spectroscopy, In *Applications of Physical Methods in Inorganic and Bioinorganic Chemistry: Handbook, Encyclopedia of Inorganic Chemistry, 2nd Edition* (Scott, R. A., and Lukehart, C. M., Eds.), pp 513-528, John Wiley & Sons,LTD, Chichester, UK.
76. Semisotnov, G. V., Rodionova, N. A., Razgulyaev, O. I., Uversky, V. N., Gripas, A. F., and Gilmanshin, R. I. (1991) Study of the "molten globule" intermediate state in protein folding by a hydrophobic fluorescent probe, *Biopolymers* 31, 119-128.
77. Weiss, I. M., and Liebhaber, S. A. (1994) Erythroid cell-specific determinants of alpha-globin mRNA stability, *Mol Cell Biol* 14, 8123-8132.
78. Weiss, I. M., and Liebhaber, S. A. (1995) Erythroid cell-specific mRNA stability elements in the alpha 2-globin 3' nontranslated region, *Mol Cell Biol* 15, 2457-2465.
79. Collier, B., Goobar-Larsson, L., Sokolowski, M., and Schwartz, S. (1998) Translational inhibition in vitro of human papillomavirus type 16 L2 mRNA mediated through interaction with heterogenous ribonucleoprotein K and poly(rC)-binding proteins 1 and 2, *J Biol Chem* 273, 22648-22656.
80. Ostareck, D. H., Ostareck-Lederer, A., Wilm, M., Thiele, B. J., Mann, M., and Hentze, M. W. (1997) mRNA silencing in erythroid differentiation: hnRNP K and hnRNP E1 regulate 15-lipoxygenase translation from the 3' end, *Cell* 89, 597-606.

81. Blyn, L. B., Swiderek, K. M., Richards, O., Stahl, D. C., Semler, B. L., and Ehrenfeld, E. (1996) Poly(rC) binding protein 2 binds to stem-loop IV of the poliovirus RNA 5' noncoding region: identification by automated liquid chromatography-tandem mass spectrometry, *Proc Natl Acad Sci U S A* 93, 11115-11120.
82. Gamarnik, A. V., and Andino, R. (1997) Two functional complexes formed by KH domain containing proteins with the 5' noncoding region of poliovirus RNA, *RNA* 3, 882-892.
83. Charroux, B., Angelats, C., Fasano, L., Kerridge, S., and Vola, C. (1999) The levels of the bancal product, a *Drosophila* homologue of vertebrate hnRNP K protein, affect cell proliferation and apoptosis in imaginal disc cells, *Mol Cell Biol* 19, 7846-7856.
84. Zhu, J., and Chen, X. (2000) MCG10, a novel p53 target gene that encodes a KH domain RNA-binding protein, is capable of inducing apoptosis and cell cycle arrest in G(2)-M, *Mol Cell Biol* 20, 5602-5618.
85. Michelotti, E. F., Michelotti, G. A., Aronsohn, A. I., and Levens, D. (1996) Heterogeneous nuclear ribonucleoprotein K is a transcription factor, *Mol Cell Biol* 16, 2350-2360.
86. Tomonaga, T., and Levens, D. (1996) Activating transcription from single stranded DNA, *Proc Natl Acad Sci U S A* 93, 5830-5835.
87. Sivashanmugam, A., Murray, V., Cui, C., Zhang, Y., Wang, J., and Li, Q. (2009) Practical protocols for production of very high yields of recombinant proteins using *Escherichia coli*, *Protein Sci* 18, 936-948.

88. Chong, S., Mersha, F. B., Comb, D. G., Scott, M. E., Landry, D., Vence, L. M., Perler, F. B., Benner, J., Kucera, R. B., Hirvonen, C. A., Pelletier, J. J., Paulus, H., and Xu, M. Q. (1997) Single-column purification of free recombinant proteins using a self-cleavable affinity tag derived from a protein splicing element, *Gene* 192, 271-281.
89. Chong, S., Montello, G. E., Zhang, A., Cantor, E. J., Liao, W., Xu, M. Q., and Benner, J. (1998) Utilizing the C-terminal cleavage activity of a protein splicing element to purify recombinant proteins in a single chromatographic step, *Nucleic Acids Res* 26, 5109-5115.
90. George, G. N. G., SJ;Pickering IJ. (2001) In *EXAF-SPAK*.
91. Rehr, J. J., and Ankudinov, A. L. (2001) Progress and challenges in the theory and interpretation of X-ray spectra, *J Synchrotron Radiat* 8, 61-65.
92. Bencze, K. Z., Kondapalli, K. C., and Stemmler, T. L. (2006) *X-Ray Absorption Spectroscopy*, John Wiley & Sons, Ltd.
93. Wood, R. J. R., AG (2006) *Iron*, Vol. 10, Lippincott Williams and Wilkins, Philadelphia, PA.
94. Crichton, R. (1991) *Inorganic Biochemistry of Iron Metabolism*, West Sussex:Ellis Horwood Ltd.
95. WHO. (2002) The World Health Report 2002-Reducing Risks, Promoting Health Life Styles.
96. Beutler, E. (2006) Hemochromatosis: genetics and pathophysiology, *Annu Rev Med* 57, 331-347.

97. Heeney, M. M., and Andrews, N. C. (2004) Iron homeostasis and inherited iron overload disorders: an overview, *Hematol Oncol Clin North Am* 18, 1379-1403, ix.
98. Ajioka, R. S., and Kushner, J. P. (2002) Hereditary hemochromatosis, *Semin Hematol* 39, 235-241.
99. Rouault, T. A., and Tong, W. H. (2008) Iron-sulfur cluster biogenesis and human disease, *Trends Genet* 24, 398-407.
100. O'Halloran, T. V., and Culotta, V. C. (2000) Metallochaperones, an intracellular shuttle service for metal ions, *J Biol Chem* 275, 25057-25060.
101. Waldron, K. J., Rutherford, J. C., Ford, D., and Robinson, N. J. (2009) Metalloproteins and metal sensing, *Nature* 460, 823-830.
102. Dupont, C. L., Butcher, A., Valas, R. E., Bourne, P. E., and Caetano-Anolles, G. (2010) History of biological metal utilization inferred through phylogenomic analysis of protein structures, *Proc Natl Acad Sci U S A* 107, 10567-10572.
103. Outten, C. E., and O'Halloran, T. V. (2001) Femtomolar sensitivity of metalloregulatory proteins controlling zinc homeostasis, *Science* 292, 2488-2492.
104. Rosenzweig, A. C. (2002) Metallochaperones: bind and deliver, *Chem Biol* 9, 673-677.
105. Stemmler, T. L., Lesuisse, E., Pain, D., and Dancis, A. (2010) Frataxin and mitochondrial FeS cluster biogenesis, *J Biol Chem* 285, 26737-26743.

106. Crichton, R. R. (2009) Intracellular Iron Storage and Biomineralization, In *Iron Metabolism: From Molecular Mechanisms to Clinical Consequences* (Crichton, R. R., Ed.), pp 183-215, Wiley, West Sussex.
107. Hintze, K. J., and Theil, E. C. (2006) Cellular regulation and molecular interactions of the ferritins, *Cell Mol Life Sci* 63, 591-600.
108. Chaudhury, A., Chander, P., and Howe, P. H. (2010) Heterogeneous nuclear ribonucleoproteins (hnRNPs) in cellular processes: Focus on hnRNP E1's multifunctional regulatory roles, *RNA* 16, 1449-1462.
109. Ostareck-Lederer, A., and Ostareck, D. H. (2004) Control of mRNA translation and stability in haematopoietic cells: the function of hnRNPs K and E1/E2, *Biol Cell* 96, 407-411.
110. Shanklin, J., Guy, J. E., Mishra, G., and Lindqvist, Y. (2009) Desaturases: emerging models for understanding functional diversification of diiron-containing enzymes, *J Biol Chem* 284, 18559-18563.
111. Kaelin, W. G., Jr., and Ratcliffe, P. J. (2008) Oxygen sensing by metazoans: the central role of the HIF hydroxylase pathway, *Mol Cell* 30, 393-402.
112. Loenarz, C., and Schofield, C. J. (2008) Expanding chemical biology of 2-oxoglutarate oxygenases, *Nat Chem Biol* 4, 152-156.
113. Ozer, A., and Bruick, R. K. (2007) Non-heme dioxygenases: cellular sensors and regulators jelly rolled into one?, *Nat Chem Biol* 3, 144-153.
114. Ivan, M., Kondo, K., Yang, H., Kim, W., Valiando, J., Ohh, M., Salic, A., Asara, J. M., Lane, W. S., and Kaelin, W. G., Jr. (2001) HIF α targeted

- for VHL-mediated destruction by proline hydroxylation: implications for O₂ sensing, *Science* 292, 464-468.
115. Jaakkola, P., Mole, D. R., Tian, Y. M., Wilson, M. I., Gielbert, J., Gaskell, S. J., Kriegsheim, A., Hebestreit, H. F., Mukherji, M., Schofield, C. J., Maxwell, P. H., Pugh, C. W., and Ratcliffe, P. J. (2001) Targeting of HIF- α to the von Hippel-Lindau ubiquitylation complex by O₂-regulated prolyl hydroxylation, *Science* 292, 468-472.
116. Bruick, R. K., and McKnight, S. L. (2001) A conserved family of prolyl-4-hydroxylases that modify HIF, *Science* 294, 1337-1340.
117. Epstein, A. C., Gleadle, J. M., McNeill, L. A., Hewitson, K. S., O'Rourke, J., Mole, D. R., Mukherji, M., Metzen, E., Wilson, M. I., Dhanda, A., Tian, Y. M., Masson, N., Hamilton, D. L., Jaakkola, P., Barstead, R., Hodgkin, J., Maxwell, P. H., Pugh, C. W., Schofield, C. J., and Ratcliffe, P. J. (2001) *C. elegans* EGL-9 and mammalian homologs define a family of dioxygenases that regulate HIF by prolyl hydroxylation, *Cell* 107, 43-54.
118. Berra, E., Benizri, E., Ginouves, A., Volmat, V., Roux, D., and Pouyssegur, J. (2003) HIF prolyl-hydroxylase 2 is the key oxygen sensor setting low steady-state levels of HIF-1 α in normoxia, *EMBO J* 22, 4082-4090.
119. Hewitson, K. S., McNeill, L. A., Riordan, M. V., Tian, Y. M., Bullock, A. N., Welford, R. W., Elkins, J. M., Oldham, N. J., Bhattacharya, S., Gleadle, J. M., Ratcliffe, P. J., Pugh, C. W., and Schofield, C. J. (2002) Hypoxia-inducible factor (HIF) asparagine hydroxylase is identical to factor

- inhibiting HIF (FIH) and is related to the cupin structural family, *J Biol Chem* 277, 26351-26355.
120. Lando, D., Peet, D. J., Gorman, J. J., Whelan, D. A., Whitelaw, M. L., and Bruick, R. K. (2002) FIH-1 is an asparaginyl hydroxylase enzyme that regulates the transcriptional activity of hypoxia-inducible factor, *Genes Dev* 16, 1466-1471.
121. Lando, D., Peet, D. J., Whelan, D. A., Gorman, J. J., and Whitelaw, M. L. (2002) Asparagine hydroxylation of the HIF transactivation domain a hypoxic switch, *Science* 295, 858-861.
122. Shah, Y. M., Matsubara, T., Ito, S., Yim, S. H., and Gonzalez, F. J. (2009) Intestinal hypoxia-inducible transcription factors are essential for iron absorption following iron deficiency, *Cell Metab* 9, 152-164.
123. Pfaffl, M. W. (2001) A new mathematical model for relative quantification in real-time RT-PCR, *Nucleic Acids Res* 29, e45.
124. Tian, H., McKnight, S. L., and Russell, D. W. (1997) Endothelial PAS domain protein 1 (EPAS1), a transcription factor selectively expressed in endothelial cells, *Genes Dev* 11, 72-82.
125. Aprelikova, O., Pandolfi, S., Tackett, S., Ferreira, M., Salnikow, K., Ward, Y., Risinger, J. I., Barrett, J. C., and Niederhuber, J. (2009) Melanoma antigen-11 inhibits the hypoxia-inducible factor prolyl hydroxylase 2 and activates hypoxic response, *Cancer Res* 69, 616-624.

126. Tuckerman, J. R., Zhao, Y., Hewitson, K. S., Tian, Y. M., Pugh, C. W., Ratcliffe, P. J., and Mole, D. R. (2004) Determination and comparison of specific activity of the HIF-prolyl hydroxylases, *FEBS Lett* 576, 145-150.
127. Zhang, N., Fu, Z., Linke, S., Chicher, J., Gorman, J. J., Visk, D., Haddad, G. G., Poellinger, L., Peet, D. J., Powell, F., and Johnson, R. S. (2010) The asparaginyl hydroxylase factor inhibiting HIF-1alpha is an essential regulator of metabolism, *Cell Metab* 11, 364-378.
128. Tateishi, K., Okada, Y., Kallin, E. M., and Zhang, Y. (2009) Role of Jhdm2a in regulating metabolic gene expression and obesity resistance, *Nature* 458, 757-761.
129. Dina, C., Meyre, D., Gallina, S., Durand, E., Korner, A., Jacobson, P., Carlsson, L. M., Kiess, W., Vatin, V., Lecoecur, C., Delplanque, J., Vaillant, E., Pattou, F., Ruiz, J., Weill, J., Levy-Marchal, C., Horber, F., Potoczna, N., Hercberg, S., Le Stunff, C., Bougneres, P., Kovacs, P., Marre, M., Balkau, B., Cauchi, S., Chevre, J. C., and Froguel, P. (2007) Variation in FTO contributes to childhood obesity and severe adult obesity, *Nat Genet* 39, 724-726.
130. Frayling, T. M., Timpson, N. J., Weedon, M. N., Zeggini, E., Freathy, R. M., Lindgren, C. M., Perry, J. R., Elliott, K. S., Lango, H., Rayner, N. W., Shields, B., Harries, L. W., Barrett, J. C., Ellard, S., Groves, C. J., Knight, B., Patch, A. M., Ness, A. R., Ebrahim, S., Lawlor, D. A., Ring, S. M., Ben-Shlomo, Y., Jarvelin, M. R., Sovio, U., Bennett, A. J., Melzer, D., Ferrucci, L., Loos, R. J., Barroso, I., Wareham, N. J., Karpe, F., Owen, K. R.,

- Cardon, L. R., Walker, M., Hitman, G. A., Palmer, C. N., Doney, A. S., Morris, A. D., Smith, G. D., Hattersley, A. T., and McCarthy, M. I. (2007) A common variant in the FTO gene is associated with body mass index and predisposes to childhood and adult obesity, *Science* 316, 889-894.
131. Scott, L. J., Mohlke, K. L., Bonnycastle, L. L., Willer, C. J., Li, Y., Duren, W. L., Erdos, M. R., Stringham, H. M., Chines, P. S., Jackson, A. U., Prokunina-Olsson, L., Ding, C. J., Swift, A. J., Narisu, N., Hu, T., Pruim, R., Xiao, R., Li, X. Y., Conneely, K. N., Riebow, N. L., Sprau, A. G., Tong, M., White, P. P., Hetrick, K. N., Barnhart, M. W., Bark, C. W., Goldstein, J. L., Watkins, L., Xiang, F., Saramies, J., Buchanan, T. A., Watanabe, R. M., Valle, T. T., Kinnunen, L., Abecasis, G. R., Pugh, E. W., Doheny, K. F., Bergman, R. N., Tuomilehto, J., Collins, F. S., and Boehnke, M. (2007) A genome-wide association study of type 2 diabetes in Finns detects multiple susceptibility variants, *Science* 316, 1341-1345.
132. Scuteri, A., Sanna, S., Chen, W. M., Uda, M., Albai, G., Strait, J., Najjar, S., Nagaraja, R., Orru, M., Usala, G., Dei, M., Lai, S., Maschio, A., Busonero, F., Mulas, A., Ehret, G. B., Fink, A. A., Weder, A. B., Cooper, R. S., Galan, P., Chakravarti, A., Schlessinger, D., Cao, A., Lakatta, E., and Abecasis, G. R. (2007) Genome-wide association scan shows genetic variants in the FTO gene are associated with obesity-related traits, *PLoS Genet* 3, e115.

133. Fischer, J., Koch, L., Emmerling, C., Vierkotten, J., Peters, T., Bruning, J. C., and Ruther, U. (2009) Inactivation of the Fto gene protects from obesity, *Nature* 458, 894-898.
134. Aisen, P., Wessling-Resnick, M., and Leibold, E. A. (1999) Iron metabolism, *Curr Opin Chem Biol* 3, 200-206.
135. Aisen, P., Leibman, A., and Zweier, J. (1978) Stoichiometric and site characteristics of the binding of iron to human transferrin, *J Biol Chem* 253, 1930-1937.
136. Cook, J. D., Kondapalli, K. C., Rawat, S., Childs, W. C., Murugesan, Y., Dancis, A., and Stemmler, T. L. (2010) Molecular details of the yeast frataxin-Isu1 interaction during mitochondrial Fe-S cluster assembly, *Biochemistry* 49, 8756-8765.

ABSTRACT**CHARACTERIZATION OF POLY (rC) BINDING PROTEIN (PCBP2) AND FRATAXIN**

by

SUDIPA GHIMIRE-RIJAL**May 2011****Advisor:** Prof. Timothy L. Stemmler**Major:** Biochemistry and Molecular Biology**Degree:** Masters in Science

Iron is a micronutrient that acts as a cofactor in many prosthetic groups involving itself in almost every biological process. Iron is the key component in our body fluid, flowing in our veins all the time. Iron deficiency disorders affects more than 9 million people worldwide. Similarly, a high level of iron is associated with various disorders which suggest that in order for body to function properly level of iron should be tightly regulated. Many iron binding proteins help in maintaining cellular iron homeostasis by keeping iron in reduced form.

Working on the hypothesis that Poly (rC) Binding Protein family serve as iron chaperone, research presented here shows that PCBP2 binds ferrous iron with micromolar binding affinity. The structural data on PCBP2 shows that thus bound iron is in 6-coordinate O/N ligand environment. Data presented here characterizes PCBP2 as a dimeric protein, with high helical content. Characterization of PCBP2 will serve as a base for exploring the roles of PCBP2 in cellular iron homeostasis.

AUTOBIOGRAPHICAL STATEMENT

Name: Sudipa Ghimire-Rijal
Date of Birth: 25 February, 1984
Father's name: Dr. Iswor Chandra Ghimire
Mother's name: Srijana Ghimire

Education:

Master's of Science, Wayne State University, (2009-2011)
Major: Biochemistry and Molecular Biology
Advisor: Prof. Timothy L. Stemmler

Bachelor of Science, Wayne State University, (Jan-May 2009)
Major: Biology

Bachelor of Science, Tribhuvan University, Kathmandu, Nepal (2002-2005)
Major: Biology

Publications:

1. Poorna Subramanian, Andria Rodrigues, **Sudipa Ghimire-Rijal** and Timothy L. Stemmler, "Iron Chaperones for Mitochondrial Fe-S Cluster Biosynthesis and Ferritin Iron Storage" *Cur. Opin. Chem. Biol.*, **2010**, *In Press*.
2. Anajli Nandal, Poorna Subramanian, **Sudipa Ghimire-Rijal**, Timothy L. Stemmler, Richard K. Bruick, and Caroline C. Philpott: "Activation of the HIF Prolyl Hydroxylase PHD2 by the Iron Chaperones PCBP1 and PCBP2," *manuscript in preparation*.
3. Swati Rawat, **Sudipa Ghimire-Rijal**, Yogapriya Murugesan and Timothy L. Stemmler, "Characteristics of the Drosophila Frataxin-ISU Interaction that Promotes Mitochondrial Fe-S Cluster Assembly," *manuscript in preparation*.
4. **Sudipa Ghimire-Rijal**, Poorna Subramanian, Timothy L. Stemmler, "Structural and Functional Analysis of Iron Chaperones PCBP1 and PCBP2," *manuscript in preparation*.